Université de Neuchâtel **Faculté des Sciences**

Ligand Design for Transition Metal Catalysis:

From α-Olefin Polymerization to Enantioselective Hydrogenation of Prochiral Olefins

Thèse présentée à la Faculté des Sciences
de l'Université de Neuchâtel
pour l'obtention du titre de Docteur ès Sciences par

Séverine Duclos

Chimiste diplômée de l'Université de Brest (France)

Institut de Chimie **Mai 2002**

IMPRIMATUR POUR LA THESE

Ligand design for transition metal catalysis: from α-olefin polymerization to enantioselective reduction of prochiral alkenes

de Mme Séverine Duclos

UNIVERSITE DE NEUCHATEL

FACULTE DES SCIENCES

La Faculté des sciences de l'Université de Neuchâtel sur le rapport des membres du jury,

MM. T. Ward (directeur de thèse),
G. Süss-Fink et J.-L. Reymond (Berne)

autorise l'impression de la présente thèse.

Neuchâtel, le 31 mai 2002

Le doyen:

F. Zwahlen

A ma famille

Pour ma grand-mère

"Everything should be made as simple as possible, but not simpler."

Albert Einstein (1879-1955)

Acknowledgments

The work presented in this manuscript has been achieved in the group of Prof. Dr. Thomas R. Ward at the University of Bern (August 1997 - August 2000) and at the University of Neuchâtel (September 2000 - July 2002) and would have not been possible without the participation of the following persons to which I would like to express all my gratitude, namely,

Prof. Dr. Thomas R. Ward for the opportunity to make my Ph.D in his research group, for his faithful supervision, the enriching discussions and for the interest he gave to this work,

the Swiss National Science Foundation for financial support,

Members of my jury, Prof. Dr. J.-L. Reymond and Prof. Dr. G. Süss-Fink,

Prof. Dr. J.-L. Reymond and M. Reymond for their collaboration in the biological part of this work,

The groups of Dr. S. Schürch (Bern), Prof. Dr. J. Schäller (Bern) and Prof. Dr. R. Tabacchi (Neuchâtel) for mass spectroscopy,

The group of Prof. Dr. P. Bigler (Bern), Mr. H. Bursian and Dr. S. Claude (Neuchâtel) for NMR,

The group of Prof. Dr. H. Stoekli-Evans (Neuchâtel) and Dr. B. Therrien (Bern) for crystallography,

All my colleagues who worked with me in the laboratory at Bern (Andreas Lutz, Bruno Therrien, Cristof Brändli) and at Neuchâtel (Andreas Loosli, Jerôme Collot, Dr. Andrea Zocchi, Nicolas Humbert, Dr. Julieta Gradinaru, Edith Joseph, Daniel Berdat, Myriem Skander) for the enjoyable working atmosphere, their help and their support,

All my friends in Bern and in Neuchâtel for their presence and their active participation to

make these five years in Switzerland unbelievable and particularly Dr. Caroline Schenkels, Dr. Giancarlo Francese, Dr. Nicolas Bensel, Dr. florence Berezovski, Emmanuel Leroy, les M&M's...

Table of Contents

Summary

The aim of the present thesis has been to rationally design organic ligands and study their coordination- and catalytic properties. Three distinct chapters are presented.

The coordination properties of Kläui's tripodal ligand $[CpCo\{(O)PR_2\}_3]^-$ (which is abbreviated by L_R^-; R = OEt (L_{OEt}^-) or R = Et (L_{Et}^-)), toward zirconium (IV) have been investigated and compared to those of related cyclopentadienyl complexes. Addition of one or two equivalents of L_{OEt}^- or L_{Et}^- to $[ZrCl_4(THF)_2]$ or $[ZrCpCl_3]$ afford the complexes $[Zr_2(L'_{OEt})_4]$ (**1**), $[Zr(L_{OEt})_2](OTos)_2$ ((**3**)$(OTos)_2$), $[Zr(L_{OEt})Cl_3]$ (**4**) and $[Zr(L_{Et})_2]Cl_2$ ((**5**)Cl_2), which have been characterized by X-ray crystallography. Labile $[Zr(L_{OEt})_2Cl_2]$ (**2**) undergoes Arbuzov dealkylation to yield the dinuclear complex **1**.

The synthesis and coordination properties of mixed N,O-compartmental ligands is described. Macrocyclic ligands H_2L_A (**12**) and H_2L_B (**19**) were designed to mimic transition-state analogs for the production of catalytic antibodies for C-H activation reactions. Reaction of ligand **12** with vanadyl cations yields the dinuclear complex $[(VO)_2(L_A)]^{2+}$ (**13**) which was characterized by X-ray crystallography. Amputated ligands HL_C (**21**) and H_3L_D (**22**) react with various transition metal cations to yield complexes which are designed to act as coenzymes for the catalytic antibodies. The nickel complex $[Ni_2(L_C)](CF_3COO)_3(MeOH)$ was structurally characterized by X-ray crystallography.

Pseudo-enantiomers of mixed phosphine-phosphinite ligands $POP_{o\text{-}An}$ (**2**) and $_{o\text{-}An}POP$ (**4**) have been synthesized. Platinum complex $[Pt(_{o\text{-}An}POP)Cl_2]$ (**7**) has been characterized by X-ray crystallography. The contribution of electronic asymmetry has been quantified for enantioselective hydrogenation of prochiral olefins.

Résumé

Le but cette thèse a été de concevoir des ligands organiques et d'étudier leurs propriétés de coordination et catalytiques avec des métaux de transition. Trois chapitres distincts sont présentés ici.

Les propriétés de coordination du ligand $[CpCo\{(O)PR_2\}_3]^-$, (noté L_R^-, R = OEt (L_{OEt}^-) ou R = Et (L_{Et}^-)), vis-à-vis du zirconium (IV) ont été etudiées et comparées à celles de complexes analogues du cyclopentadienyl. L'addition d'un ou deux équivalents de L_{OEt}^- ou L_{Et}^- à $[ZrCl_4(THF)_]$ ou [ZrCpCl] conduit aux complexes $[Zr_2(L'_{OEt})_4]$ (**1**), $[Zr(L_{OEt})_2](OTos)_2$ ((**3**)$(OTos)_2$), $[Zr(L_{OEt})Cl_3]$ (**4**) et $[Zr(L_{Et})_2]Cl_2$ ((**5**)Cl_2) caractérisés cristallographiquement par diffraction de rayons X. Le complexe labile $[Zr(L_{OEt})_2Cl_2]$ (**2**) subit une déalkylation d'Arbuzov pour donner le complexe dinucléaire **1**.

La synthèse et les propriétés de coordination de ligands compartimentés sont décrites. Les ligands macrocycliques H_2L_A (**12**) et H_2L_B (**19**) ont été conçus dans le but de mimer des analogues d'état de transition, pour la production d'anticorps catalytiques possédant de potentielles propriétés d'activation de liaisons C-H. La réaction du ligand **12** avec des cations vanadyl conduit à la formation du complexe dinucléaire $[(VO)_2(L_A)]^{2+}$ (**13**) caractérisé par diffraction de rayons X. Les ligands amputés HL_C (**21**) et H_3L_D (**22**) réagissent avec divers cations de métaux de transition pour donner des complexes, conçus afin d'être utilisés comme coenzymes pour les anticorps catalytiques. Le complexe du nickel $[Ni_2(L_C)](CF_3COO)_3(MeOH)$ a également été caractérisé par diffraction de rayons X.

Des *pseudo*-énantiomères de ligands phosphine-phosphinites $POP_{o\text{-}An}$ (**2**) et $_{o\text{-}An}POP$ (**4**)ont été synthétisés. Le complexe du platine $[Pt(_{o\text{-}An}POP)Cl_2]$ (**7**) a été caractérisé par diffraction de rayons X. La contribution de l'asymétrie électronique a été quantifiée pour l'hydrogénation énantiosélective d'oléfines prochirales.

List of Abbreviations

Anal. calc.	Analysis calculated
arom.	Aromatic
BINAP	(*R*)-2,2'-bis(diphenylphosphino)-1,1'-binaphthyl
9-BBN	9-Borabicyclo[3.3.1]nonane
Boc	*t*-Butoxycarbonyl
BOP	(Benzotriazol-1-yloxy)-tris-(dimethylamino)-phosphonium hexafluorophosphate
BSA (Part 2)	Bovine Serum Albumin
BSA (Part 3)	N,O-bis(trimethylsilyl)acetamide
Bu	Butyl
Cbz	(Benzyloxy)carbonyl
COD	1,5-Cyclooctadiene
Conf.	Configuration
Conv.	Conversion
Cp	Cyclopentadienyl
Cy	Cyclohexyl
DABCO	1,4-Diaza[2.2.2]bicyclooctane
DIOP	(*R*, *R*)-2, 3-*o*-isopropylidene-2, 3-dihydroxy-1, 4-bis(diphenylphosphino)-butane
DIPAMP	(*R*, *R*)-1, 2-bis[(o-methoxyphenyl)-phenylphosphino]ethane
DMF	Dimethylformamide
DMSO	Dimethylsulfoxyde
DNA	Desoxyribo Nucleic Acid
dpopyr	(*S*)-(*N*-diphenylphosphino)(2-diphenylphosphinoxymethyl)pyrrolidine
DuPhos	Alkyl 1,2-bis (phospholano)benzene
EBT-5	Edge Bridged Tetrahedral

EDCI	1-(3-Dimethylaminopropyl-3-ethyl carbodiimid) chlorohydrate
EDTA	Ethylenediamine-*N*, *N*, *N′* ,*N′*-tetraacetic acid
ee	Enantiomeric excess
EI	Electronic Ionisation
ELISA	Enzyme Linked Immuno-Sorbent Assay
equiv.	Equivalent(s)
ESI	Electron Spray Ionisation
Et	Ethyl
Fab	Fragment antigen binding
GC	Gas Chromatography
h	Hour(s)
HBTU	*o*-(Benzotriazol)-1-yl-*N*, *N*, *N′* ,*N′*-tetramethyluronium hexafluorophosphate
HOBT	Hydroxybenzotriazol
HPLC	High Performance Liquid Chromatography
Hz	Hertz
Ig	Immunoglobulin
i-PrOH	Isopropanol
IR	Infra Red
Josiphos	(*R*)-1-[(*S*)-(diphenylphosphino)ferrocenyl]ethyldi-alkylphosphine
kDa	Kilo Dalton
KLH	Keyhole Limpet Hemocyanin
LSIMS	Liquid Secondary Ion Mass Spectroscopy
M	Molar
MALDI	Matrix Assisted Laser Desorption and Ionisation
Me	Methyl
MeCN	Acetonitrile
mg	Milligram
min	Minute(s)
ml	Milliliter
MMM	4-Methylmorpholine

MOM	Methoxymethyl
MS	Mass Spectroscopy
NBD	Norbonadiene
NHS	*N*-hydroxysuccinimid
NMR	Nuclear Magnetic Resonance
obs	Observed
PBS	Phosphate Saline Buffer
PHOX	Phosphooxazoline
POP	(*R*)-1,3-[bis(diphenylphosphin)]-2-phenyl-1-oxa-propane
POPPY	(*R*)-3-diphenylphosphin-1-dipyrrolylphosphin-2-phenyl-1-oxa-propane
ppm	Parts per million
QUINAP	1-(2-diphenylphosphino-1-naphthyl)isoquinoline
r.t.	Room temperature
RNA	Ribo Nucleic Acid
RPHPLC	Reversed-Phase High Performance Liquid Chromatography
S-NHS	Sulfo-*N*-hydroxysuccinimid
SPY-5	Square Pyramid
TB-5	Trigonal Bipyramid
TFA	Trifluoro Acetic Acid
th	Theoretical
THF	Tetrahydrofuran
TLC	Thin Layer Chromatography
TMEDA	Tetramethylenediamine
Tos	Tosylate
t_R	Retention time
TRAP	(*S*,*S*)-2,2''-bis[(*R*)-1-(dialkylphosphino)ethyl]-1,1'-biferrocene
TSU (TSTU)	2-Succinimido-1, 1, 3, 3- tetramethyluronium tetrafluoroborate

General Introduction

The Oxford dictionnary defines a catalyst as a substance, that without itself undergoing any permanent chemical change, increases the rate of a reaction. Chemists distinguish three classes of catalysts: heterogeneous catalysts, enzymes and homogeneous catalysts.

Heterogeneous catalysts are often the most active catalysts but typically operate at high temperature. As a consequence, they lack selectivity. Such catalysts find wide applications in the production of bulk chemicals. The 1963 Nobel Prize in chemisty was awarded to K. Ziegler and G. Natta for the discovery and development of the ethylene polymerization, a heterogeneous process catalyzed by $TiCl_3$.

Enzymes consist of high molecular weight proteins which operate under mild conditions and display high activity and selectivity. In addition to the protein, some enzymes require co-enzymes which are small organic or inorganic molecules indispensable for activity. The 1988 Nobel Prize in chemistry was awarded to J. Deisenhofer, H. Michel and R. Huber for the elucidation of the structure and the activity of the photosynthetic reaction center.

Homogeneous catalysts most often consist of a transition metal and an organic ligand. Such catalysts can be fine-tuned by rationally (or randomly) varying the ligand steric and electronic properties. The 2001 Nobel Prize in Chemistry was awarded to B. K. Sharpless, R. Noyori and W. S. Knowles for their contribution in the field of enantioselective catalysis. These catalysts are finding increasing applications in the synthesis of high added value chemicals (pharmaceuticals, additives...).

The aim of the present thesis is to rationally design organic ligands and study their coordination- and catalytic properties. Three distinct chapters are presented.

Although today most of the polyethylene production relies on heterogeneous catalysts, the need for homogeneous cataysts is very high. Indeed, the stereospecific polymerization of α-olefins yields polymers with fascinating properties depending on the tacticity. Cationic bent metallocene derivatives of the early transition metals ($[Cp_2MX_2]^{n+}$) are finding important uses as homogeneous catalysts for olefins polymerization. Current research efforts in the area focus on the design and synthesis of sterically modified metallocene ligands. In this context, we have been interested to study the coordination properties, toward d^0 metals (Zr(IV)), of the anionic Co(III)-based oxygen tripod $[CpCo\{PR_2(O)\}_3]^-$ (R = OEt or Et), which has long been recognized as a cyclopentadienyl analog.

Enzymes containing carboxylate-bridged dinuclear iron centers are members of a select class of metalloenzymes capable of activating dioxygen for either oxygen transport (respiration) or oxidation chemistry. The soluble MMOH (methane monooxygenase hydroxylase), which falls into this latter category, is capable of selectively oxidazing methane under ambient conditions to yield methanol. This metalloenzyme and its reactivity inspired the design of dinuclear transition-state analogs for the production of catalytic antibodies with potential C–H activation properties.

Transition metal-catalyzed asymmetric reactions are one of the most efficient method for preparing enantiomerically pure products. The work in the area of enantioselective hydrogenation reactions has focused to a great extent on the synthesis of enantiopure transition metal catalysts incorporating C_2 symmetric diphosphine ligands. Recently however, *electronically asymmetric ligands* have shown high potential in enantioselective catalysis. With the aim of quantifying the importance of electronic asymmetry in enantioselective catalysis, we have designed a new class of electronically asymmetric phosphine-phosphinite bidentate ligands which are nearly achiral from a steric point of view.

Part 1 :

Coordination Properties of Kläui's Tripodal Oxygen Donor Toward Zirconium (IV)

1 Introduction

The discovery of ferrocene in 1951 [1,2] has contributed to the large development of organometallic chemistry and more particularly of early transition metal chemistry which is dominated by systems incorporating cyclopentadienyl ligands [3,4].

In the field of homogeneous catalysis, d^0 bent metallocene complexes $[Cp_2MX_2]^{n+}$ (Cp = η^5-C_5H_5) display unrivalled catalytic properties. They are used as catalysts for polymerization of α-olefins (Ziegler-Natta catalyst) [5-7], in reductive coupling [8-10] or hydrogenation [11-13].

Much effort has been invested to improve on existing metallocene catalyst [14-16]. The search for new non-cyclopentadienyl ligand systems is currently of considerable interest to provide the next generation of catalysts [17-25]. This research is focused on organometallic molecules with N- or O- donor ancillary ligands [26-28] or boron-based ligands [29-31]. For examples, chelating diamine titanium complex [15], bis(imido) chromium complex [16] and zirconium (diisopropylamino)borabenzene complexes [32] are tested as catalysts for polymerization of α-olefins (Scheme 1.1). But, to date most useful systems still incorporate bent {Cp_2M}-fragments in many disguises [32-34].

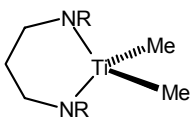

R = 2,6 i-$Pr_2C_6H_3$, 2,6 $Me_2C_6H_3$

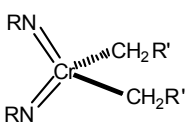

R = 2,6 i-$Pr_2C_6H_3$, t-Bu
R' = Ph, H

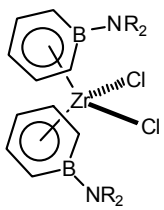

R = i-Pr

a b c

Scheme 1.1 Non comprehensive selection of non-Cp complexes tested as catalysts for polymerization of α-olefins.

Five-coordinate complexes [MCp_2L_3] adopt prototypical square pyramid (SPY-5) or trigonal bipyramid (TB-5) geometries. These geometries and their interconversion along the Berry pathway as well as the reactivity potential of the corresponding compounds have been thoroughly studied, often as a function of the number of metal d electrons [35-42].

However d^0 [MCp_2L_3] compounds cannot be categorized as either SPY-5 or TB-5. This is the case for complexes such as [$TaCp_2H_3$] [43], [$ZrCp_2Cl(\eta^2–CH_3CO)$] [44] and [$ZrCp_2Cl(\eta^4–C_4H_6)$] [45,46] (Scheme 1.2).

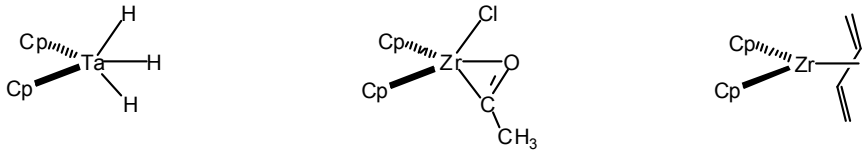

a b c

Scheme 1.2 Complexes [$TaCp_2H_3$] (a), [$ZrCp_2Cl(\eta^2–CH_3CO)$] (b) and [$ZrCp_2Cl(\eta^4–C_4H_6)$] (c).

They adopt an unusual geometry called edge bridged tetrahedral (EBT-5) [47]. This geometry results from a distortion along a reversed-Berry pathway and is characterized by a planar MX_3-arrangment with acute X–M–X angles (symbolized 2α). It is the *overlap* between the π-donor ligand L_π and the d^0-metal M which determines the efficiency of this distortion away from the trigonal bipyramidal geometry and thus the acuteness of the X–M–X angle. The π-orbitals of a cylindrical π-donor (L_π), which are responsible for the reversed Berry distortion, have the same symmetry as the doubly degenerate orbitals of facial terdentate ligands. As such terdentate ligands have a very strong overlap with the metal, such ligands could force a d^0 metal into an EBT-5 geometry [ML_2X_3] (Scheme 1.3).

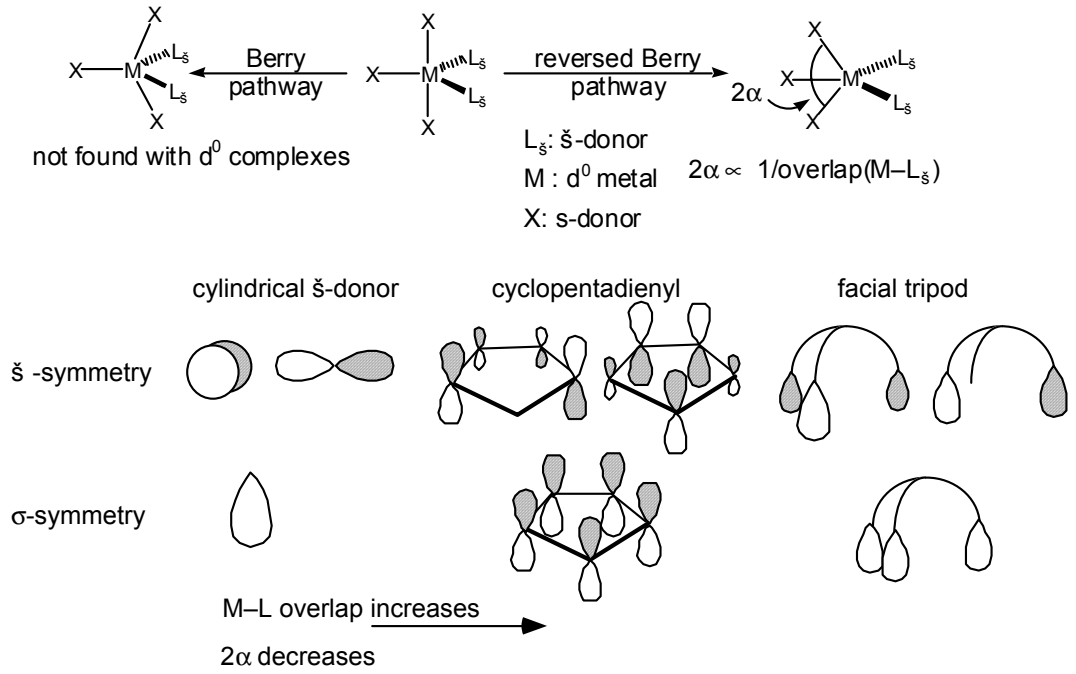

Scheme 1.3 Steric and electronic factors leading to a reversed-Berry distorsion for d^0 complexes.

The anionic Co(III)-based oxygen tripod $[CpCo\{PR_2(O)\}_3]^-$, abbreviated L_R^- (R = OEt or Et, abbreviated L_{OEt}^- and L_{Et}^- respectively), developped by Kläui *et al.* has long been recognized as a cyclopentadienyl analog (Scheme 1.4) [48,49].

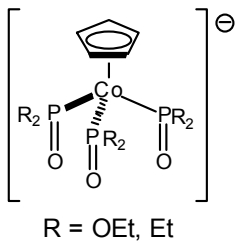

Scheme 1.4 Kläui's tripodal ligand (L_R^-).

Studies of the electronic spectra of the L_R^- metal complexes show that the ligands occupy a high position in the spectrochemical series; i.e. they are very weak and hard donor ligands. They are chemically remarkably inert and suitable to stabilize metal ions and fragments with transition metal centers in various oxidation states [50-52].

Despite its hardness, the coordination chemistry of L_R^- with d^0 metals has received

only little attention [53-57]. This prompted us to investigate the reactivity of Zr(IV) towards L_R^-.

2 Reactivity of Zr(IV) toward L_R- (R = OEt or Et) ligands

2.1 Reactivity of Zr(IV) toward NaL_{OEt}

2.1.1 Arbuzov rearrangment of $[Zr(L_{OEt})_2Cl_2]$ (2) in $[Zr_2(L'_{OEt})_4]$ (1)

Reaction of $[ZrCl_4(THF)_2]$ with two equivalents of NaL_{OEt} in THF at r.t. for 24 h yields, after NaCl filtration and solvent removal, a yellow powder. $^{31}P\{^1H\}$ NMR analysis of the crude reaction mixture indicates the presence of four different P nuclei in a 2:2:1:1 ratio, inconsistent with the expected $[Zr(L_{OEt})_2Cl_2]$ (**2**). Recrystallization from Et_2O affords X-ray quality crystals in 75 % yield. The low temperature X-ray analysis reveals a dinuclear structure $[Zr_2(L'_{OEt})_4]$ (**1**) with seven coordinate zirconiums and devoid of chlorides. This structure, reminiscent of that obtained by Nolan *et al.* for the reaction of YCl_3 with two equivalents of NaL_{OEt} as well as Yeo *et al.* for $ZrCl_4$ with two equivalents of L_{OMe}^-, arises from an Arbuzov dealkylation of two phosphonate alkyl groups for each Zr atom with concomitant ClEt evolution [54,57]. The resulting ligand bears a dianionic charge and can potentially act as a bridging ligand. Although all four ligands present in the dinuclear structure have lost an ethyl group as a result of the Arbuzov reaction, only two of these act as bridging ligands, resulting in a ZrO_7 coordination environment. The molecular structure of $[Zr_2(L'_{OEt})_4]$ (**1**) is depicted in Figure 1.1. Selected bond distances and angles are summarized in Table 1.1. The synthetic route is outlined in Scheme 1.5.

The above reaction can conveniently be monitored by ^{31}P NMR. It appears that the L_{OEt}^-–Cl^- ligand exchange is rapid at r.t. (< 5 min). The singlet at 120 ppm is tentatively assigned to $[Zr(L_{OEt})_2Cl_2]$ (**2**). All attempts to isolate this intermediate have yielded only impure material, contaminated with the rearranged product $[Zr_2(L'_{OEt})_4]$ (**1**). The Arbuzov

rearrangment is complete within 18 h at r.t.

In an attempt to isolate a $[Zr(L_{OEt})_2L_2]$ complex, a THF solution of $[ZrCl_4(THF)_2]$ was treated with two equivalents of NaL_{OEt}, immediately followed by an alkylating agent, i.e. MeLi, $ZnEt_2$, EtMgBr. In all cases, we observed by ^{31}P NMR a ligand displacement (rather than a Cl^-/$Alkyl^-$ exchange) from the zirconium to afford ML_{OEt} (M= Li, MgBr, ZnEt). This metathesis reaction is rationalized by the very high affinity of L_{OEt}^- for such metals, as reflected by their high binding constants [48].

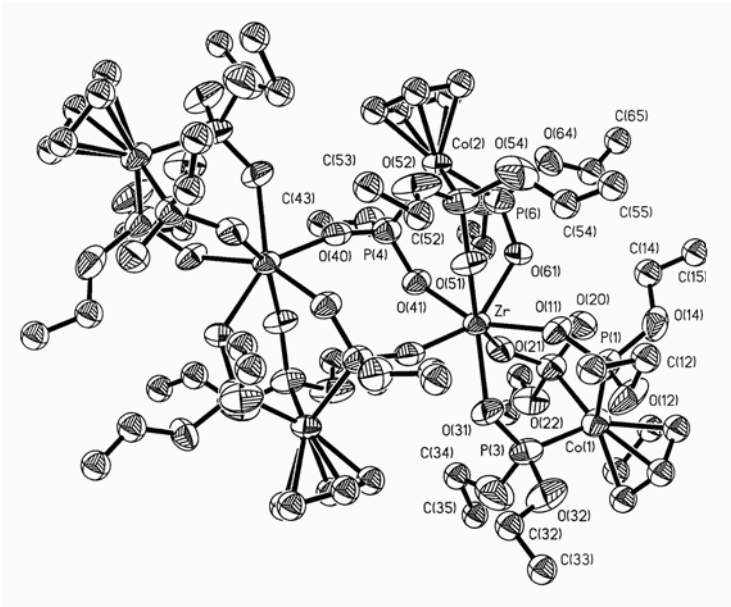

Figure 1.1 Molecular structure of $[Zr_2(L'_{OEt})_4]$ (**1**). Thermal ellipsoids are at the 50% probability level; H atoms and disorder are omitted for clarity.

Table 1.1 Selected interatomic distances (Å) and angles (deg) for $[Zr_2(L'_{OEt})_4]$ (**1**).

Zr-O(21)	2.064(8)	P(2)-O(20)	1.465(11)
Zr-O(41)	2.100(9)	P(2)-O(21)	1.551(9)
Zr-O(40)#1	2.105(10)	P(3)-O(31)	1.513(9)
Zr-O(11)	2.130(8)	P(4)-O(40)	1.517(10)
Zr-O(51)	2.159(8)	P(4)-O(41)	1.537(9)
Zr-O(61)	2.224(9)	P(5)-O(51)	1.520(9)

Zr-O(31)	2.247(9)	P(6)-O(61)	1.523(9)
P(1)-O(11)	1.529(9)		
O(21)-Zr-O(41)	89.1(3)	O(41)-Zr-O(61)	77.8(3)
O(21)-Zr-O(40)#1	124.9(4)	O(40)#1-Zr-O(61)	147.6(3)
O(41)-Zr-O(40)#1	80.1(4)	O(11)-Zr-O(61)	75.4(3)
O(21)-Zr-O(11)	90.5(3)	O(51)-Zr-O(61)	76.7(3)
O(41)-Zr-O(11)	152.7(4)	O(21)-Zr-O(31)	77.2(3)
O(40)#1-Zr-O(11)	121.5(4)	O(41)-Zr-O(31)	130.6(4)
O(21)-Zr-O(51)	154.8(3)	O(40)#1-Zr-O(31)	70.6(3)
O(41)-Zr-O(51)	85.9(3)	O(11)-Zr-O(31)	75.7(4)
O(40)#1-Zr-O(51)	78.5(4)	O(51)-Zr-O(31)	124.0(3)
O(11)-Zr-O(51)	82.9(3)	O(61)-Zr-O(31)	141.5(3)
O(21)-Zr-O(61)	78.1(3)		

Symmetry transformations used to generate equivalent atoms: #1 -x,-y,-z

2.1.2 Isolation of $[Zr(L_{OEt})_2](OTos)_2$ ((3)$(OTos)_2$) from the in situ generated $[Zr(L_{OEt})_2Cl_2]$ (2)

The *in situ* generated $[Zr(L_{OEt})_2Cl_2]$ (**2**) was treated with two equivalents of [AgOTos] (Tos = *p*-$CH_3C_6H_4SO_2$). After AgCl filtration and solvent evaporation, the product was recrystallized from THF/hexane. All spectroscopic data were consistent with $[Zr(L_{OEt})_2(OTos)_2]$. An X-ray analysis of the latter however revealed a dicationic octahedral zirconium species, the tosylates acting as counterions: $[Zr(L_{OEt})_2](OTos)_2$ ((**3**)$(OTos)_2$). This contrasts with Thewalt's recently published $[ZrCp_2(OTos)(H_2O)_2](OTos)$. In this latter case, the tosylates efficiently interact with the Zr (Zr–O = 2.169(5) Å) [58]. The synthetic route is outlined in Scheme 1.5. The molecular structure and selected metrical data for $[Zr(L_{OEt})_2](OTos)_2$ ((**3**)$(OTos)_2$) are presented in Figure 1.2 and Table 1.2 respectively.

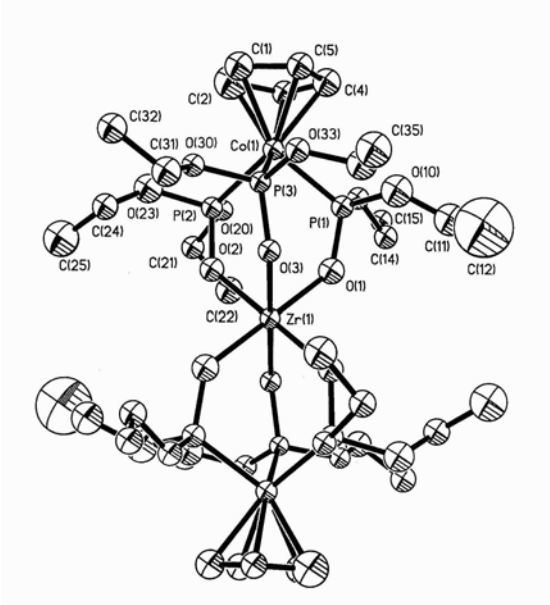

Figure 1.2 Molecular structure of $[Zr(L_{OEt})_2](OTos)_2$ ((**3**)$(OTos)_2$). Thermal ellipsoids are at the 50% probability level; Only one molecule displayed; H atoms and OTos are omitted for clarity.

Table 1.2 Selected interatomic distances (Å) and angles (deg) for $[Zr(L_{OEt})_2](OTos)_2$ ((**3**)$(OTos)_2$).

Zr(1)-O(1)#1	2.066(3)	O(1)#1-Zr(1)-O(2)#1	85.95(10)
Zr(1)-O(1)	2.067(3)	O(1)-Zr(1)-O(2)#1	94.05(10)
Zr(1)-O(2)	2.068(3)	O(2)-Zr(1)-O(2)#1	180.0
Zr(1)-O(2)#1	2.068(3)	O(1)#1-Zr(1)-O(3)#1	87.38(10)
Zr(1)-O(3)#1	2.077(3)	O(1)-Zr(1)-O(3)#1	92.62(10)
Zr(1)-O(3)	2.077(3)	O(2)-Zr(1)-O(3)#1	93.14(10)
P(1)-O(1)	1.544(3)	O(2)#1-Zr(1)-O(3)#1	86.86(10)
P(2)-O(2)	1.544(3)	O(1)#1-Zr(1)-O(3)	92.62(10)
P(3)-O(3)	1.548(3)	O(1)-Zr(1)-O(3)	87.38(10)
O(1)#1-Zr(1)-O(1)	180.0	O(2)-Zr(1)-O(3)	86.86(10)
O(1)#1-Zr(1)-O(2)	94.05(10)	O(2)#1-Zr(1)-O(3)	93.14(10)
O(1)-Zr(1)-O(2)	85.95(10)	O(6)#2-Zr(2)-O(6)	179.999(1)

Two nearly identical independent molecules in the unit cell, only one considered in this table. Symmetry transformations used to generate equivalent atoms: #1 -x,-y+2,-z #2 -x+1,-y+1,-z+1

2.1.3 Synthesis of $[Zr(L_{OEt})Cl_3]$ (4)

Next, we reacted $[ZrCpCl_3]$ with one equivalent of NaL_{OEt} in various solvents (THF, Et_2O, toluene). $^{31}P\{^1H\}$ NMR analysis of the crude mixture reveals a singlet at +119 ppm, consistent with an η^3-coordination of L_{OEt}^- to zirconium. Recrystallization from CH_2Cl_2/C_6H_6 affords a pure crystalline product. ^1H and ^{13}C NMR spectra of the latter display a single cyclopentadienyl resonance with an integral of five rather that ten as would be expected for $[ZrCpL_{OEt}Cl_2]$. The above spectroscopic data suggest that, rather than displacing a chloride from $[ZrCpCl_3]$, L_{OEt}^- displaces the η^5-Cp to afford $[Zr(L_{OEt})Cl_3]$ (**4**). This was confirmed by an X-ray analysis. The molecular structure of $[Zr(L_{OEt})Cl_3]$ (**4**) is depicted in Figure 1.3. Selected bond distances and angles are summarized in Table 1.3. The synthetic route is outlined in Scheme 1.5. It is interesting to note that $[Zr(L_{OEt})Cl_3]$ does not undergo the Arbuzov dealkylation, even upon prolonged heating in THF. This suggests that

only free- rather that coordinated chlorides can induce the rearrangement. The octahedral structure obtained for $[Zr(L_{OEt})_2](OTos)_2$ ((**3**)$(OTos)_2$) suggests that the chlorides in $[Zr(L_{OEt})_2Cl_2]$ (**2**) are either loosely bound or dissociated.

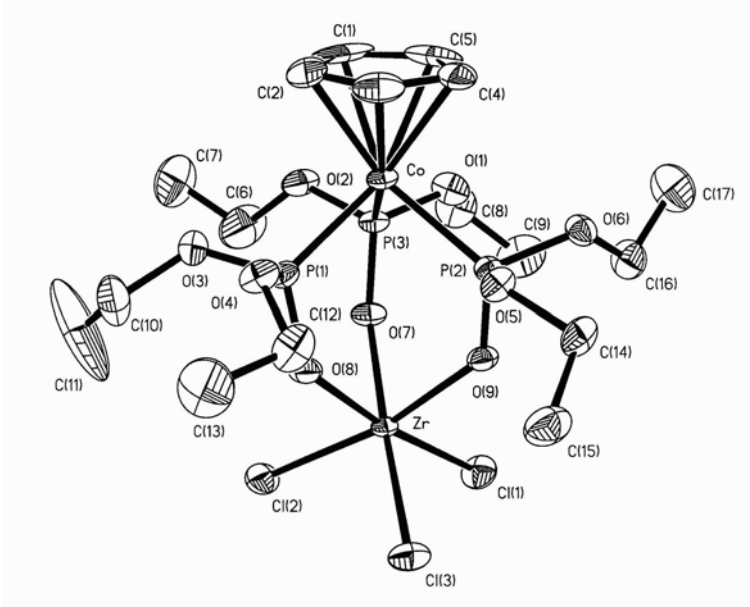

Figure 1.3 Molecular structure of $[Zr(L_{OEt})Cl_3]$ (**4**). Thermal ellipsoids are at the 50% probability level; H atoms and solvents molecules are omitted for clarity.

Table 1.3 Selected interatomic distances (Å) and angles (deg) for $[Zr(L_{OEt})Cl_3]$ (**4**).

Zr-O(7)	2.088(2)	Zr-Cl(3)	2.4414(10)
Zr-O(8)	2.094(2)	Zr-Cl(2)	2.4433(10)
Zr-O(9)	2.098(2)	Zr-Cl(1)	2.4460(9)
O(3)-C(10)	1.457(4)	P(1)-O(8)	1.537(2)
O(5)-C(14)	1.465(4)	P(2)-O(9)	1.539(2)
O(2)-C(6)	1.427(4)	P(3)-O(7)	1.537(2)
O(7)-Zr-O(8)	84.66(8)	O(9)-Zr-Cl(3)	90.54(6)
O(7)-Zr-O(9)	82.98(8)	O(7)-Zr-Cl(2)	89.33(6)
O(8)-Zr-O(9)	82.84(8)	O(8)-Zr-Cl(2)	89.51(6)
O(7)-Zr-Cl(3)	172.03(5)	O(9)-Zr-Cl(2)	169.61(6)
O(8)-Zr-Cl(3)	89.94(7)	Cl(3)-Zr-Cl(2)	96.50(4)
O(7)-Zr-Cl(1)	91.27(6)	Cl(3)-Zr-Cl(1)	93.51(4)
O(8)-Zr-Cl(1)	173.17(6)	Cl(2)-Zr-Cl(1)	95.95(4)
O(9)-Zr-Cl(1)	91.23(6)	P(1)-O(8)-Zr	136.55(13)
P(3)-O(7)-Zr	136.25(12)		

2.2 Reactivity of Zr(IV) toward NaL_{Et}: synthesis of $[Zr(L_{Et})_2]Cl_2$ ((5)Cl_2)

To circumvent the Arbuzov rearrangment, we synthesised the alkyl-substituted ligand L_{Et}^- and reacted it with 0.5 equivalent of $[ZrCl_4(THF)_2]$ in THF [59]. Upon coordination, the ^{31}P NMR signal shifts from 109 ppm to 136 ppm. All spectroscopic data were consistent with $[Zr(L_{Et})Cl_2]$. Crystals grown from CH_2Cl_2 were submitted to X-ray analysis. The structure is octahedral around the zirconium with a ZrO_6 environment: $[Zr(L_{Et})_2]Cl_2$ ((**5**)Cl_2). The chlorides are fully dissociated (Zr–Cl = 7.250(1) Å). Despite the charge and the propensity of zirconium to afford complexes with coordination numbers higher than six, it thus appears that the tripodal ligands L_R^- are too bulky to allow eight coordination around Zr(IV). The molecular structure is presented in Figure 1.4. Selected bond distances and angles are summarized in Table 1.4. The synthetic route is outlined in Scheme 1.5.

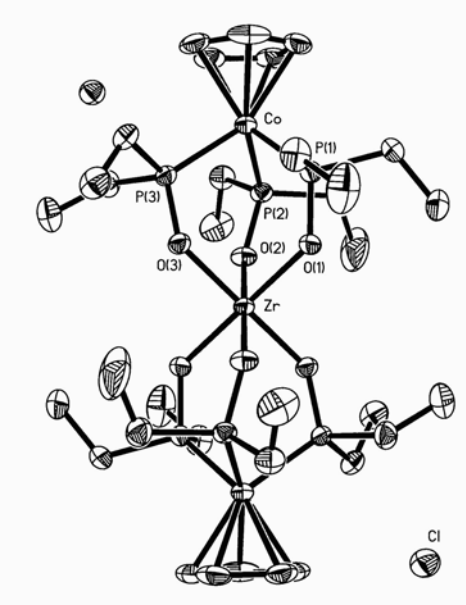

Figure 1.4 Molecular structure of $[Zr(L_{Et})_2]Cl_2$ ((**5**)Cl_2). Thermal ellipsoids are at the 50% probability level; H atoms are omitted for clarity.

Table 1.4 Selected interatomic distances (Å), angles and torsion angles (deg) for $[Zr(L_{Et})_2]Cl_2$ ((**5**)Cl_2).

Zr-O(1)	2.069(2)	O(1)-Zr-O(2)	86.22(9)
Zr-O(3)	2.072(2)	O(1)-Zr-O(3)	85.12(8)
Zr-O(2)	2.073(2)	O(3)-Zr-O(2)	86.00(8)
P(3)-O(3)	1.566(2)	O(1)-Zr-O(2)#1	93.78(9)
P(2)-O(2)	1.568(2)	O(1)-Zr-O(3)#1	94.88(9)
P(1)-O(1)	1.563(2)	O(3)-Zr-O(2)#1	94.00(8)
Zr-Cl	7.2495(9)	P(1)-O(1)-Zr	133.77(13)
Co-P(3)	2.2064(9)	P(2)-O(2)-Zr	133.19(13)
Co-P(1)	2.2065(9)	P(3)-O(3)-Zr	132.11(12)
Co-P(2)	2.2178(9)		

Symmetry transformations used to generate equivalent atoms: #1 -x+1,-y+1,-z+1

3 Conclusion

Scheme 1.5 summarizes the reactivity of $[ZrCl_4(THF)_2]$ towards L_R^- (R = OEt, Et). In contrast to the Cp_2M-based chemistry, this chemistry is characterized by octahedral environments around zirconium. The Arbuzov rearrangment can readily be alleviated by use of L_{Et}^-, but the steric requirements of the tripod are such that the chorides are fully dissociated in $[Zr(L_{Et})_2]Cl_2$. Thus, L_R^- does not behave like a Cp^- analog in the chemistry described here.

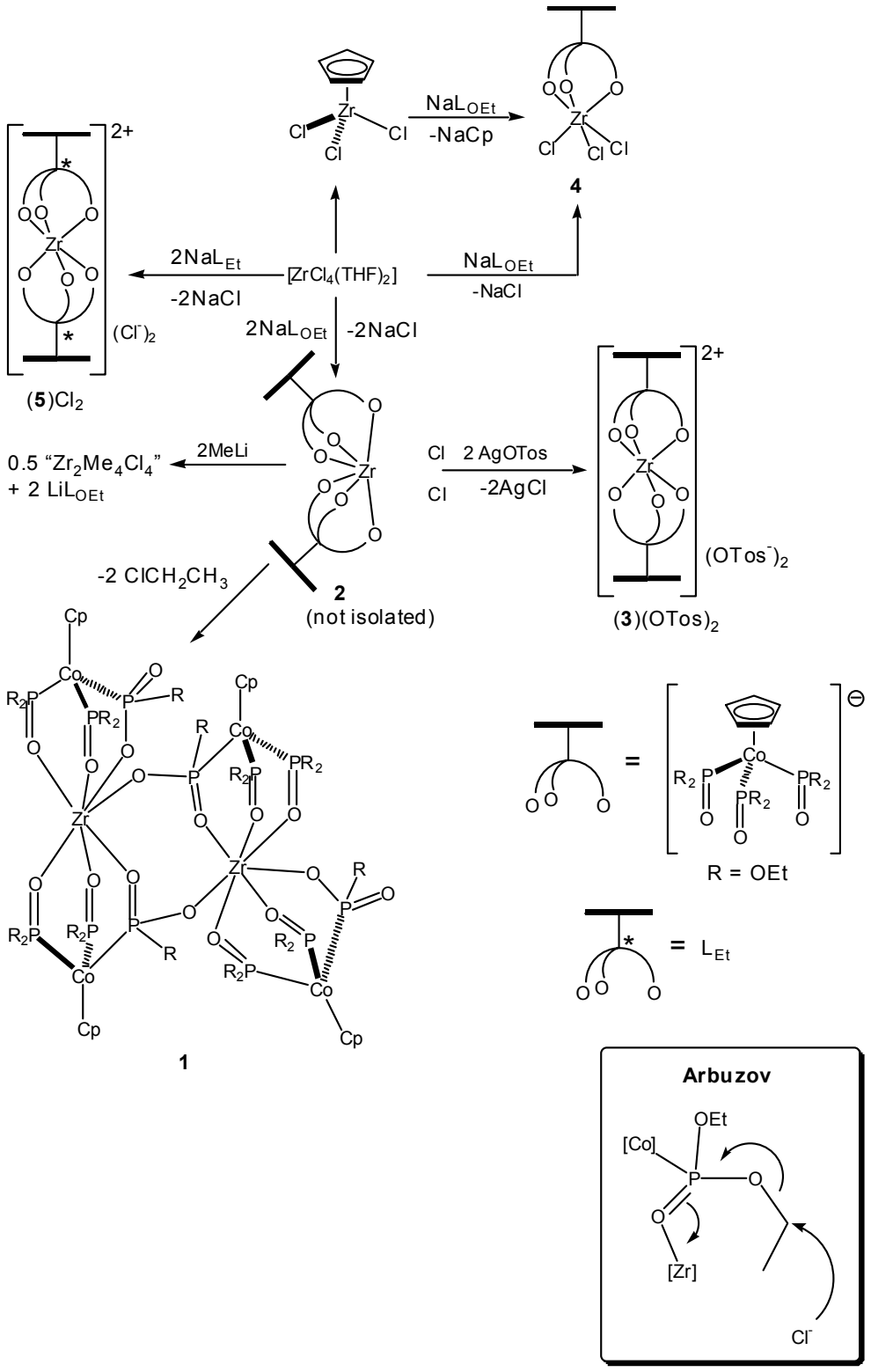

Scheme 1.5 Summary of the reactivity of $[ZrCl_4(THF)_2]$ toward L_R^-.

4 Experimental Section

4.1 General considerations

NMR spectra were recorded on either a VARIAN XL 200 (^{31}P) or BRUKER AM 300 (^{1}H, ^{13}C). Chemical shifts are given in ppm and coupling constant in Hz. Signals are referenced against H_3PO_4 (^{31}P, external reference) and tetramethylsilane (^{1}H, ^{13}C internal reference).

Combustion analyses were carried out by Novartis, Basel.

All experiments were carried out under a nitrogen atmosphere using standard Schlenk techniques.

All solvents were distilled under nitrogen with standard desicating agents.

The compounds NaL_{OEt} [60] and NaL_{Et} [59] were prepared by litterature methods.

4.2 Synthesis of Zr complexes

[$Zr_2(L'_{OEt})_4$]

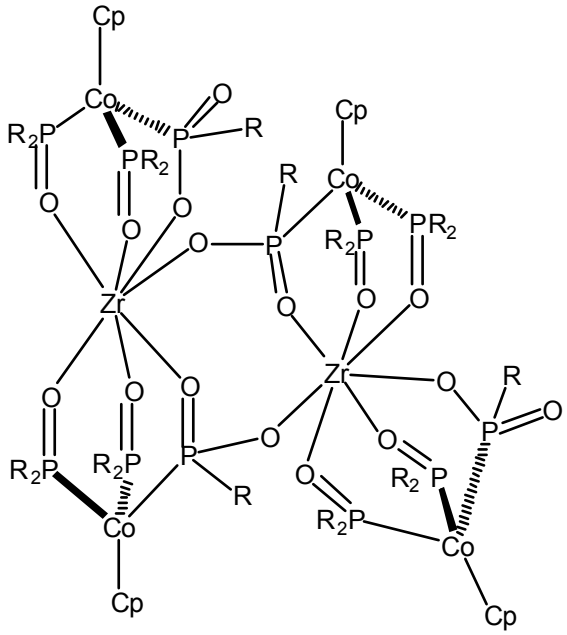

Compound **1**

A THF solution (2 mL) of NaL_{OEt} (0.25 g, 0.44 mmol) was added to $ZrCl_4(THF)_2$ (0.08 g, 0.22 mmol) in THF (3 mL). The mixture was stirred at r.t. for 24 h. After NaCl filtration, the solution was evaporated *in vacuo* to afford a yellow powder. Suitable crystals for X-ray diffraction were obtained by recrystallization from diethylether to yield $[Zr_2(L'_{OEt})_4]$ (**1**) (0.36 g, 0.16 mmol, 75%).

^1H NMR ($CDCl_3$): 1.24 (m, 15H, CH_3); 3.70-4.22 (m, 8H, $P(OC\mathbf{H}_2\text{-}CH_3)_2$); 4.44 (m, 2H, $P(OC\mathbf{H}_2\text{-}CH_3)$); 5.10 (s, 5H, Cp).

^{13}C NMR ($CDCl_3$): 17.14, 17.80 (CH_3); 59.08, 59.94, 60.64, 60.74, 61.01, 61.11, 62.37, 63.51, 68.60 (CH_2); 90.46 (Cp).

$^{31}P\{^1H\}$ NMR ($CDCl_3$): 80.98 (t, $^2J_{P\text{-}P}$=136.16 Hz, 1P, $P(OCH_2\text{-}CH_3)$); 80.68 (t, $J_{P\text{-}P}$=135.36 Hz, 1P, $P(OCH_2\text{-}CH_3)$); 135.14 (d, 2P, $P(OCH_2\text{-}CH_3)_2$); 135.48 (d, 2P, $P(OCH_2\text{-}CH_3)_2$).

Anal. calc. for $C_{60}H_{120}O_{36}P_{12}Co_4Zr_2$: C, 32.65; H, 5.48; P, 16.84; found: C, 32.68; H, 5.49; P, 17.45.

$[Zr(L_{OEt})_2Cl_2]$

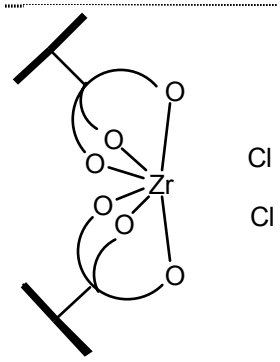

Compound **2**

A THF solution (3mL) of NaL_{OEt} (0.51 g, 0.88 mmol) was added to a THF solution (5 mL) of

$ZrCl_4(THF)_2$ (0.16 g, 0.44 mmol). After filtration, solvents were evaporated under reduced pressure to give a yellow powder. All attempts to purify the product yielded $[Zr(L_{OEt})_2Cl_2]$ (**2**), contaminated with the rearranged product **1**. The crude product was thus directly used for the next step.

^{1}H NMR ($CDCl_3$): 1.28 (t, $^3J_{H-H}$=6.80 Hz, 18 H, CH_3); 4.11 (m, 12H, CH_2); 5.20 (s, 5H, Cp).

^{13}C NMR ($CDCl_3$): 17.13 (CH_3); 63.47 (CH_2); 90.95 (Cp).

^{31}P NMR (THF/C_6D_6): 120 (s)

$[Zr(L_{OEt})_2](OTos)_2$

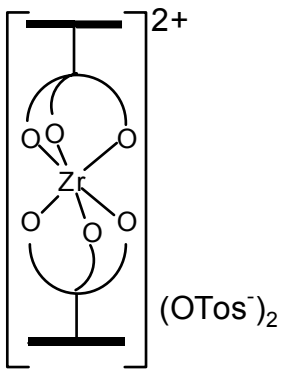

Compound (**3**)$(OTos)_2$

A THF solution (8 mL) of $[Zr(L_{OEt})_2Cl_2]$ (**2**) was treated with two equivalents of AgOTos (0.24 g, 0.88 mmol) in THF (20 mL). The mixture was filtered and the solvent was removed *in vacuo* to give $[Zr(L_{OEt})_2](OTos)_2$ ((**3**)$(OTos)_2$) as a pale yellow powder. Slow diffusion of hexane through a THF solution of (**3**)$(OTos)_2$ affords yellow crystals in 80 % yield (0.53 g, 0.35 mmol).

^{1}H NMR ($CDCl_3$): 1.29 (t, $^3J_{H-H}$=7.2 Hz, 18H, OCH_2-C**H**$_3$); 2.31 (s, 3H, arom. CC**H**$_3$); 4.11 (m, 12H, OC**H**$_2$-CH_3); 5.28 (s, 5H, Cp); 7.09 (d, $^3J_{H-H}$=8.08 Hz, 2H, arom. CH); 7.81 (d, 2H, arom. CH).

^{13}C NMR ($CDCl_3$): 17.14, 17.17 (**C**H_3-CH_2O); 21.94 (arom. C**C**H_3); 63.67 (CH_3-**C**H_2O);

91.35 (Cp); 126.94, 128.95 (arom. C).

^{31}P NMR ($CDCl_3$): 123 (s).

Anal. calc. for $C_{48}H_{84}O_{24}P_6S_2Co_2Zr$: C, 38.33; H, 5.63; found: C, 37.35; H, 5.64.

[Zr(L_{OEt})Cl_3]

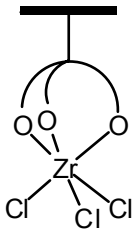

Compound **4**

A THF solution (2 mL) of NaL_{OEt} (0.20 g, 0.35 mmol) and $CpZrCl_3$ (0.09 g, 0.35 mmol) in THF (6 mL) were mixed and stirred at r.t. for 10 min. After filtration, solvents were evaporated *in vacuo* to give of a yellow solid. The crude product was washed with hexane and recrystallized by adding C_6H_6 to a CH_2Cl_2 solution of [Zr(L_{OEt})Cl_3] (**4**) (0.18 g, 0.24 mmol, 70%).

^{1}H NMR ($CDCl_3$): 1.32 (t, $^3J_{H-H}$=6.98 Hz, 18H, C**H**$_3$-CH_2O); 4.20 (m, 12H, CH_3-C**H**$_2$O); 5.18 (s, 5H, Cp).

^{13}C NMR ($CDCl_3$): 17.15 (CH_3); 64.06 (CH_2); 90.73 (Cp).

^{31}P NMR ($CDCl_3$): 122 (s); (THF d_8): 119 (s).

Anal. calc. for $C_{17}H_{35}Cl_3O_9P_3CoZr$ (+ 0.5 C_6D_6 + 1 H_2O): C, 30.29; H, 5.46; found: C, 30.09; H, 6.29.

EI (m/z): 64 (M^+).

[Zr(L_{Et})$_2$]Cl_2

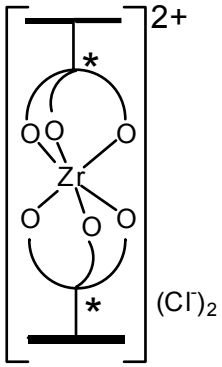

Compound (**5**)Cl_2

A THF solution (3 mL) of NaL_{Et} (0.25 g, 0.52 mmol) was added to a THF solution (5 mL) of $[ZrCl_4(THF)_2]$ (0.10 g, 0.26 mmol). After 5 min of stirring the solution was filtered and evaporated *in vacuo*. The residue was then placed in a Soxhlet extractor and extracted under N_2 with CH_2Cl_2, affording yellow crystals suitable for X-ray analysis in 75 % yield (0.20 g, 0.19 mmol).

^1H NMR ($CDCl_3$): 1.18 (m, 18H, CH_3); 1.99 (m, 6H, CH_2); 2.24 (m, 6H, CH_2); 5.02 (s, 5H, Cp).

^{13}C NMR ($CDCl_3$): 8.73 (CH_3); 31.95 (CH_2); 88.18 (Cp).

^{31}P NMR (CH_2Cl_2/C_6D_6): 136 (s).

Anal. calc. for $C_{34}H_{70}Cl_2O_6P_6Co_2Zr$ (+ CH_2Cl_2): C, 37.30; H, 6.40; found: C, 36.90; H, 6.2.

EI (m/z): 64 (M^+).

5 X-ray Crystallography

5.1 Structure determination

X-ray diffraction data for **1**, (**3**)$(OTos)_2$ and (**5**)Cl_2 were collected on a Siemens SMART CCD diffractometer [61] at low temperature using monochromatized graphite Mo-Kα radiation (0.71073 Å). The relevant structure determination parameters are summarized in Table 1.5. A complete hemisphere of data was scanned on ω□0.3° with a run time of 20 or 60 sec. (unless otherwise stated) at the detector resolution of 512X512 pixels and a detector distance of 5.18 cm (for compounds **1** and (**5**)Cl_2) and 5.93 cm (compound (**3**)$(OTos)_2$). A total of 1271 frames were collected for each data set. Cell constants were obtained from forty-five 60 sec. frames. The collected frames were processed with the SAINT program [62] that automatically performs Lorentz and polarization corrections. Empirical absorption corrections were made using the XPREP program from the SHELXTL [63] software.

The Data collection for compound **4** was carried out at 160K on a Stoe IPDS system equipped with MoKαradiation. Two hundred images with Δϕ□1° were exposed during four min each. The image plate was set to 80mm, which resulted in a maximum 2θ of 48.4°. Reflection profiles varied from 9 to 21 pixels and the effective mosaic spread was 0.009. An inspection of reciprocal space ascertained the diffraction figure to be exceptionally pure and to correspond to the cell given in Table 1.5. The crystal was bounded by {010} and {001} pinacoids and a {110} prism; a numerical absorption correction yielded an agreement factor for equivalent intensities of 0.0311 and transmission factors between 0.6411 and 0.7562. The intensities were further corrected for Lorentz and polarization effects.

All structures were solved by direct methods and the refinement was done by full matrix least square of F^2 using SHELXL96 [64] (beta-test version). All non-hydrogen atoms were refined anisotropically while hydrogen atoms (for compounds **1** and (**5**)Cl_2), included at calculated positions, were refined in the riding model with group atomic displacement

parameters. For compounds (**3**)$(OTos)_2$ and **4**, the hydrogens were kept riding on their associated carbon atoms and their isotropic displacement parameters were set to 1.2 or 1.5 times the U_{eq} of their associated carbons. Weights used were $[\sigma^2(F_o)^2]^{-1}$.

The slightly elevated residual densities and R_{int} value for **1** are a result of a poor quality crystal with disordered ethyl group. To avoid that we tried different crystals at different temperatures without any success. But in our view the accuracy of the stucture determination does not significantly detract from the reality.

5.2 Crystallographic data

The crystallographic data of all compounds are summarized in Table 1.5.

Table 1.5 Summary of the crystallographic data for compounds **1** and (**3**)$(OTos)_2$.

Compound	**1**	(**3**)$(OTos)_2$
Formula	$C_{60}H_{120}Co_4O_{36}P_{12}Zr_2$	$C_{48}H_{84}Co_2O_{24}P_6S_2Zr$
Formula weight	2207.36	1504.22
Crystal system	monoclinic	triclinic
Space group	$P2_1/n$	$P\bar{1}$
a, Å	12.569(2)	13.857(5)
b, Å	22.170(5)	15.254(5)
c, Å	16.279(3)	17.875(5)
α, deg		78.303(5)
β, deg	94.11(1)	77.686(5)
γ, deg		64.709(5)
V, $Å^3$	4524.6(1)	3311(2)
Z	2	2
ρ_{calcd}, mg/m^3	1.620	1.527
μ, mm^{-1}	1.230	0.937
F(000)	2272	1572
Crystal size, mm	0.08 x 0.10 x 0.10	0.09 x 0.22 x 0.30
T, K	203(2)	190(2)
Exposure time/sec	60	60
Scan range, deg	$1.55 < \theta < 26.56$	$1.49 < \theta < 25.55$
Total no. of data	10418	13859
no. of unique obsd data	7308	10142
no. of variables	604	752
Goodness-of-fit	1.202	2.822
R(int)	0.0896	0.0271
Final R_1[a] $[I>2\sigma(I)]$	0.0984	0.0449
Final wR_2[b] (all data)	0.2781	0.1026
Max resid density, e $Å^{-3}$	1.745 and -1.057	0.910 and -0.548

[a]$R_1 = \Sigma||F_o| - |F_c||/\Sigma|F_o|$. [b]$wR_2(F_o^2) = \{\Sigma[w(F_o^2 - F_c^2)^2]/\Sigma[w(F_o^2)]\}$. $w = 1/[\sigma^2(F_o^2) + P^2 + P]$ where $P = (F_o^2 + 2F_c^2)/3$

Table 1.5 Summary of the crystallographic data for compounds **4** and (**5**)Cl_2.

Compound	**4**	(**5**)Cl_2
Formula	$C_{20}H_{38}Cl_3CoO_9P_3Zr$	$C_{34}H_{70}Cl_2Co_2O_6P_6Zr \cdot 2\ CH_2Cl_2$
Formula weight	771.91	1210.62
Crystal system	monoclinic	triclinic
Space group	$P2_1/n$	$P\bar{1}$
a, Å	10.752(2)	10.7538(5)
b, Å	16.255(3)	10.9314(5)
c, Å	18.561(4)	13.6390(5)
α, deg		97.496(1)
β, deg	102.93(3)	104.689(1)
γ, deg		99.350(1)
V, Å^3	3162(1)	1505.4(1)
Z	4	1
ρ_{calcd}, mg/m^3	1.622	1.523
μ, mm^{-1}	1.302	1.356
F(000)	1572	708
Crystal size, mm	0.22 x 0.22 x 0.09	0.09 x 0.18 x 0.40
T, K	180(2)	200(2)
Exposure time/sec		20
Scan range, deg	$1.68 < \theta < 23.90$	$1.57 < \theta < 26.58$
Total no. of data	19311	7681
no. of unique obsd data	4769	5483
no. of variables	335	326
Goodness-of-fit	4.309	1.099
R(int)	0.0311	0.0284
Final R_1[a] [I>2σ(I)]	0.0290	0.0377
Final wR_2[b] (all data)	0.0625	0.0955
Max resid density, e Å^{-3}	0.506 and -0.466	0.829 and -0.671

[a]$R_1 = \Sigma||F_o| - |F_c||/\Sigma|F_o|$. [b]$wR_2(F_o^2) = \{\Sigma[w(F_o^2 - F_c^2)^2]/\Sigma\ [w(F_o^2)]\}$. $w = 1/[\sigma^2(F_o^2) + P^2 + P]$ where $P = (F_o^2 + 2F_c^2)/3$

6 References

EN.REFLIST

Part 2 :

Design and Synthesis of Compartmental Ligands and their Complexes for the Production of Catalytic Antibodies

1 Introduction

1.1 Monoclonal antibodies: background and principles

The immunosystem develops antibodies (also called immunoproteins or immunoglobulins) to protect organisms against external substances, the antigens, that are recognized as nonself. The antibodies recognize the antigen, form aggregates with it, and so prevent it from harming to the organism. The specific affinity of the antibody is not raised against the entire macromolecule but only against a defined site of the antigen called the epitope. A large variety of antigens can ellicit an immunoresponse, and a variety of antibodies are synthesized against any single antigen.

Antibodies are secreted by plasma cells, which are derived from B lymphocytes (B cells). Once stimulated *in vivo*, B lymphocytes undergo a process of proliferation, differenciation and maturation. Identical cells producing one type of antibody that arise from one unique cell are said to be monoclonal.

There are five different classes of immunoglobulins: IgA, IgD, IgE, IgG and IgM. Immunoglobulin G is a Y shaped protein which consists of two light (L) and two heavy (H) protein chains joined by disulfide linkages. Each light chain (and each heavy chain) is made up of several domains and consists of two homologous units, V_L and C_L (V_H and C_H for the heavy chain) where V and C indicate the polypeptide chain's variable and constant regions (Figure 2.1). The antigen-binding site is formed at the ends of the arms of the Y, where a heavy chain variable domain (V_H) and a light chain variable domain (V_L) come close together [1,2].

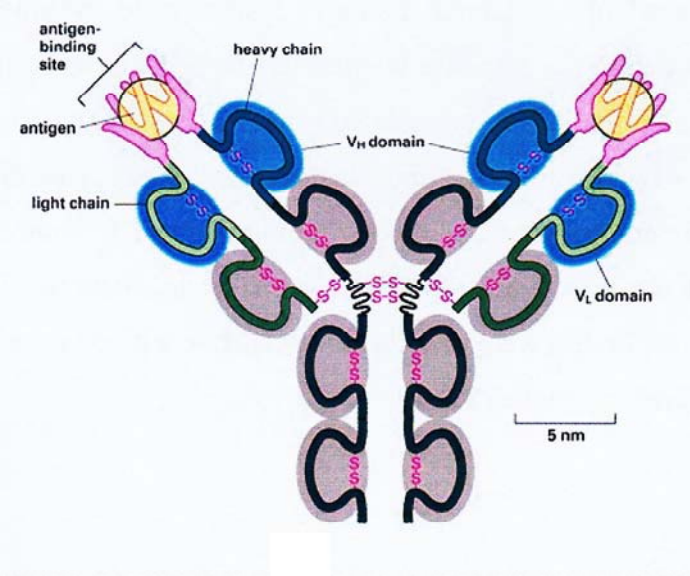

Figure 2.1 Schematic drawing of an IgG molecule [3].

Antibody diversity is generated by several different mechanisms [4]. Genetic information for this diversity is contained in more than 1000 small segments of DNA. There is a multitude of possibilities to join these segments together and to form the heavy and light chains. Consequently, it has been estimated that at least 90000 different heavy chains and 3000 different light chains can be produced. Almost any heavy chain can combine with almost any light chain to produce a functional antibody. The number of different antibody molecules a new B cell can choose from this combinatorial association is increased to 3000 X 90000 = 270 milllion. Moreover, because in mature B cells point mutation can be introduced for the variable domains, the actual number of antibody molecules with different antigen binding sites is several orders of magnitude higher.

1.2 Catalytic antibodies: basic concepts

Enzymatic catalysis was defined by Haldane [5] and later by Pauling [6,7] as the selective binding to a transition state. The fundamental processes that determine binding in enzymes and antibodies are the same. The only difference between the actions of enzymes and antibodies is that whereas enzymes bind most readily to high-energy activated states, antibodies bind to low-energy structures.

This led Jencks to propose in 1969 that an antibody designed to recognize a stable transition state analog of a chemical reaction might catalyze this latter. The combining sites of an antibody are complementary to the transition state and accelerate the reaction by forcing bound substrates to resemble the transition state [8].

It was not until 1986 that Lerner and Schultz independently demonstrated this long standing hypothesis [9,10]. Both groups isolated catalytic antibodies with hydrolase activity from immunizations with haptens containing a phosphonate and a phosphate group respectively as stable analogs for the tetrahedral intermediate involved in the hydrolysis of the ester linkage, see Figure 2.2. It was the first example of a catalytic antibody specific for a transition state analog and numerous factors were considered in designing it. First, esters undergo important structural and electronic changes during the reaction from substrate to product. This facilitates differential binding and stabilization of the transition state. Second, hydrolytic reactions of this type do not necessarily require active side chains and can occur by simple polarization of the carbonyl group concurrent with the delivery of water.

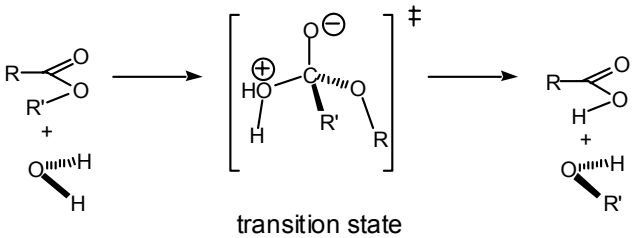

transition state

(a)

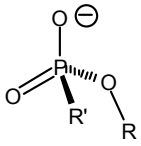

stable transition state analog (hapten)

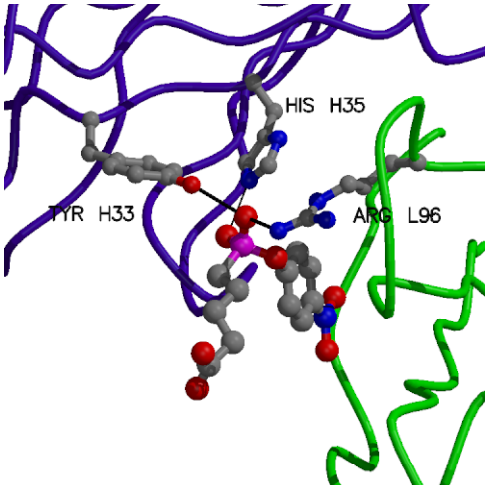

(b)

Figure 2.2 Immunization with a stable transition state analog for a given reaction yields antibodies which may display catalytic activity for this reaction (a) as they are combinatorially optimized to stabilize the transition state analog (b).

In recent years, X-ray structural characterization of several transition state analogs-catalytic antibodies has greatly contributed to the understanding of the weak interactions which participate to the stabilization of the host-guest complex (i.e. the protein-transition state (analog)). The X-ray structure of the phosphonate transition state analog-catalytic antibody complex is presented in Figure 2.2.b. As can be appreciated, the protein forms a *well defined active site* which is exquisitely tailored to accommodate and thus stabilize the transition state (analog) by means of weak interactions [11].

1.3 Production of monoclonal catalytic antibodies

Haptens are usually small molecules that cover a range of natural and synthetic molecules. Molecular size plays an important role in eliciting the immune response. Low molecular weight antigens (less than 1 kDa) are not good immunogens. Nethertheless, it is possible to generate antibodies against substances that are not antigenic by coupling them onto a strongly immunogenic carrier protein, like Keyhole Limpet Haemocyanin (KLH).

A catalytic antibody for a given reaction (an ester hydrolysis in this case) is made by injecting a transition state analog (a) coupled to the carrier protein into an experimental animal (typically a mouse) (Figure 2.3). Spleen cells are taken from the animal and fused with myeloma cells, which are cancerous cells derived from the immune system and have the property of infinite life *in vitro* without interfering with the property of producing antibodies. The resulting fused cells, called hybridoma cells, divide indefinitely, making it possible to obtain clones of cells, each hybrid clone secreting a monoclonal antibody that has unique binding pocket. After selection, antibody specific to the transition state analog is isolated. This antibody may also be capable of binding to the transition state itself (b) and thereby catalyzing the reaction [12].

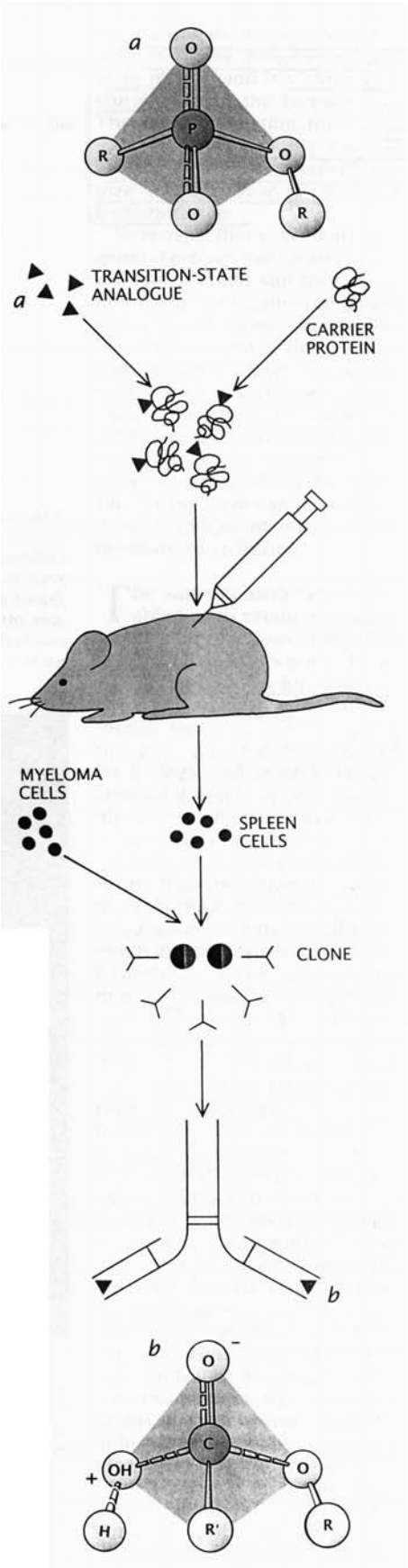

Figure 2.3 Production of monoclonal antibodies [12].

1.4 Catalytic antibodies in organic synthesis

In the past fifteen years, the field of catalytic antibodies has considerably expanded, producing hundreds of novel catalytic antibodies for a wide variety of organic transformations [13-15]. Catalytic antibodies with either (*R*) or (*S*) substrate specificity are used in kinetic resolution processes [16-18]. They are used in disfavored chemical reactions [19] and they are also valuable catalysts in asymmetric reactions [20,21]. Reymond et *al.* provided evidence of how an antibody could catalyze the carbon protonation of a prochiral enol ether (Scheme 2.1) [22].

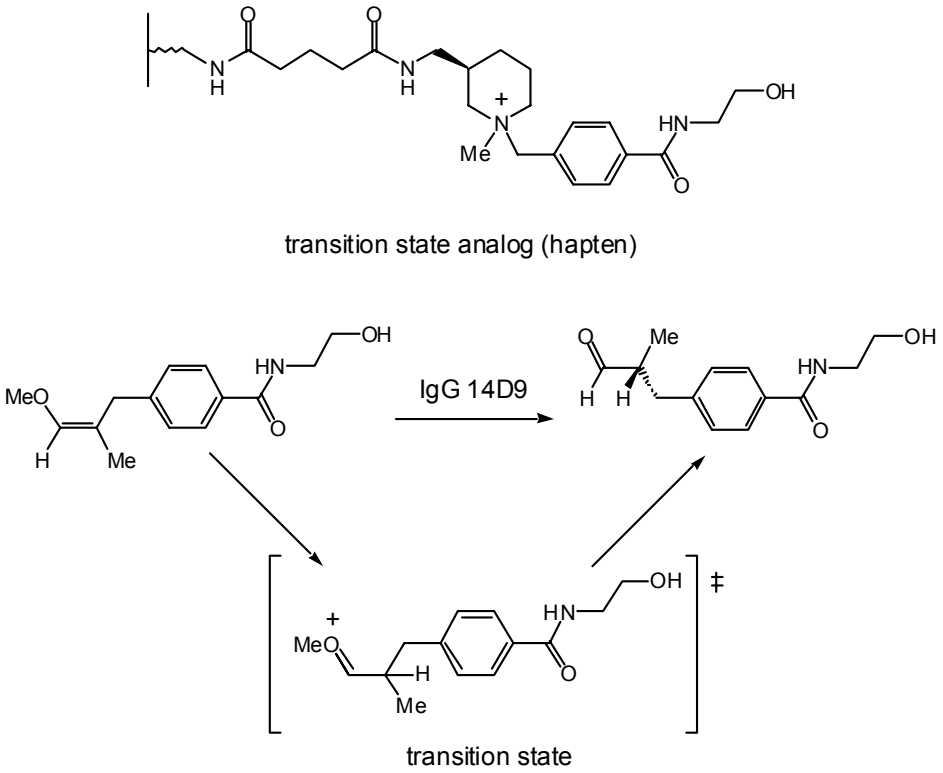

Scheme 2.1 Antibody 14D9 obtained from immunization with N-methylpiperidinium salt as hapten catalyzes enantioselective hydrolysis of the ester.

The N-methylpiperidinium salt used to generate antibodies can be expected to induce carboxyl groups into the antibody binding pocket. These groups should be in an optimal position to stabilize the oxo carbenium ion and furthermore assist the carbon protonation of

enol ethers. Moreover, binding interactions to the tetrahedral ammonium center of hapten can also induce a geometry in the antibody combining site. This favors the pyramidalization of the trigonal carbon undergoing protonation. The antibody 14D9 obtained after immunization was found to not only catalyze the hydrolysis of the enol ether but also to provide the product with a good enantiomeric excess.

Catalytic antibodies have now been induced with haptens that are designed to use a number of different strategies for effecting catalysis: distortion, charge stabilization and proximity have all been used to advantage [23]. Selective recognition of antigens is achieved through interactions similar to those involved in enzyme-substrate binding, and include van der Waals interactions, hydrogen bonding and other electrostatic and hydrophobic effects. The antibody can use an ensemble of weak interactions to bind its antigen with adequate affinity.

To date, most of the effort has focused primarily on organic transition state analogs, with perhaps an "exotic" element (Si, S, P) present to mimic a transition state geometry for carbon. In comparison, catalytic antibodies that incorporate transition metal ions have received much less attention although a few reports exist on porphyrin-containing catalytic antibodies [24-31]. Schwabacher et *al.* isolated antibodies from immunization with either Fe^{3+} or Co^{3+} porphyrin complexes illustrated in Figure 2.4 [32].

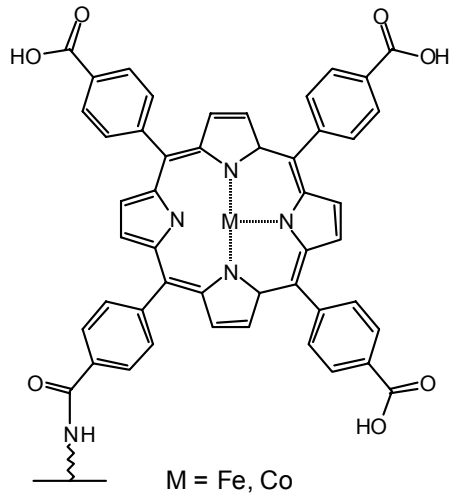

Figure 2.4 Antibodies elicited against metal porphyrin complex were isolated by the Schwabacher's group.

Latter the Schultz group reported an antibody-catalyzed porphyrin metallation reaction [33]. In their strategy, antibodies were elicited by a distorted N-methyl porphyrin hapten supposed to mimic the transition state for porphyrin metallation. They obtained antibodies which could catalyze Zn^{2+} and Cu^{2+} insertion into a porphyrin chelate.

Moreover, many enzymes use nonamino acid cofactors (such as nicotinamides, flavins and heme units) to catalyse reactions. Antibodies can also incorporate cofactors into their active site to expand the types of their antibody-catalyzed reactions. A strategy to introduce cofactors into an antibody's combining site has been reported by Janda et co-workers (Scheme 2.2) [35].

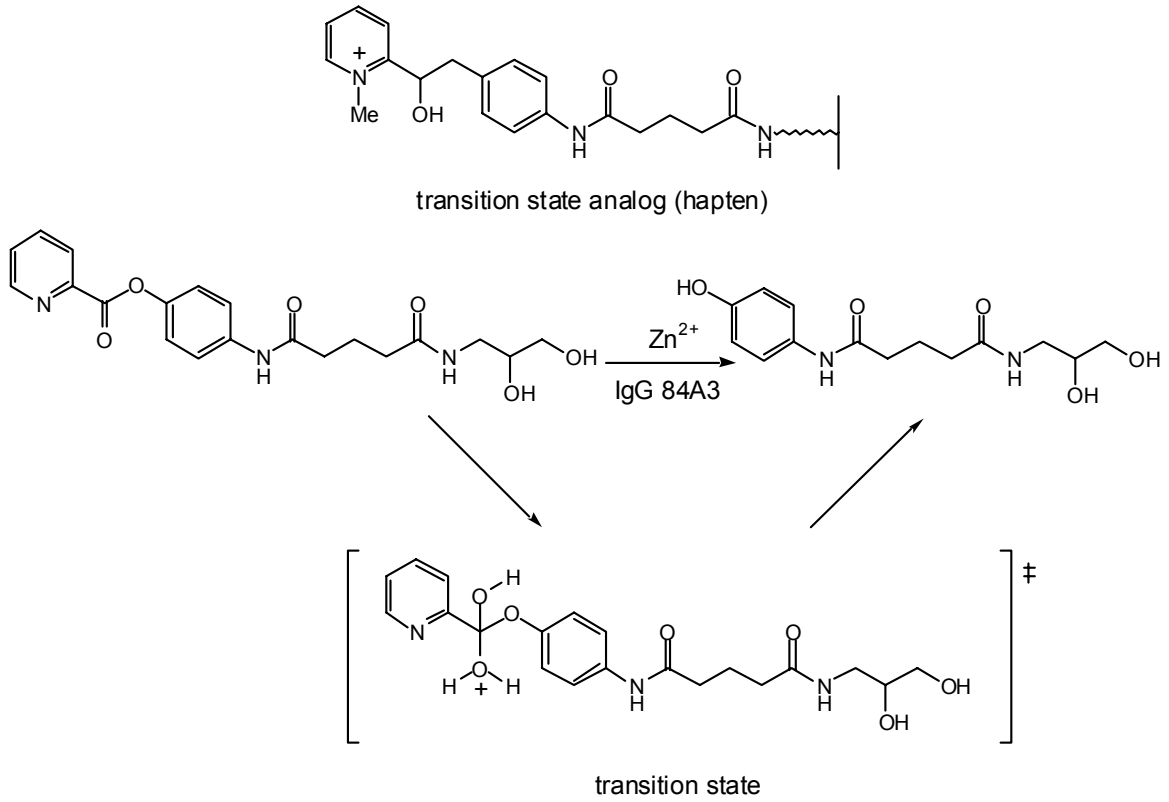

Scheme 2.2 The antibody 84A3, obtained from immunization using pyridium salt as hapten, catalyzes the hydrolysis of the ester in the presence of Zn^{2+} as cofactor.

Using a "bait and switch approach" (in this terminology, the hapten serves as "bait" for attracting catalytic functions in the induction of the antibody; it is then "switched" for the

substrat [34]), they elicited antibodies, from a pyridinium salt as analog of the transition state, capable of catalyzing the hydrolysis of an ester. The antibody reaction is metal-ion dependent and specific, actually only Zn^{2+} functions as a cofactor.

A monoclonal antibody, elicited against a water soluble tin (IV) porphyrin containing an axial α-naphtoxy ligand, binds a ruthenium porphyrin cofactor to form a novel catalytic assembly that catalyzes the enantioselective oxidation of aromatic sulfides to sulfoxides [36]. Monoclonal antibodies directed towards mercuric ions have also been elicited by immunization with a glutathione-Hg derivative and they have been used to detect mercuric ions in aqueous samples [37,38].

Recently, Meares et *al* have isolated antibodies with infinite affinity by preventing the dissociation of the hapten from the antibody [39]. They have demonstrated that the S95C Fab, which is a mutant of the antibody CHA255 (antibody which possesses high affinity for (*S*)-benzyl-EDTA-indium chelates [40]), binds covalently to an EDTA-In complex called AABE-In (Figure 2.5).

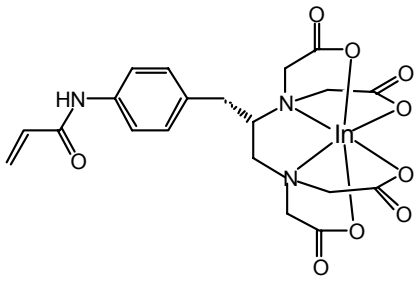

Figure 2.5 (*S*)-1-p-acrylamidobenzyl-EDTA-indium (AABE-In) binds covalently to the S95C Fab antibody.

1.5 Metalloenzymes as models for hapten design

Many enzymes contain a metallic center (a metallobiosite) that is essential for catalysis. These are called metalloenzymes [41]. It has been estimated that approximately one third of all enzymes require a metal ions (other than sodium) as coenzymes for their catalytic activity [42]. The most famous example of a mononuclear metal complex acting as coenzyme is maybe the coenzyme B_{12} (5'-deoxyadenosylcobaltamin) (Figure 2.6). It serves as a cofactor in various enzymatic rections (reactions catalyzed by glutamate mutase, diol dehydrase and ethanolamine ammmonia lyase for example) in which an hydrogen atom is interchanged with a substituent on an adjacent carbon atom [43,44].

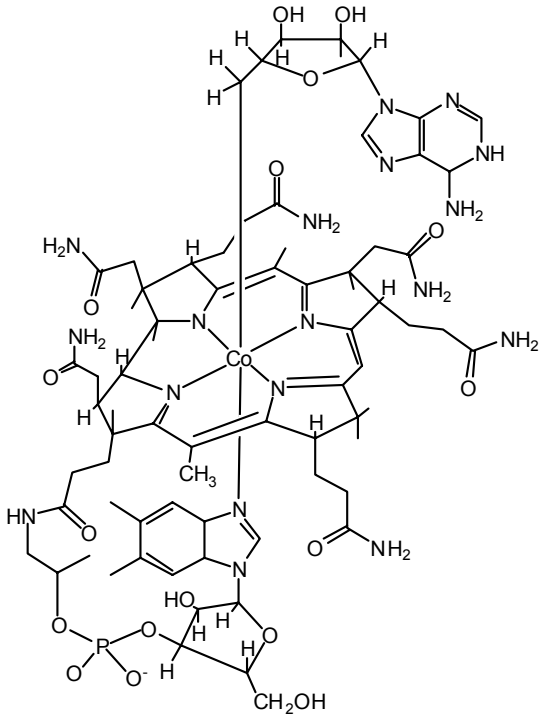

Figure 2.6 Coenzyme B_{12}.

In enzymes which possess a bimetallic center, the two metals work more or less independently [41]. They are required for distinct functions either structural or catalytic, and they can catalyze different steps in a multistep sequence. Heterobimetallic centers appear to employ the two metals in different functions and homobimetallic centers can operate together as a unit to enable stabilization of transition states involving concerted steps such as nucleophilic ligand substitution reactions.

Carboxylate-bridged non-heme diiron active sites have emerged in the past decade as a

new common structural motif for an increasing number of metalloproteins that bind and/or activate dioxygen [45-48]. The proteins belonging to this class include: the invertabrate respiratory protein hemerythrin (Hr) [49-51] as well as the hydroxylase component of methane monooxygenase (MMOH) [52-56] found in a methanotrophic bacteria (Figure 2.7). Hemerythrin binds the dioxygen and transports it whereas methane monooxygenase activate dioxygen and includes it in the selective oxidation of methane to methanol.

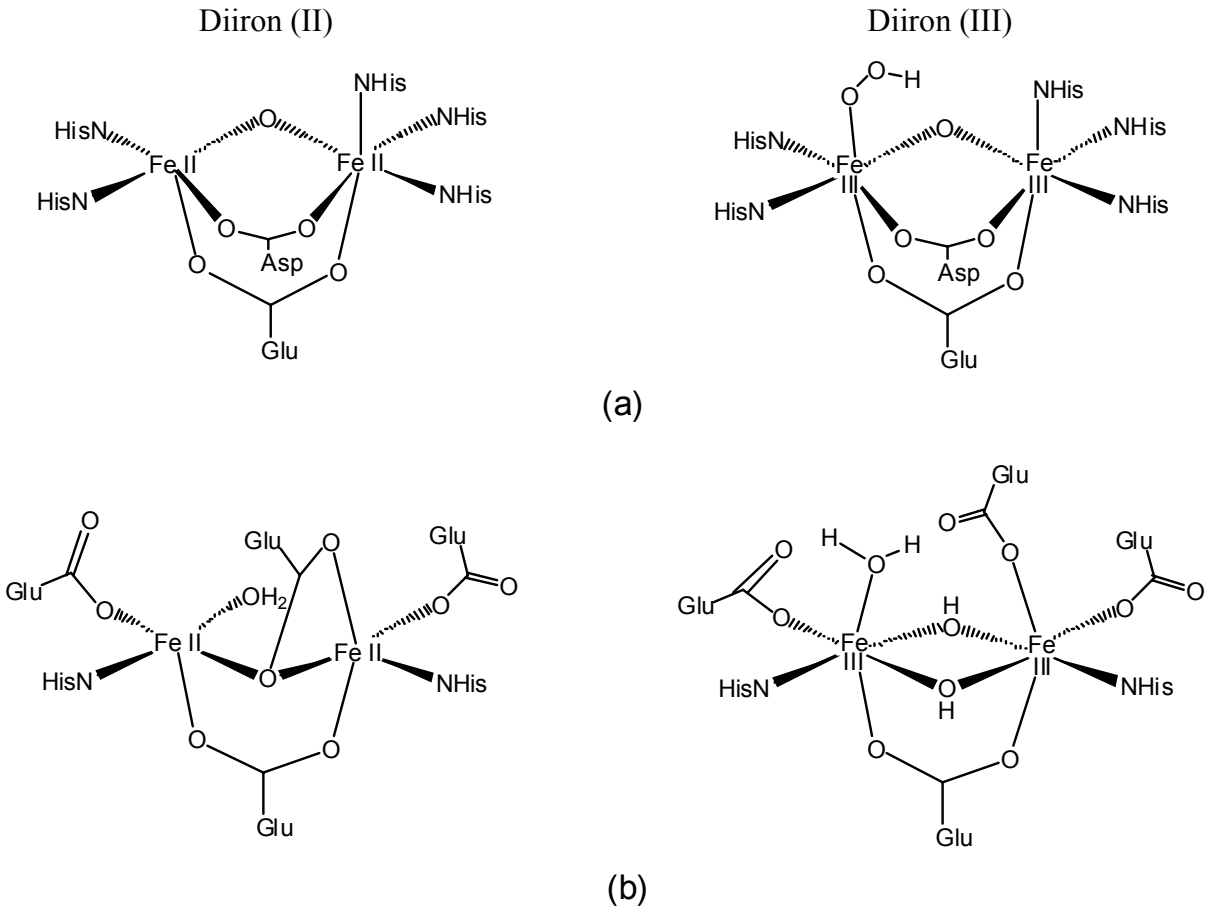

Figure 2.7 Non-heme diiron actives sites of hemerythrin (a) and methane monooxygenase hydroxylase component (b).

Despite the broad interest in carboxylate-bridged bimetallic activation of small molecules [41,42], we are not aware of any attempt of eliciting an immune response with a bimetallic hapten. And to our knowledge, no dinuclear metal complex-coenzyme has ever been incorporated in a catalytic antibody.

This part reports the design, synthesis and characterization of dinuclear transition-state analogs for the production of catalytic antibodies as well as coenzymes for subsequent incorporation into the resulting host proteins.

2 Hapten- and coenzyme design

The lack of precise knowledge concerning the transition-state geometry of transition metal-catalyzed reactions renders the rational design of a transition-state analog (hapten) difficult. To circumvent this problem, we rely on our knowledge of metalloenzyme mimics, which are known to promote or catalyze certain reactions even in the absence of proteins.

Over the years, the Robson compartmental ligand and its derivatives have proven versatile for the activation of small molecules as well as for the modelling of the active-site of various metalloenzymes [57-59]. The template condensation of the ligand itself suggests that such systems are capable of hydroxylating aromatic substrates (Scheme 2.3).

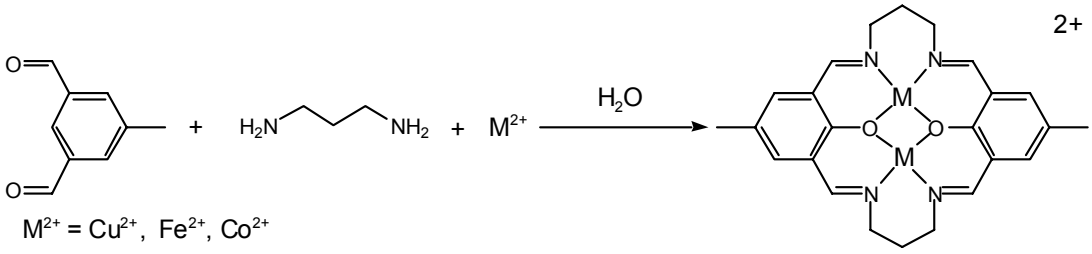

Scheme 2.3 Template synthesis of a Robson-type compartmental ligand via the hydroxylation of the aromatic moieties.

Furthermore, we speculated that the presence of two phenyl moieties in a hapten may be strongly immunogenic, potentially forming a precise "imprint" for later recognition of the coenzyme and for delivering an aromatic substrate to be functionalized (e.g. hydroxylated) during catalysis.

In addition to their thermodynamic stability and inertness, indispensible criteria for immunization purposes, Robson-type complexes are known to possess catalytic- or stoechiometric activity in various biologically relevant transformations, including catalase [60-65], catecholase [66-69] as well as oxygenase [66,70].

We thus set out to synthesize an inert Robson-type complex as a transition-state analog for the hydroxylation of benzene derivatives. Concerning the coenzymes to be incorporated in the host proteins, catalytically active metals should be incorporated in a *structurally-related but amputated ligand* thus allowing substrate (i.e. benzene) activation and functionalization. Several features were considered in designing the transition-state analog as well as the coenzyme: a) the appropriate skeleton; b) the metals and the co-ligands which complete the coordination sphere.

a) In order to elicit an immune response, a hapten should be conjugated to a carrier protein, typically keyhole lympet hemocyanin (KLH). For this purpose, either a free carboxylic acid or an amine was remotely anchored to the Robson-ligand. Furthermore, to prevent hydrolysis of the imine functionalities of the Robson ligand, these were reduced to the corresponding secondary amines.

For the coenzymes, one of the phenol moieties of the hapten was amputated, thus yielding an equatorial pentadentate donor ligand. In conjunction with the protein raised against a full ligand, it was speculated that a hydrophobic pocket would favour the approach of an incoming substrate (i.e. an aromatic moiety to be hydroxylated).

It has long been recognized that subtle differences in the coordination environment of iron enzymes play a determining role in the fate of coordinated oxygen. While oxygen-rich environment (such as found in methane monooxygenase) are better suited for dioxygen activation, a nitrogen-rich ligand sphere favours reversible dioxygen coordination (such as in hemerythrin) [41,42]. Thus, both N_4O- and N_2O_3 donor set ligands were synthesized for the coenzymes.

b) In order to allow for O_2 coordination and subsequent activation, a divanadyl moiety was choosen as transition-state analog. On one hand, the vanadyl unit is one of the most stable diatomic moieties. On the other hand, it was speculated that the presence of terminal oxide ligands in the hapten would elicit the presence of hydrogen donors in the active site of the antibody, which could help activate the coordinated dioxygen for subsequent reactions with the organic substrate to be hydroxylated. Due to the pronounced *trans*-effect of the oxo-donors, vanadyl complexes often display a 5+1 geometry, the sixth ligand located *trans* to the oxo being weakly bound. It was speculated that these sites may be occupied by a bridging

carboxylate provided by the protein upon immunization (i.e. "bait and switch" catalysis) [10].

The coenzyme should contain *catalytically active* metals coordinated to an amputated ligand. The remaining coordination sites should be occupied by labile ligands, to allow docking on a bridging carboxylate elicited by the divanadyl hapten.

A summary of the design criteria for the hapten and coenzymes is outlined in Scheme 2.4.

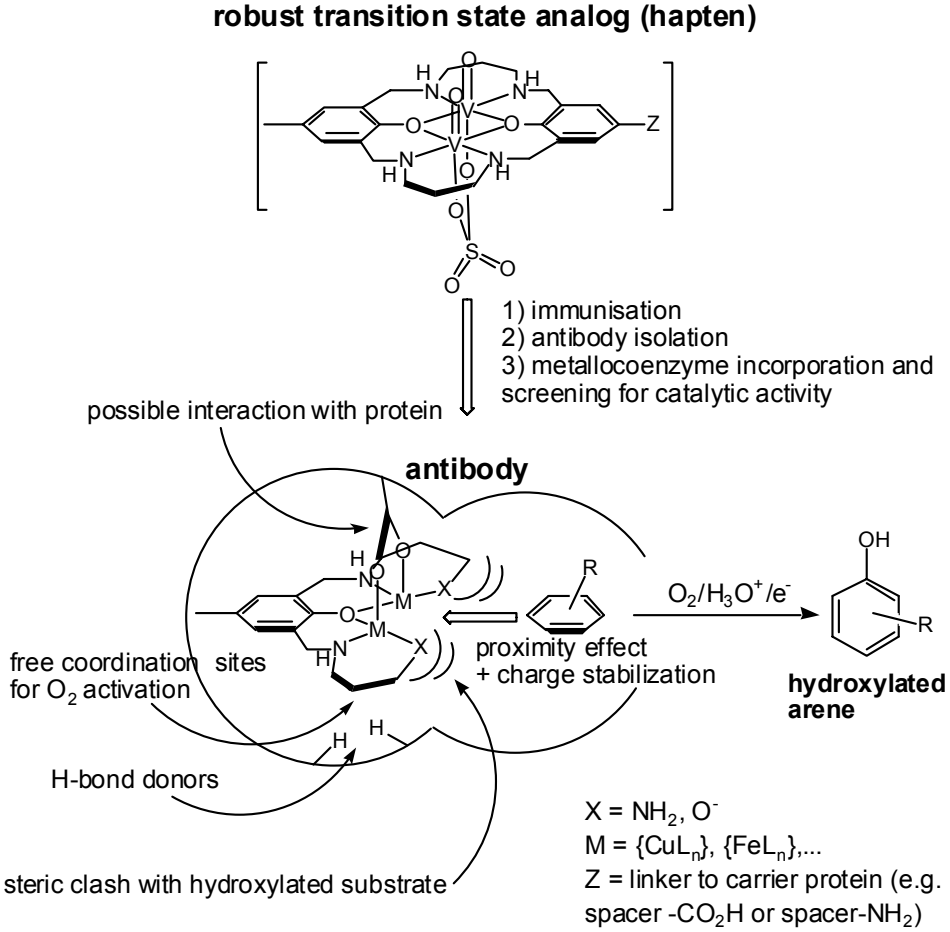

Scheme 2.4 Design of a dinuclear transition-state analog and coenzymes based on compartmental ligands for the production of catalytic antibodies.

3 Hapten synthesis and characterization

3.1 Introduction

Since a hapten must be conjugated to a carrier protein, a reactive functionality (carboxylic acid or amine) was covalently linked via a spacer to one of the aromatic moieties of the compartmental ligand, yielding an asymmetric N_4O_2 hexadentate ligand.

3.2 Synthesis of the aromatic moiety containing the spacer

3.2.1 Synthesis of an aromatic spacer to be bis-hydroxymethylated

Based on a patent describing the synthesis of 3-(3,5-dihydroxymethyl-4-hydroxybenzene)propanoic acid by reaction of 3-(4-hydroxybenzene)propanoic acid in formaldehyde in presence of base [71], we applied this synthesis to its analogs i.e. three or four methylene groups instead of two.

The bis-hydroxymethylated product **1** is obtained from 4-(4-hydroxybenzene)butanoic acid by small modification of the original procedure and subjected to MnO_2 oxidation to afford the dialdehyde product **2** in a modest overall yield (34%) (Scheme 2.5). The bis-hydroxymethylation of 5-(4-hydroxybenzene)pentanoic acid failed. It appears that the introduction of one extra carbon in the chain changes dramatically the reactivity of the substrate. For this reason, another approach was attempted to provide the compartmental ligand.

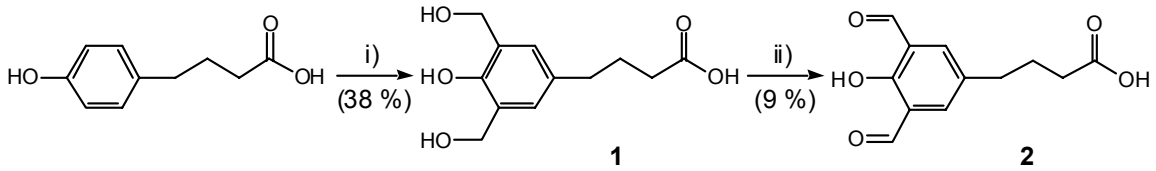

Scheme 2.5 Synthetic route to compound **2**.

i) Formaldehyde (2.5 equiv.), NaOH 5M. ii) MnO_2 (15 equiv.), $CHCl_3$.

3.2.2 Synthesis of an aromatic spacer to be hydroxylated via the Robson's hydroxylation

The reaction between ethyl undecylenate, 9-BBN and 5-bromobenzene-1,3-dicarbaldehyde affords the coupled product 11-(3,5-dicarbaldehydebenzene) ethylundecanoate **3**. Based on the template synthesis of a Robson-type compartmental ligand, which proceeds via hydroxylation of the aromatic moities [58], compound **3** was condensed with 5-methylbenzene-1,3-dicarbaldehyde, 1,3-diaminopropane and various M^{2+} salts (M= Cu, Ni or Zn) in alcoholic solvants (MeOH or i-PrOH) (Scheme 2.6). The colored powder generally obtained after these reactions was submitted to several characterization methods (UV-Vis, IR, MS). Recrystallization attempts were also undertaken. Despite all efforts, no unambiguous proof of the formation of the dinuclear complex **4** was obtained. Another approach was thus undertaken.

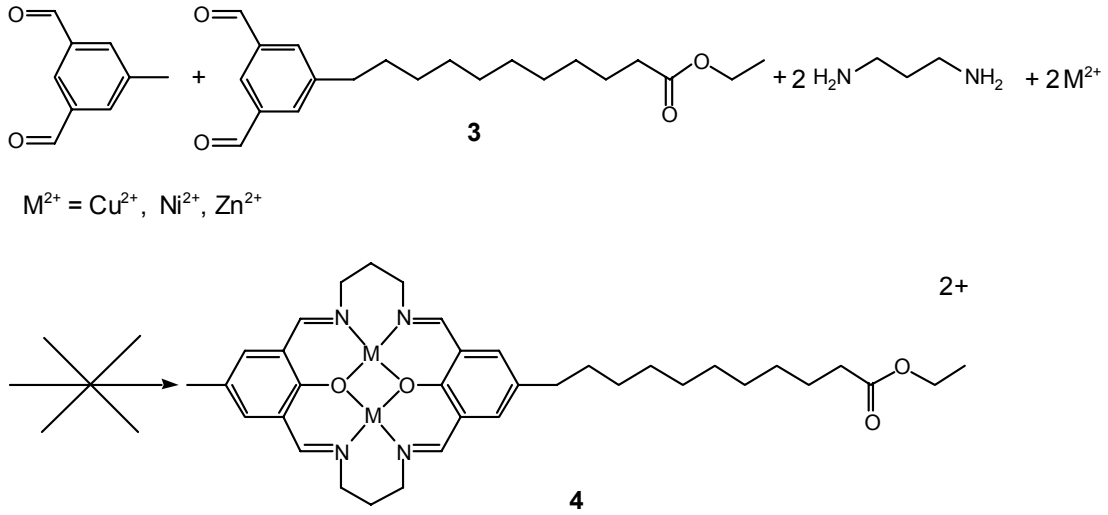

Scheme 2.6 Synthetic route for the synthesis of an asymmetric compartmental ligand

according to Robson's hydroxylation.

3.2.3 Synthesis of a spacer with a reactive functionality (carboxylic acid or amine) to be linked to the aromatic moiety

In this approach, the spacer with a reactive functionality (carboxylic acid or amine) was synthesized and subsequently linked via a C-C bond to the aromatic moiety. The synthetic routes are described in Schemes 2.7 and 2.8.

In the case of spacer with the acid functionality, the coupling step was performed by means of palladium-catalyzed coupling between alkyne **6** and the MOM-protected bromophenol **5**. Deprotection of the coupled product **7** was possible only by addition of stoechiometric amounts of NaI under acidic conditions to afford phenol **8** (Scheme 2.7).

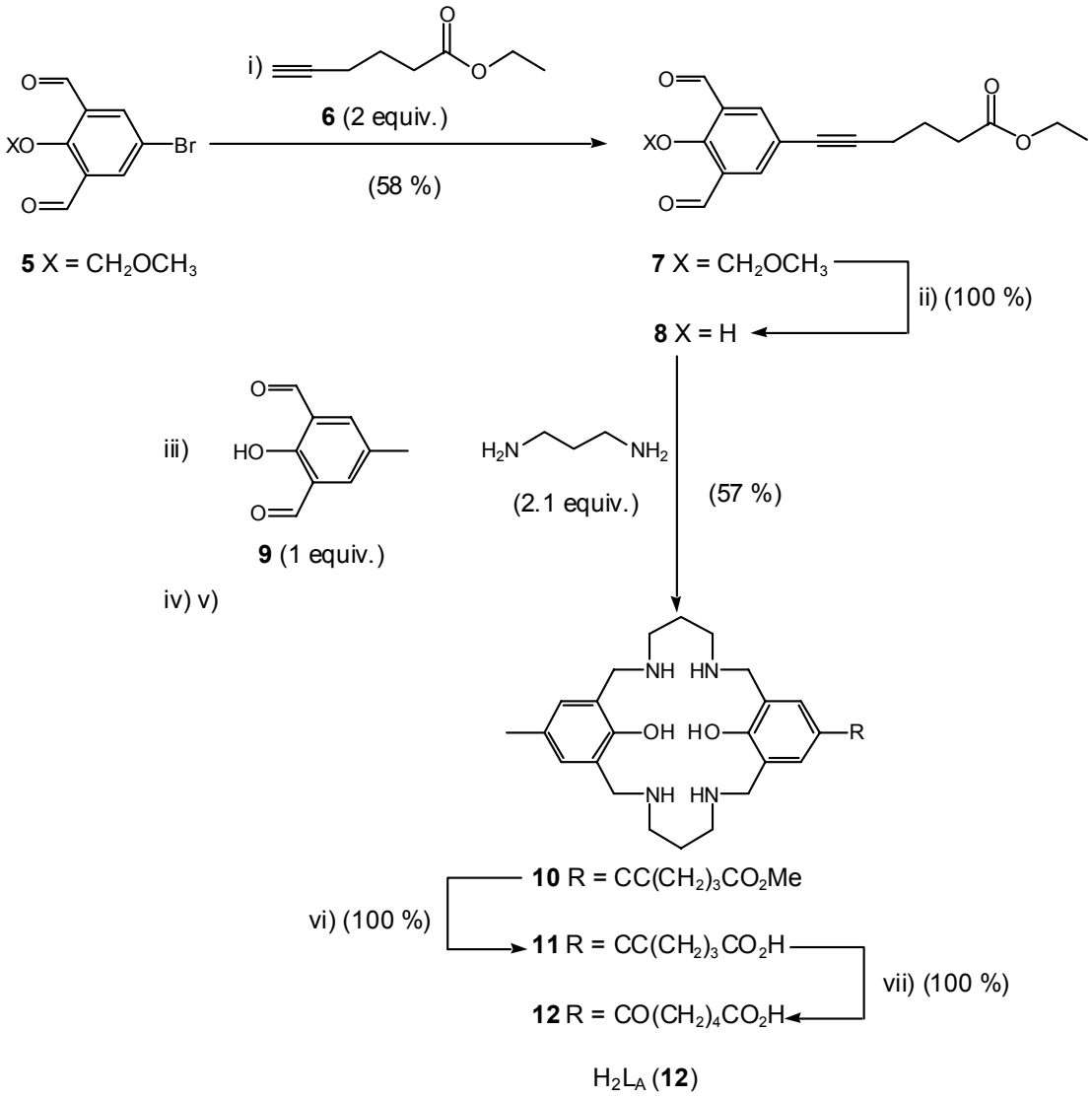

Scheme 2.7 Synthesis of ligand H_2L_A (**12**).

i) $Pd(PPh_3)_4$ (0.04 equiv.), CuI (0.05 equiv.), THF, piperidine, reflux. ii) NaI (1 equiv.), cat. HCl, acetone, 50˚C. iii) $Pb(OAc)_2 \cdot 3H_2O$ (1 equiv.), $Pb(NO_3)_2$ (1 equiv.), MeOH, DMF, reflux. iv) $NaBH_4$, MeOH, r.t. v) MeOH, H_2SO_4 (8M), r.t. vi) LiOH (20 equiv.), MeOH, H_2O, r.t. vii) MeOH, TFA (10%), r.t.

The synthesis of spacer containing a primary amine for conjugation purposes follows a similar route (Scheme 2.8). Ester **6** was reacted in neat 1,3-diaminopropane to afford the amino-amide **14** which was Boc-protected to afford alkyne **15**. Coupling with MOM-protected bromo-phenol **5** yielded, after deprotection with NaI, the dialdehyde **17**.

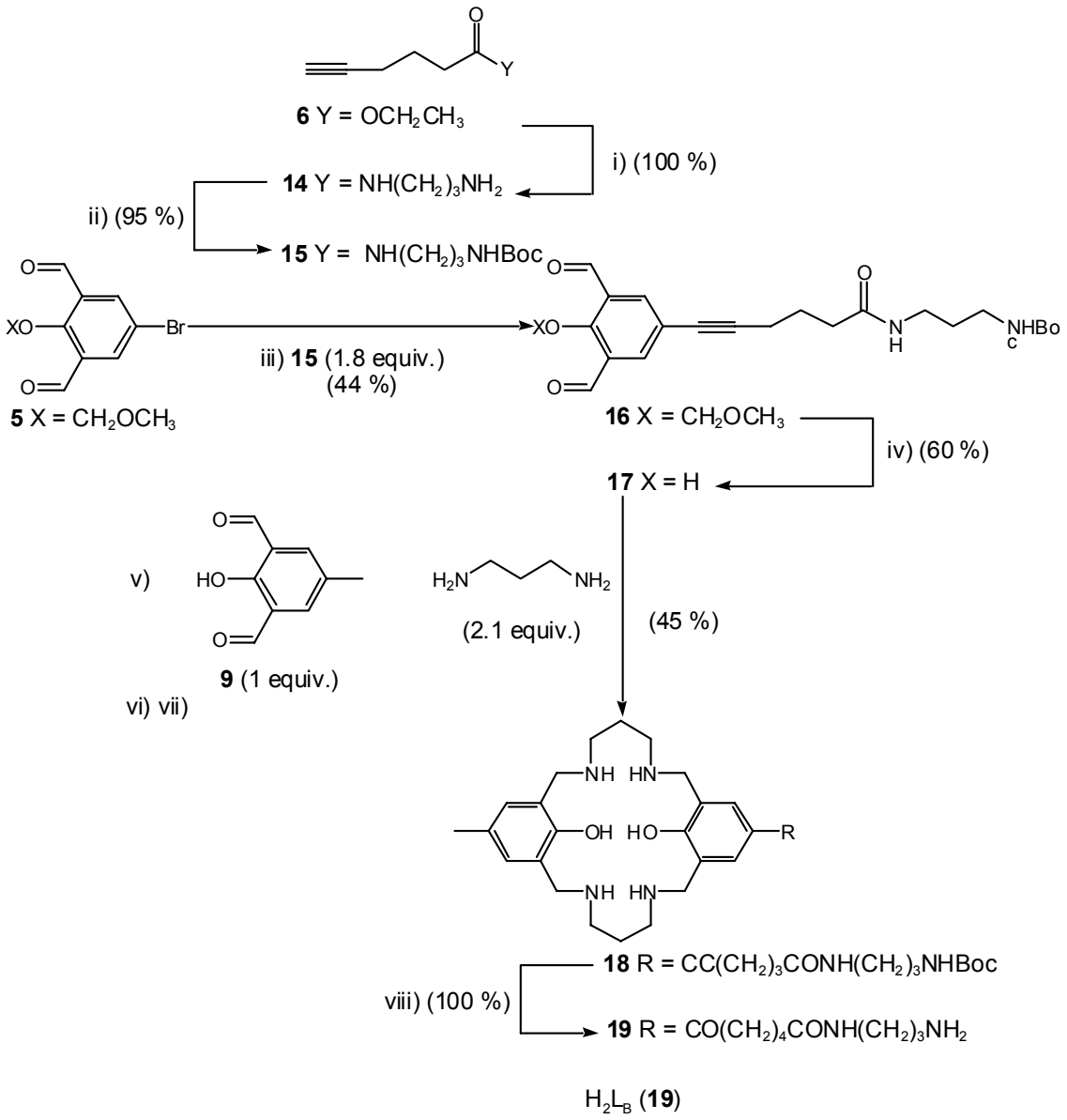

Scheme 2.8 Synthesis of ligand H_2L_B (**19**).

i) Neat 1,3-diaminopropane, 60˚C. ii) $(Boc)_2O$ (1.5 equiv.), dioxane, saturated solution $NaHCO_3$, 0˚C. iii) $PdP(Ph_3)_4$ (0. 04 equiv.), CuI (0.05 equiv.), THF, piperidine, reflux. iv) NaI (1 equiv.), cat. HCl, acetone, 50˚C. v) $Pb(OAc)_2 \cdot 3H_2O$ (1 equiv.), $Pb(NO_3)_2$ (1 equiv.), MeOH, DMF, reflux. vi) $NaBH_4$, MeOH, r.t. vii) MeOH, H_2SO_4 (8M), r.t. viii) TFA (10%), 60˚C.

3.3 Synthesis and purification of the compartmental ligands: H_2L_A (12) and H_2L_B (19)

Template condensation of ester **8** with dialdehyde **9**, 1,3-diaminopropane and lead salts yielded a bright yellow precipitate which could not be solubilized [72]. Therefore, the suspension was reduced by $NaBH_4$ and subsequently acidified with H_2SO_4 to afford a mixture of the three free ligands, including the asymmetric compartmental ligand **10**. Reversed-Phase High Performance Liquid Chromatography (RPHPLC) using an H_2O/CH_3CN (TFA 0.1%) gradient elution allowed separation of all three compartmental ligands resulting from the cross-condensation of both aldehydes. The ^{1}H-NMR analysis of the isolated ligand revealed that the ethyl-ester functionality had been *trans*-esterified to the corresponding methyl-ester **10**. Furthermore, the alkyne functionality had partially been hydrated to afford a ketone. Therefore, the methyl-ester was saponified and the alkyne was fully hydrated to afford the ligand H_2L_A (**12**) in 33 % overall isolated yield.

The synthesis of the ligand H_2L_B (**19**) was achieved according the same procedure. Template cross-condensation of amino-protected **17** with dialdehyde **9**, imine reduction, ligand separation, triple bond hydration and Boc-deprotection yields the ligand H_2L_B (**19**) in 12% overall isolated yield.

3.4 Synthesis of the divanadyl haptens: $[(VO)_2(L_A)]^{2+}$ (13) and $[(VO)_2(L_B)]^{2+}$ (20)

3.4.1 Synthesis and characterization

Addition of two equivalents of $[VO(SO_4)] \cdot 3H_2O$ in methanol in the presence of triethylamine to either hexadentate ligands H_2L_A (**12**) or H_2L_B (**19**) affords the desired

haptens $[(VO)_2(L_A)]^{2+}$ (**13**) and $[(VO)_2(L_B)]^{2+}$ (**20**) quantitatively.

Depending on the acid used in electron-spray ionization, mass spectral analysis resulted in different molecular weights. For example, when formic acid was used, the molecular peak appeared at m/z = 703.30 which corresponds to **13** + $HCOO^-$. Upon addition of trifluoroacetic acid, the molecular peak occurs at **13** + CF_3COO^- (m/z = 771.5), suggesting a weakly coordinated carboxylic acid, in line with our design concept.

3.4.2 X-ray structure analysis of $[(VO)_2(L_A\text{-}H^+)]_2(CF_3COO)_2$

Recrystallization of the salt $[(VO)_2(L_A)]^{2+}$ (**13**) in methanol affords violet crystals suitable for X-ray diffraction studies. The refined structure of $[(VO)_2(L_A\text{-}H^+)]_2(CF_3COO)_2$ is depicted in Figure 2.8. Most importantly, both vanadyls occupy eclipsed axial positions with a weakly bound bridging carboxylate in *trans*-position. Although solution studies (i.e. MS data) suggest that various carboxylates can occupy the bridging sites *trans* to both vanadyls, the solid-state structure reveals that the bridging carboxylate is provided intramolecularly. The metrical data closely ressemble those of the related sulfate-bridged compound recently reported by Nag and coworkers (Table 2.1) [73].

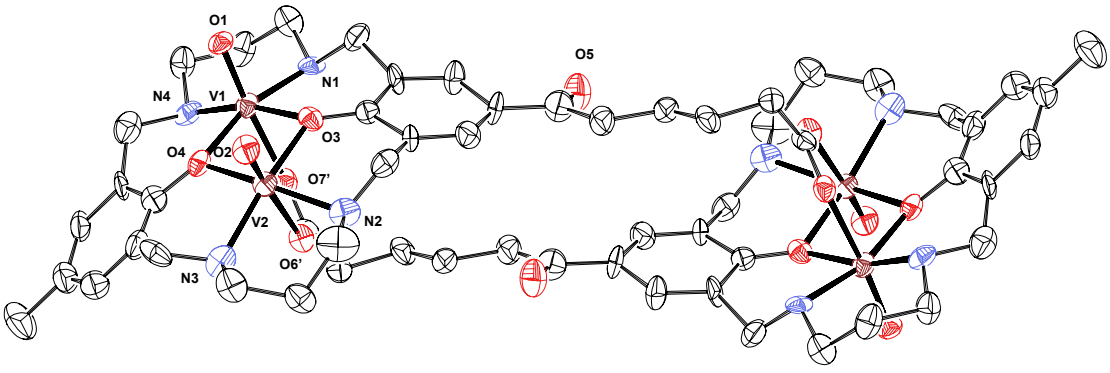

Figure 2.8 Molecular structure of $[(VO)_2(L_A\text{-}H^+)]_2(CF_3COO)_2$. Thermal ellipsoids are at the 50% probability level. Hydrogen atoms and counter ions (2 $CF_3CO_2^-$) are omitted for clarity.

Table 2.1 Selected bond lengths [Å] and angles [°] for $[(VO)_2(L_A\text{-}H^+)]_2(CF_3COO)_2$. Comparison with $[(VO)_2\ (\mu\text{-}SO_4)\ L(R^1)_2]$ [73].

	$[(VO)_2(L_A\text{-}H^+)]_2(CF_3COO)_2$	$[(VO)_2\ (\mu\text{-}SO_4)\ L(R^1)_2]$
V(1)-O(1)	1.600(5)	1.590(6)
V(1)-O(4)	2.027(6)	2.029(6)
V(1)-O(3)	2.067(6)	2.020(6)
V(1)-O(7')	2.134(6)	2.173(6)
V(1)-V(2)	3.0511(15)	3.077(7)
V(2)-O(2)	1.579(5)	1.573(6)
V(2)-O(3)	2.047(6)	2.016(6)
V(2)-O(4)	2.050(6)	2.005(6)
V(2)-O(6')	2.126(6)	2.180 (6)
V(1)-N(1)	2.152(7)	2.091(7)
V(1)-N(4)	2.113(8)	2.093(8)
V(2)-N(2)	2.138(8)	2.103(8)
V(2)-N(3)	2.093(8)	2.132(7)
V(2)-O(3)-V(1)	95.7(3)	99.0(3)
V(1)-O(4)-V(2)	96.9(3)	99.7(3)
V(displ.) [a]	0.27[a]	0.264[a]

[a]) V(1) displacement towards the vanadyl oxygen from the plane N(1)N(4)O(3)O(4).

4 Conjugation of the hapten to a carrier protein and

immunization

In order to test the stability of these complexes under immunization conditions, divanadyl complex $[(VO)_2(L_A)]^{2+}$ (**13**) is incubated in the presence of an excess of BSA (Bovine Serum Albumin) at 37°C at pH 7. HPLC analysis of the mixture after one week revealed that the divanadyl complex **13** is totally inert under these conditions.

The hapten **13** was conjugated to the carrier protein KLH using standard protocols (EDCI, NHS). MS analysis of the hapten coupled to BSA suggested that two molecules of $[(VO)_2(L_A)]^{2+}$ (**13**) (M((**13**) + H_2O - H^+) = 656·5 g.mol^{-1}) were coupled to the protein (average of two measures of BSA (67005 g·mol^{-1}) minus average of two measures of hapten (68317 g·mol^{-1}) equals 1312 g·mol^{-1} i.e. 2*656.5 g·mol^{-1}). As we can observed in Figure 2.9, peaks obtained by MALDI-MS are very broad thereby it's sometimes difficut to assign that the difference of mass is due to hapten.

Immunizations were performed and ELISA tests, realized after 1 month revealed that no antibody was produced against the hapten. Mice were boosted a second time with the hapten-KLH complex (one mouse died after this second injection). Unfortunately, all ELISA screens were negative. It was strongly suspected that the hapten was probably not conjugated to the carrier protein.

Different coupling methods were thus tested, first with phenethylamine as substitute for the protein (easier to analyze by mass spectroscopy) and then with ligand **12** or complex **13** as substrates. The synthesis of the activated ester was performed with various reagents such as EDCI+SNHS, HBTU+NEt_3 [74], TSU+N(i-Pr)$_2$Et [75], MMM+BOP+HOBT [76] and BOP+NEt_3 [77]. The couplings were also carried out in various solvents (DMF, DMSO and water).

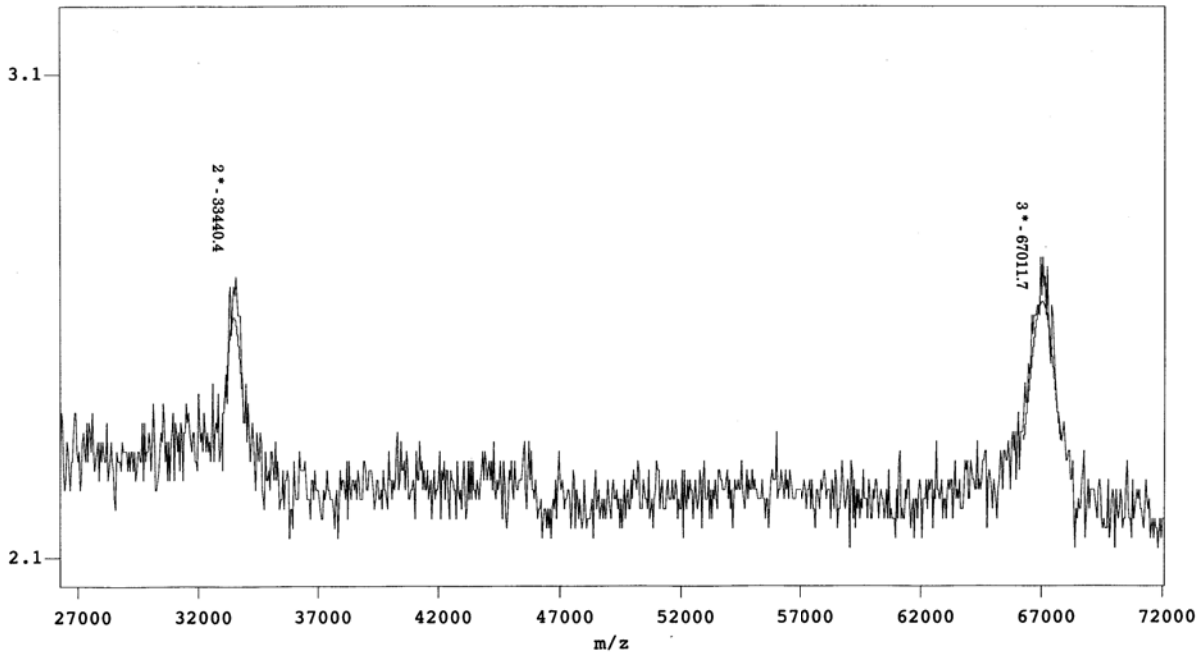

(a)

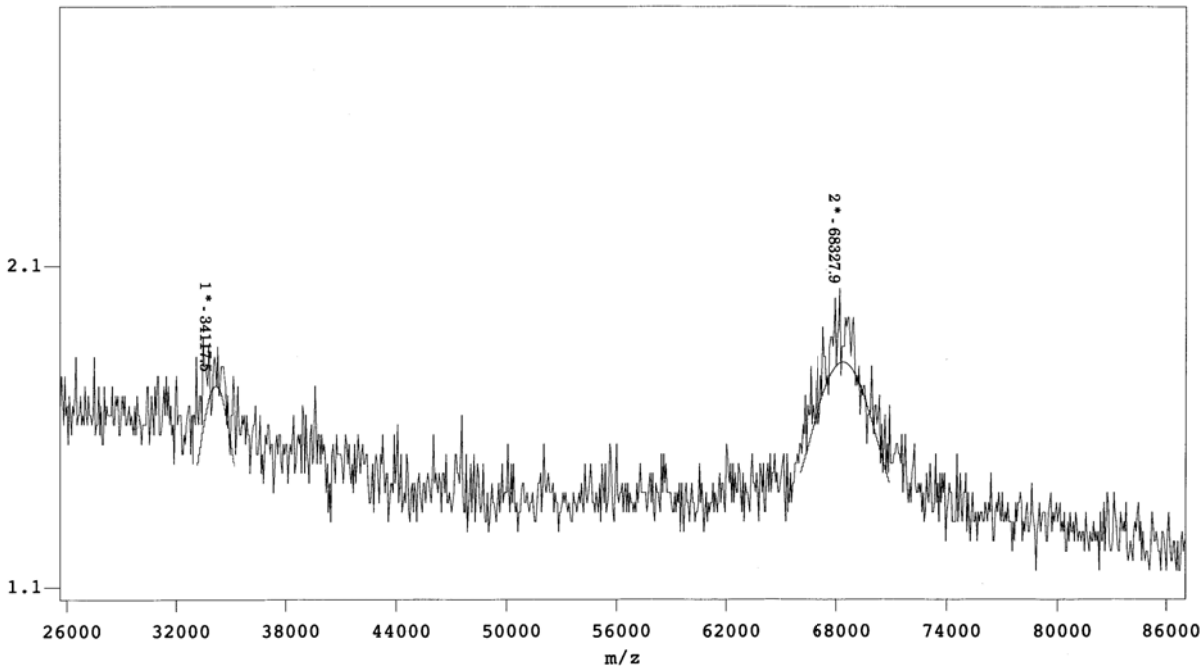

(b)

Figure 2.9 MALDI spectra of BSA (a) and product resulting of coupling of **13** to BSA (b).

Objective analysis of the MS-data (Figure 2.9) led us to suspect that the conjugation step (between the hapten and the protein) was unsuccessful. In all cases, the complex which is mostly soluble in DMF or DMSO precipitates upon mixing with the protein which is

dissolved in water or aqueous buffer solutions. This suggests that the failure to conjugate the divanadyl complex **13** to a protein is due to incompatible solubility between the protein and the hapten.

An alternative solution was envisaged to use a protein which is stable in organic solvants. For this purpose, subtilysin was choosen. However again here, all conjugation attempts failed.

5 Coenzyme synthesis and characterization

5.1 Synthesis of ligands HL_C (21) and H_3L_D (22)

As outlined above, the coenzyme should contain a pentadentate ligand structurally related to the hexadentate ligand **12** used for immunization. In order to tune the coenzyme reactivity, both N_4O or N_2O_3 donor sets were synthesized, according the the synthetic route outlined in Scheme 2.9 [78].

Schiff-base condensation between dialdehyde **9** and two equivalents of either 1,3-diaminopropane or 3-amino-1-propanol affords, after imine reduction, ligand HL_C (**21**) (after acidic Boc-deprotection) and ligand H_3L_D (**22**) in 38% and 93% yield respectively. Both ligands were obtained as TFA-salt after RPHLPC purification.

5.2 Coenzyme synthesis

5.2.1 Screening and coordination properties of ligands HL_C (21) and H_3L_D (22)

Screening of the coordination properties of both ligands HL_C (**21**) and H_3L_D (**22**) was performed in a 96 well plate using two equivalents of various metal salts (including Ni, Cu, Mn, Co and Cr) and excess base. The color changes and mass spectral analysis suggests that coordination occurs in most cases.

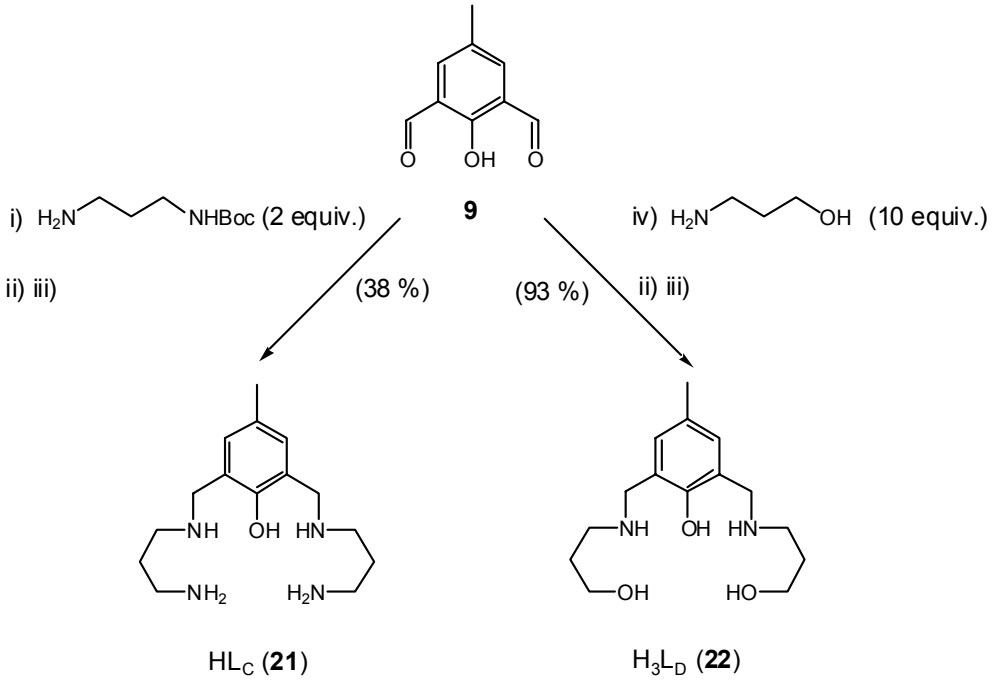

Scheme 2.9 Synthesis of pentadentate ligands HL_C (**21**) and H_3L_D (**22**).

i) MeOH, r.t. ii) $NaBH_4$ (10 equiv.), MeOH, r.t. iii) MeOH, TFA (10 %) r.t. iv) Benzene, reflux.

5.2.2 Crystal structures analysis of a dinickel coenzyme

To acertain this, a preparative reaction was carried out between $NiCl_2 \cdot 6H_2O$, triethylamine and ligand HL_C (**21**) in methanolic medium affording cationic salt $[Ni_2(L_C)]^{2+}$ (**23**). Slow evaporation of the methanol afforded crystals suitable for X-ray analysis. The first crystals diffracted poorly and the resulting data set could not be fully refined, but the structure of (**23**)$(CF_3COO)_2(MeOH)_2Cl$ is instructive (Figure 2.10(a)). A second crop of crystals was obtained under very similar recrystallization conditions. These crystals however diffracted much better and the anisotropically refined structure of (**23**)$(CF_3COO)_3(MeOH)$ is depicted in Figure 2.10(b). Bond –length and –angle data for complex (**23**)$(CF_3COO)_3(MeOH)$ are collected in Table 2.2.

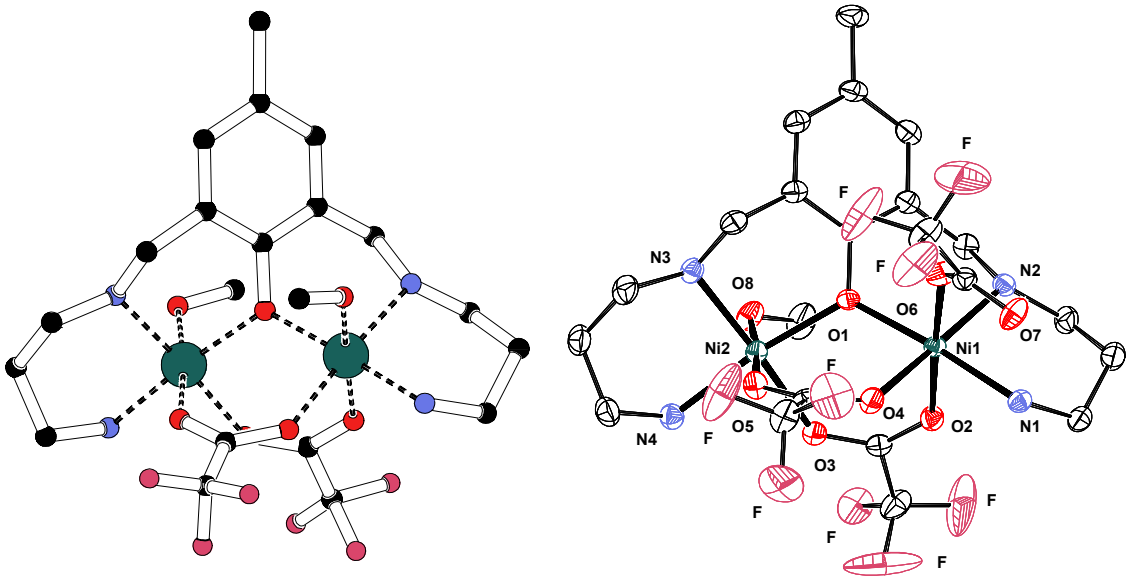

(a) (b)

Figure 2.10 Molecular structures of a) (**23**)$(CF_3COO)_2(MeOH)_2Cl$ and b) (**23**)$(CF_3COO)_3(MeOH)$. Thermal ellipsoids are at the 50% probability level. Hydrogen atoms are omitted for clarity.

Table 2.2 Selected bond lengths [Å] and angles [°] for (**23**)$(CF_3COO)_3(MeOH)$.

N(1)-Ni(1)	2.079(3)	Ni(1)-O(4)	2.096(2)
N(2)-Ni(1)	2.104(2)	Ni(1)-O(6)	2.107(2)
N(3)-Ni(2)	2.090(2)	Ni(2)-O(1)	2.0281(19)
N(4)-Ni(2)	2.077(2)	Ni(2)-O(5)	2.040(2)
Ni(1)-O(1)	2.027(2)	Ni(2)-O(3)	2.097(2)
Ni(1)-O(2)	2.073(2)	Ni(2)-O(8)	2.148(2)
Ni(1)-Ni(2)	3.520(5)	Ni(1)-O(1)-Ni(2)	120.49(10)

Although similar, these structures differ in one remarkable aspect. In the unrefined structure of (**23**)$(CF_3COO)_2(MeOH)_2Cl$, which includes Cl^- as a counter ion, the N_4O donor set occupies the equatorial plane of the nearly C_s-symmetric bi-octahedral complex. In the refined structure of (**23**)$(CF_3COO)_3(MeOH)$, the angle between the planes spanned by O(1)N(3)N(4)O(3) and O(1)N(2)N(1)O(4) is 64.15˚. This suggests that the ligand is highly flexible which should be a major advantage, allowing the coenzyme to adapt its geometry to the cavity within the antibody. Furthermore, the bridging triflates should readily be displaced by a more nucleophilic carboxylate provided by the protein in the catalytic cavity.

6 Conclusion

With the aim of producing catalytic antibodies incorporating dinuclear coenzymes, we have designed mixed N,O-compartmental ligands and studied their coordination properties.

Macrocyclic ligands H_2L_A (**12**) and H_2L_B (**19**) react with vanadyl cations to yield octahedral complexes $[(VO)_2(L_A)]^{2+}$ (**13**) and $[(VO)_2(L_B)]^{2+}$ (**20**) to be used as transition-state analogs (haptens) for the production of catalytic antibodies with C-H bond activation properties. In designing these transition-state analogs, several key features were taken into account including: a) the transition-state analog is inert and stable under physiological conditions, b) the transition-state analog possesses two immunogenic aromatic moieties, c) the transition-state analog contains a functional group which can be used to conjugate the hapten to a carrier protein and d) the transition-state analog possesses two “free” coordination sites which may elicit the presence of a (bridging) carboxylate in the active site of the protein.

For use as coenzymes, compartmental pentadentate ligands HL_C (**21**) and H_3L_D (**22**) were synthesized. These react smoothly with catalytically active transition metals to yield dinuclear coordination compounds which are structurally related to the transition-state analog $[(VO)_2(L_A)]^{2+}$ (**13**) but lack a bridging phenol moiety. The nickel complex $[Ni_2(L_C)](CF_3COO)_3(MeOH)$ was structurally characterized by X-ray.

One exciting aspect of catalytic antibody technology is its ability to deliver tailored catalysts for reactions that are difficult to carry out selectively using existing methods. Antibodies and enzymes use the same set of molecular interactions to bind their respective ligands and stabilize transition states. But can antibodies attain enzyme like efficiency to be useful? This question was recently raised by Hilvert in his "critical analysis of antibody catalysis" [79]. Antibodies appear to be less successful than enzymes in their ability to discriminate transition states and ground states [13]. This is probably due to the simple strategy used to generate them (imperfect transition-state analog). Nature optimizes catalytic activity of enzymes for millions of years whereas Man has just begun to explore the field of

catalytic antibodies.

Catalytic antibody technology combines programmable design with the combinatorial diversity of the immune system. Now that the approach is well established, attention must be paid to strategies for optimizing catalytic efficiency and promoting more demanding transformations.

Concerning the hapten, incorporating design features that maximize transition-state affinity while minimizing ground state stabilization, as well as strategies to facilitate product release should be considered as a major challenge. More extensive screening of the immune response may increase the probability of finding highly active clones. New strategies to optimize existing active sites should be developed. The combinatorial processes of the immune system can be mimicked in vitro and libraries of macromolecules generated relatively easily using the tools of molecular biology. Analogous to catalytic antibody experiments, catalytic RNAs and DNAs have been obtained from large libraries of nucleic acids by selection for binding to the transition-state analogs [80,81] or by direct selection for function [82].

In our case, one possibility to continue on the subject could be to react macrocyclic ligands H_2L_A and H_2L_B with various other metal transition cations in order to find a better water soluble complex. One other solution could be the one-pot reaction of ligand with metal and protein. This method, without isolation of the metal complex, seems to be traditionally done in molecular biology laboratories [83].

7 Experimental Section

7.1 General considerations

5-bromo-2-hydroxybenzene-1,3-dicarbaldehyde [84], 5-bromobenzene-1,3-dicarbaldehyde [85] and (4-hydroxyphenyl) but-4-anoic acid [86] n=3) were prepared according to published procedures. All other starting materials were purchased from *Fluka AG* or *Aldrich* and were used without further purification. THF was dried over Na and distilled under N_2.

NMR Spectra: Bruker AM-300 spectrometer; chemical shifts δ in ppm relative to residual solvent peak, coupling constants J in Hz.

Mass spectra: EI = Electron Ionisation; FAB = Fast Atom Bombardment, (matrix: nitrobenzylalcohol); ESI = Electron Spray Ionisation (solvent: CH_3CN/H_2O 1:1 + 0.5% HCOOH unless stated otherwise); only molecular peak (rel. %) and the most intense peak are given.

UV-Vis: λ_{max}/nm (ε/$dm^3/mol^{-1}/cm^{-1}$); MeOH.

IR: ν/cm^{-1}; KBr disc.

Elemental analysis were carried out at the E.T.H. Zürich.

RPHPLC (Reversed-Phase High Performance Liquid Chromatography) was performed on Hewlett Packard 1100 Series LC instrument using an analytical column (C18-Vydac 201TP5), detection at 230 nm, and an isocratic mode (1.5 ml/min) using an appropriate mixture of the solvents A (H_2O + 0.1% TFA) and B (CH_3CN/H_2O 1:1 + 0.1% TFA). HPLC-grade H_2O and CH_3CN were used.

Preparative RPHPLC was performed on Waters prepak cartridge 500g instrument, with a flow rate of 100 ml/min, a detection at 230 nm, and a gradient elution mode (1%/min) using 10-20 % less of B compared to the analytical conditions.

7.2 Syntheses

4-(3,5-dihydroxymethyl-4-hydroxybenzene)butanoic acid

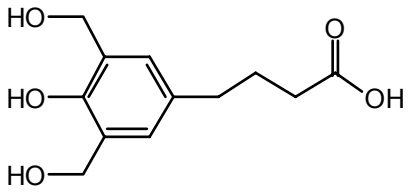

Compound **1**

A NaOH solution (5M) was added to a suspension of 4-(hydroxyphenyl) but-4-anoic acid (2.15g, 11.9 mmol) in formaldehyde (0.89g, 29.8 mmol) until dissolution. The mixture was heated at 50˚C overnight then evaporated. The crude product was dissolved in water and acidified by an HCl (1M) solution until precipitation of **1** as a white product (1.10g, 38% yield).

^{1}H NMR (CD_3OD): 1.84 (qn, J=7.35 Hz, 2H, $CH_2C\mathbf{H_2}CH_2$), 2.17 (t, 2H, CH_2), 2.48 (t, 2H, CH_2), 4.65 (s, 2H, $C\mathbf{H_2}OH$), (6.81 (s, 2 arom. H).

^{13}C-NMR (CD_3OD): 19.23, 22.15, 23.71, 61.23 (CH_2); 136.35 (arom. HC); 104.22, 133.22, 164.44 (arom. C), 171.41 (CO).

EI-MS: 240 (M^+).

4-(3,5-dicarbaldehyde-4-hydroxybenzene)butanoic acid

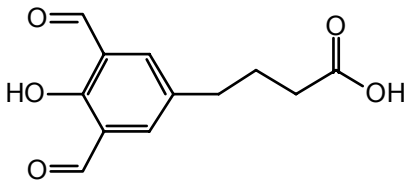

Compound **2**

MnO_2 (6.17g, 71 mmol) was added to a solution of acid **1** (1.10g, 4.60 mmol) in chloroform (300 ml). The suspension was stirred 2 days at r.t., filtered and evaporated to dryness affording the dicarbaldehyde **2** as a red powder (0,10 g, 9% yield).

^{1}H NMR ($CDCl_3$): 1.98 (qn, J=7.35 Hz, 2H, $CH_2C\mathbf{H_2}CH_2$), 2.40(t, 2H, CH_2), 2.72 (t, 2H, CH_2), 7.79 (s, 2 arom. H), 10.22 (s, 2H, HCO), 11.50 (s, 2H, OH.

^{13}C-NMR ($CDCl_3$): 19.23, 22.15, 23.71 (CH_2); 138.55 (arom. HC); 188.62 (HCO); 107.20, 132.23, 176.42 (arom. C), 177.05 (CO).

EI-MS: 236 (M^+).

11-(3,5-dicarbaldehydebenzene)undecanoate d'ethyl

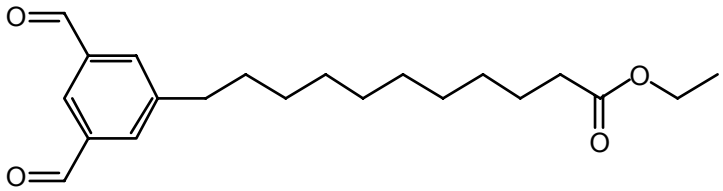

Compound **3**

A solution of ethyl undecylenate (0.62 ml, 2.58 mmol) in THF(2 mL) was added to a solution of 9-BBN (0.31 g, 2.58 mmol) in THF (8 ml) cooled at 0˚C. The reaction mixture was stirred overnight at r.t. A degazed DMF solution (20 ml) of 5-bromobenzene-1,3-dicarbaldehyde (0.5 g, 2.35 mmol), $PdCl_2$(dppf) (0.06 g, 0.07 mmol) and K_2CO_3(0.65 g, 4.70 mmol) were then added to the above borane solution. The mixture was stirred for 15 h at 50˚C and then poured into water. The crude product was extracted with ethyl acetate, washed with water, dried over $MgSO_4$ and concentrated to afford a red oil. The crude product was purified by chromatography on silicagel using ethyl acetate/hexane (1:5) as eluant to give 0.56 g (56% yield) of **3** as a white solid.

^{1}H NMR ($CDCl_3$): 1.25 (t, J=7.17 Hz, 3H, $CO_2CH_2C\mathbf{H_3}$), 1.27 (m, 12H, $(CH_2)_6$), 1.62 (m,

4H, $PhCH_2C\mathbf{H_2}(CH_2)_6C\mathbf{H_2}CH_2CO_2Et$), 2.28 (t, 2H, J=7.72 Hz, $C\mathbf{H_2}CO_2Et$), 2.77 (t, 2H, J=7.72 Hz, $PhC\mathbf{H_2}$), 4.12 (q, 2H, $CO_2C\mathbf{H_2}CH_3$), 7.97 (d, J_m=1.47 Hz, 2 arom. H), 8.19 (t, J_m, 1 arom. H), 10.09 (s, 2H, HCO).

^{13}C NMR ($CDCl_3$): 14.93 (CH_3), 25.64, 29.79, 29.80, 29.89, 30.02, 30.04, 30.09, 31.74, 35.05, 36.11 (CH_2), 60.82 ($CO_2\mathbf{C}H_2CH_3$), 129.70, 135.15 (arom. HC), 191.98 (H**C**O), 137.81, 145.99 (arom. C), 174.55 ($\mathbf{C}O_2CH_2CH_3$).

EI-MS: 346 (M^+).

5-Bromo-2-(methoxymethoxy)benzene-1,3-dicarbaldehyde

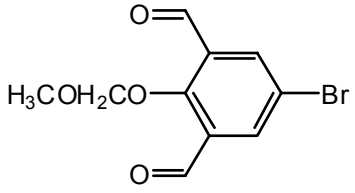

Compound **5**

To a solution of 5-bromo-2-hydroxy-1,3-benzenedicarbaldehyde (22 g, 96 mmol) in DMF (250 ml), solid K_2CO_3 (53 g, 384 mmol) was added. The mixture was cooled to 0˚C and methylchloromethylether (10 g, 124 mmol) was added dropwise. The resulting mixture was stirred for 15 h at r.t. Addition of H_2O (300 ml) resulted in a precipitate which was collected by filtration, washed with water and dried under vacuum. The crude product was purified by chromatography on silica gel (ethylacetate/hexane 1:3) to give **5** as a white powder (17.3 g, 66% yield).

^1H-NMR ($CDCl_3$): 3.62 (s, CH_3); 5.21 (s, CH_2); 8.20 (s, 2 arom. H); 10.30 (s, 2H, HCO).

^{13}C-NMR ($CDCl_3$): 59.04 (CH_3); 103.68 (CH_2); 138.02 (arom. HC); 188.17 (HCO); 119.44, 132.60, 161.48 (arom. C).

EI-MS: 272 (^{80}Br-**5**); 274 (^{82}Br-**5**) (M^+).

Ethyl hex-5-ynoate

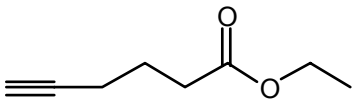

Compound **6**

A mixture of hex-5-ynoic acid (4.87 g, 43.5 mmol) and concentrated H_2SO_4 (0.5 ml) was refluxed in absolute ethanol (60 ml) for 15 h. Once cooled, a saturated solution of $NaHCO_3$ was added and the ester was extracted with CH_2Cl_2, washed with a saturated NaCl solution, dried over $MgSO_4$ and the solvent was evaporated. Distillation at 67˚C (13 mbar) gave the desired ester **6** as a colourless oil (4.70 g, 77% yield).

^{1}H-NMR ($CDCl_3$): 1.25 (t, J = 7.17, CH_3); 1,84 (tt, J = 7.35, 6.99, CH_2); 1.96 (t, J = 2.57, HC); 2.25 (dt, CCH_2); 2.43 (t, CH_2CO_2Et); 4.12 (q, CO_2CH_2Me).

^{13}C-NMR ($CDCl_3$): 14.87 (CH_3); 18.51, 24.32, 33.61 (CH_2); 61.00 (CH_2Me); 69.70 (HC); 83.95 (C); 173.69 (CO).
EI-MS: 140 (M^+).

Ethyl 6-[3,5-diformyl-4-(methoxymethoxy)-phenyl]hex-5-ynoate

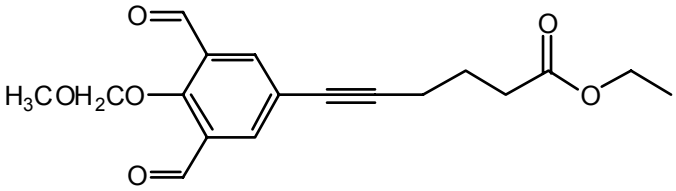

Compound **7**

A roundbottom Schlenk flask was charged with bromoarene **5** (2.0 g, 7.32 mmol), dry piperidine (50 ml) and THF (50 ml). The resulting solution was flushed with argon and alkyne **6** (2.05 g, 14.6 mmol) was added. The catalyst consisting of $Pd(PPh_3)_4$ (0.31 g, 0.29 mmol)

and CuI (0.07 g, 0.37 mmol) was added as a solid. The resulting mixture was refluxed for 40 h. After cooling at r.t., the red solution was poured into a threefold volume of ice/HCl (3:1) and immediately extracted with methylenechloride. The organic layer was dried with Na_2SO_4 and the solvent evaporated. The crude product was purified by flash chromatography (ethylacetate/hexane 1:3) to give **7** as an orange solid (1.40 g, 58% yield).

^{1}H-NMR ($CDCl_3$): 1.28 (t, J = 7.17, CH_3); 1,94 (tt, J = 7.35, 6.99, $CH_2C\mathbf{H_2}CH_2$); 2.50 (t+t, $C\mathbf{H_2}CH_2C\mathbf{H_2}$); 3.60 (s, OCH_3); 4.16 (q, $CO_2C\mathbf{H_2}Me$); 5.21 (s, OCH_2O); 8.09 (s, 2 arom. H); 10.31 (s, 2 HCO).

^{13}C-NMR ($CDCl_3$): 14.91 (CH_3); 59.03 (OCH_3); 19.46, 24.35, 33.76 (CH_2); 61.11 (CO_2CH_2Me); 103.67 (OCH_2O); 138.52 (arom. HC); 189.04 (HCO); 79.37, 92.21 (CC); 122.21, 131.07, 173.63 (arom. C).

EI-MS: 332 (M^+).

Ethyl 6-(3,5-diformyl-4-hydroxyphenyl)hex-5-ynoate

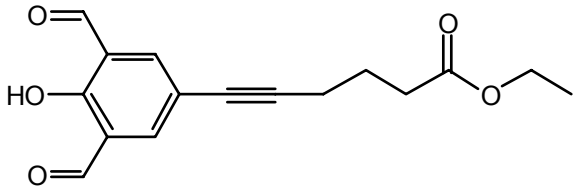

Compound **8**

MOM-protected arene **7** (1.30g, 3.91 mmol) and NaI (0.59 g, 3.91 mmol) were dissolved in acetone (15 ml). After addition of HCl (1 drop, 1M) the mixture was heated at 50˚C overnight. After cooling at r.t., the reaction mixture was acidified with HCl 1M, extracted with ethylacetate, washed with H_2O, dried with Na_2SO_4 and evaporated to give phenol **8** as an orange solid (1.13 g, quantitative yield).

^{1}H-NMR ($CDCl_3$): 1.25 (t, J = 7.17, CH_3); 1,94 (tt, J = 7.35, $CH_2C\mathbf{H_2}CH_2$); 2.49 (t,

C**H$_2$**CH$_2$C**H$_2$**); 4.16 (q, CO_2CH_2Me); 7.97 (s, 2 arom. H); 10.20 (s, 2 HCO); 11.66 (s, OH).

^{13}C-NMR ($CDCl_3$): 14.88 (CH_3); 19.45, 24.36, 33.81 (CH_2); 61.25 (CO_2CH_2Me); 138.55 (arom. HC); 189.32 (HCO); 79.65, 92.80 (CC); 117.20, 131.03, 166.42 (arom. C).

EI-MS: 288 (M^+).

Anal. calc. for $C_{16}H_{16}O_5$ + $CH_3CO_2CH_2CH_3$: C 63.82, H 6.43; found C 63.91, H 6.14.

Methyl 6-(25, 26-dihydroxy-23-methyl-3, 7, 15, 19-tetraaza-tricyclo[19.3.1.1$^{9, 13}$] hexacosa-1(24), 9, 11, 13(26), 21(25), 22-hexaen-11-yl)hex-5-ynoate

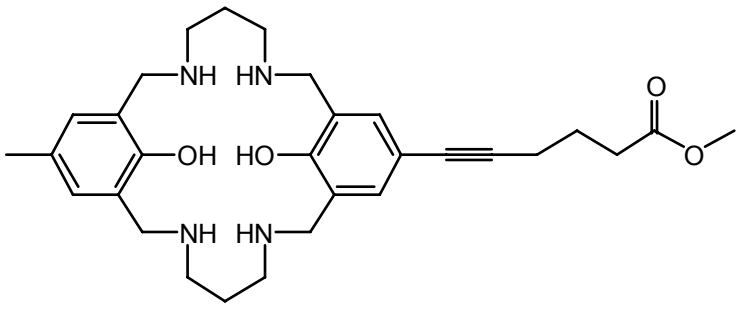

Compound **10**

Equimolar amounts of methylbenzene **9** (0.23 g, 1.39 mmol) and dicarbaldehyde **8** (0.40 g, 1.39 mmol) were dissolved in methanol (30 ml). A hot DMF solution (10 ml) containing $Pb(OAc)_2 \cdot 3H_2O$ (0.53g, 1.39 mmol) and $Pb(NO_3)_2$ (0.46 g, 1.39 mmol) was added with stirring followed by 1,3-diaminopropane (0.23 ml, 2.77 mmol). The resulting mixture was refluxed for 15 h. After evaporation of the solvent, the yellow solid was washed with methanol and dried under vacuum. Infra-red analysis of the crude product revealed the presence of a C=N streching band (ν(CN) = 1635 cm^{-1}) and the absence of the CHO streching frequency (ν(HCO) = 1685 cm^{-1}). This mixture of the three lead complexes was used without

purification for the reduction as it was insoluble. It was suspended in methanol (100 ml) and $NaBH_4$ (0.53 g, 13.9 mmol) was added portionwise. Stirring was continued overnight and the solution was filtered to remove undissolved material. The light yellow filtrate was reduced to a small volume (10 ml) and diluted with water (100 ml). The solution was then acidified with cold H_2SO_4 8M. The precipitated $PbSO_4$ was removed by filtration and washed with cold water. The filtrate was treated with ammonia (25%) until a pH of 10. The aqueous solution was extracted with chloroform, dried over Na_2SO_4 and finally evaporated to dryness to give a mixture of the three ligands (0.35 g) (i.e.: $H_2L(R^1)_2$ / $H_2LR^1R^2$ (**10**) / $H_2L(R^2)_2$ where R^1=Me, R^2=$CC(CH_2)_3CO_2Me$ and with a statistical ratio of 0.25/0.50/0.25). The asymmetric ligand **10** was isolated as a white solid (0.21 g, 57% yield) by preparative RPHPLC (60% B).

^{1}H-NMR (CD_3OD): 1.73 (tt, J = 7.35, $CH_2C\mathbf{H_2}CH_2$); 2.00 (tt, $NCH_2C\mathbf{H_2}$); 2.14 (s, $PhCH_3$); 2.32 (t, CH_2); 2.37 (t, CH_2); 2.97 (t, 4 NCH_2); 3.55 (s,3H, CH_3); 4.12 (s, 2 $PhCH_2$); 4.13 (s, 2 $PhCH_2$); 7.09 (s, 2 arom. H); 7.32 (s, 2 arom. H).

^{13}C-NMR (CD_3OD): 20.23 ($PhCH_3$); 19.25, 24.70, 25.06, 33.52, 44.84, 44.91, 46.99, 47.37 (CH_2); 52.05 (CH_3); 135.26, 137.81 (CH); 80.54, 89.80, 118.87, 121.60, 121.80, 132.98, 153.69, 155.86, 175.38 (C).

ESI-MS: 523.25 ($[M + 1]^+$).

6-(25, 26-dihydroxy-23-methyl-3, 7, 15, 19-tetraaza-tricyclo[19.3.1.1$^{9, 13}$] hexacosa-1(24), 9, 11, 13(26), 21(25), 22-hexaen-11-yl)-hex-5-ynoic acid

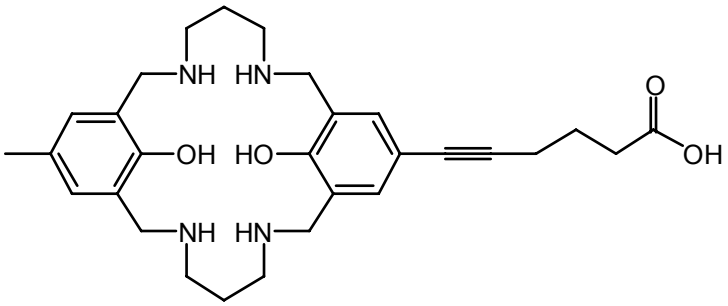

Compound **11**

Saponification of ester **10** (70 mg, 0.13 mmol) was performed in methanol (1 ml) using lithium hydroxide (60 mg, 2.68 mmol) dissolved in water (0.5 ml). After stirring 1 h at r.t., the suspension was filtered and the filtrate was treated with TFA (10%) and evaporated to dryness to give the acid **11** as a pink solid (66 mg, quantitative yield).

^{1}H-NMR (CD_3OD): 1.66 (tt, J = 7.35, $CH_2C\mathbf{H_2}CH_2$); 1.95 (tt, 2 $NCH_2C\mathbf{H_2}$); 2.07 (s, $PhCH_3$); 2.28 (t+t, 2 CH_2); 2.90 (t, 4 NCH_2); 4.06 (s, 2 $PhCH_2$); 4.08 (s, 2 $PhCH_2$); 7.03 (s, 2 arom. H); 7.26 (s, 2 arom. H).

^{13}C-NMR (CD_3OD): 20.18 (CH_3); 19.28, 24.62, 25.00, 33.73, 44.76, 44.82, 47.00, 47.37 (CH_2); 135.24, 137.82 (CH); 80.52, 89.68, 118.78, 121.49, 121.71, 132.83, 153.64, 155.79 (C); 177.44 (COOH).

ESI-MS: 509.51 ($[M + 1]^+$).

6-(25, 26-dihydroxy-23-methyl-3, 7, 15, 19-tetraaza-tricyclo[19.3.1.1$^{9, 13}$] hexacosa-1(24), 9, 11, 13(26), 21(25), 22-hexaen-11-yl)-6-oxohexanoic acid

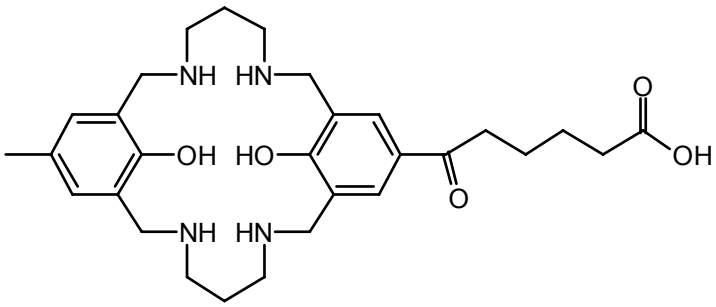

Compound H_2L_A (**12**)

Acidic hydration of alkyne **11** (66 mg, 0.13 mmol) in a methanol solution (10% TFA) for 2 days at r.t. produced the ketone **12** as a white solid in a quantitative yield (68 mg).

^{1}H-NMR (CD_3OD): 1.49 (m, $COCH_2C\mathbf{H_2}C\mathbf{H_2}CH_2CO$); 1.94 (quint., J = 7.18, 2 $NCH_2C\mathbf{H_2}CH_2N$); 2.02 (s, $PhCH_3$); 2.14 (t, J = 6.92, $COCH_2CH_2CH_2C\mathbf{H_2}CO$); 2.76 (t, J =

6.80, COC**H$_2$**CH$_2$CH$_2$CH$_2$CO); 2.88 (t, J = 6.52 , 2 NC**H$_2$**CH$_2$CH$_2$N); 2.90 (t, J = 6.50, 2 NCH$_2$CH$_2$C**H$_2$**N); 4.04 (s, 2 PhCH$_2$); 4.11 (s, 2 PhCH$_2$); 6.99 (s, 2 arom. H); 7.83 (s, 2 arom. H).

^{13}C-NMR (CD_3OD): 19.22 (CH_3); 23.74, 24.03, 24.66, 33.91, 37.42, 43.71, 43.80, 46.54, 47.36 (CH_2); 133.88, 134.14 (CH); 112.79, 115.70, 118.61, 119.86, 120.55, 121.52, (C); 177.44 (COOH); 199.20 (CO).
ESI-MS: 527.52 ($[M + 1]^+$).

$[(VO)_2(L_A)]^{2+}$

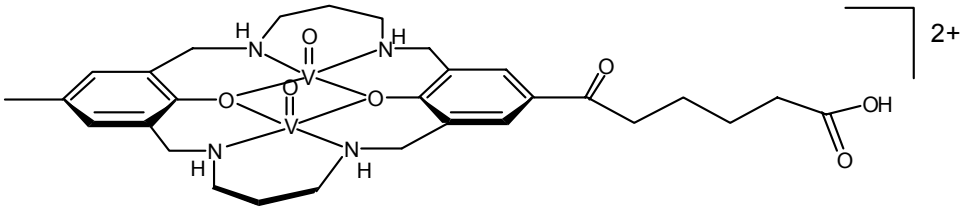

Compound **13**

Biphenol tetraamine **12** (100 mg, 0.19 mmol) was dissolved in methanol (5 ml) and triethylamine (130 µl, 0.95 mmol) was added. Trihydrated vanadyl sulfate (83 mg, 0.40 mmol) dissolved in methanol (4 ml) was added dropwise to the solution and the resulting mixture was reluxed overnight. After filtration, the solution was evaporated to dryness yielding a pale green salt **13** which was washed with cold methanol. Recrystallisation from methanol produced X-ray quality crystals (86 mg, 60% yield).

ESI-MS: 703.30 ($[M + HCOO^-]^+$).

UV-Vis : 280 (8800); 520 (70); 661 (80).

IR: 3223w ν(NH); 1600m δ(NH); 1168s, 1113s ν(S-O); 958s ν($(V=O)^+$).

Anal. calc. for $C_{29}H_{40}N_4O_7V_2$. 2 CF_3COO^- . CF_3COOH . 8.5 H_2O: C 36.50, H 5.08, N 4.86;

found C 36.20, H 4.60, N 5.29.

Typical procedure for conjugation

The hapten **13** (3 mg, $0.41.10^{-5}$ mol) was solubilized in DMF (150 µl) and H_2O (10µl). A stock solution (1.5M in 250 µl DMF and 50 µl water) of EDCI (8.14 µl, 1.3 equiv.) and stock solution (1.6 M, 200 µl DMF and 120 µl water) of NHS (7.64 µl, 1.3 equiv.) were added. The solution was stirred overnight at rt.

The activated ester solution (100 µl) was added to a solution of BSA (1 ml) in PBS (C = 5 mg/ml). The pH was adjusted between 7 and 8 by addition of a saturated solution of $NaHCO_3$ (by portions of 10 µl). The mixture was allowed to stand at 4˚C for 24 h. The protein solution was then aliquoted in 100 µl Eppendorfs and stored at -20˚C.

The same procedure was applied for the coupling of the activated ester with KLH protein (C = 5 mg/ml).

***N*-(3-aminopropyl)hex-5-ynamide**

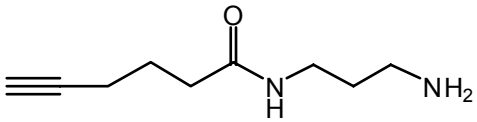

Compound **14**

The ethylester **6** (2 g, 14.3 mmol) was heated for 48 h at 60˚C in neat 1,3-diaminopropane (50 ml). After evaporation of the excess of 1,3-diaminopropane, the residue was dried overnight under high vacuum. The amide **14** was obtained as a yellow oil in a quantitative yield (2.40 g).

^{1}H-NMR ($CDCl_3$): 1.56 (tt, J = 6.61, $HNCH_2C\mathbf{H_2}$); 1.76 (tt, J = 7.35, 6.98, $CCH_2C\mathbf{H_2}$); 1.92 (t, J = 2.57, HC); 2.10 (br. s, NH_2); 2.16 (dt, CCH_2); 2.23 (t, CH_2CO); 2.70 (t, J = 6.25,

C**H$_2$**NH$_2$); 3.25 (dt, HNC**H$_2$**); 6.90 (b. t, NH).

^{13}C-NMR ($CDCl_3$): 18.39, 24.81, 32.68, 35.58, 38.05, 40.28 (CH_2); 69.61 (HC); 84.08 (C); 172.90 (CO).

EI-MS: 169 (M^+).

***tert*-butyl [3-(hex-5-ynoylamino)propyl]-carbamate**

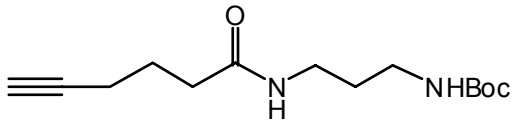

Compound **15**

A saturated solution of $NaHCO_3$ (50 ml) was added to a solution of amine **14** (2.40 g, 14 mmol) in dioxane (50 ml). The mixture was cooled to 0˚C and $(Boc)_2O$ (4.67 g, 21 mmol) in dioxane (20 ml) was slowly added. The resulting solution was strirred overnight at r.t. Extraction with ethylacetate, followed by washing with water and drying over $MgSO_4$, afforded the Boc-protected amine **15** as a yellow oil (3.65 g, 95% yield).

^{1}H-NMR ($CDCl_3$): 1.39 (s, 3 CH_3); 1.57 (quint., J = 6.25, HNCH_2C**H$_2$**); 1.82 (quint., J = 7.35, CCH_2C**H$_2$**); 1.94 (t, J = 2.70, HC); 2.21 (dt, J = 2.70, 6.90, CC**H$_2$**); 2.29 (t, J = 7.35, C**H$_2$**CO); 3.11 (q, J = 6.25, C**H$_2$**NHBoc); 3.25 (dt, J = 6.25, HNC**H$_2$**); 5.11 (br. s, NHBoc); 6.46 (br. s, NH).

^{13}C-NMR ($CDCl_3$): 28.98 (CH_3); 18.47, 24.84, 30.80, 35.71, 36.47, 37.65 (CH_2); 69.72 (HC); 79.80 (**C** 'Boc'); 85.76 (C); 147.32 (**C**O_2 'Boc'); 173.23 (CO).

EI-MS: 269 (M^+).

***tert*-butyl(3-{-[3,5-diformyl-4-(methoxymethoxy)-phenyl]-hex-5-ynoylamino}propyl)carbamate**

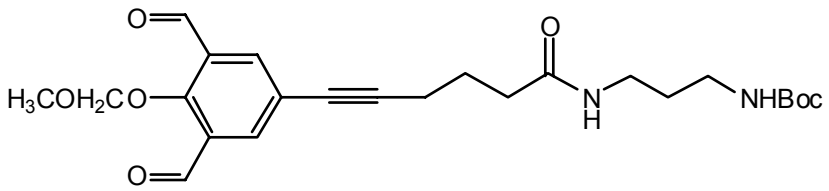

Compound **16**

The coupled product **16** was obtained using the same procedure as for compound **7**. Reaction between bromoarene **5** (2 g, 7.32 mmol) and alkyne **15** (3.53 g, 13 mmol) in the presence of $Pd(PPh_3)_4$ (0.31 g, 0.30 mmol) and CuI (0.07 g, 0.37 mmol). After workup, the resulting solid was subjected to flash chromatography (CH_2Cl_2/MeOH 20:1) to afford areno-alkyne **16** as yellow oil (1.50 g, 44% yield).

^{1}H-NMR ($CDCl_3$): 1.31 (s, 3 CH_3); 1.52 (quint., J = 6.25, 5.88, $HNCH_2C\mathbf{H_2}$); 1.84 (quint., J = 7.35, 6.98, $CCH_2C\mathbf{H_2}$); 2.28 (t, CH_2CO); 2.38 (t, CCH_2); 3.05 (q, $C\mathbf{H_2}NHBoc$); 3.19 (q, $HNC\mathbf{H_2}$); 3.49 (s, OCH_3); 5.11 (s, OCH_2O); 5.29 (t, NHBoc); 6.78 (t, J = 5.15, NHCO); 7.93 (s, 2 arom. H); 10.18 (s, 2 HCO).

^{13}C-NMR ($CDCl_3$): 28.98 (CH_3 'Boc'); 58.78 (OCH_3); 19.35, 24.86, 30.62, 35.73, 36.46, 37.61 (CH_2); 103.46 (OCH_2O); 138.21 (arom. HC); 188.90 (HCO); 79.07, 92.32 (CC); 79.60 (C 'Boc'); 121.97, 130.84, 161.29 (arom. C); 157.11 (CO_2 'Boc'); 173.11 (CO).

FAB-MS: 461 (M^+).

***tert*-butyl {3-[6-(3,5-diformyl-4-hydroxyphenyl)hex-5-ynoylamino]-propyl}-carbamate**

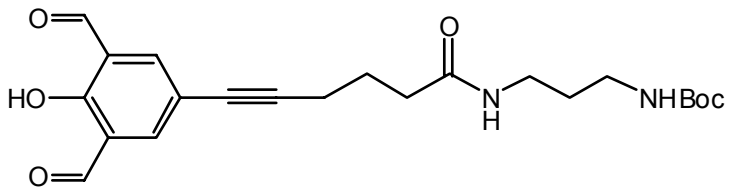

Compound **17**

Deprotection of MOM-protected **16** (0.50 g, 1.08 mmol) was carried out similary as with compound **8** using acetone (40 ml) and NaI (0.16 g, 1.08 mmol). The phenol **17** was obtained as an orange oil (0.27 g, 60% yield).

^{1}H-NMR ($CDCl_3$): 1.38 (s, 3 CH_3); 1.58 (quint., J = 6.25, 6.62, $HNCH_2C\mathbf{H_2}$); 1.93 (quint., J = 7.35, 6.99, $CCH_2C\mathbf{H_2}$); 2.34 (t, CH_2CO); 2.43 (t, CCH_2); 3.13 (q, $C\mathbf{H_2}NHBoc$); 3.26 (q, $HNC\mathbf{H_2}$); 5.11 (br. s, NHBoc); 6.62 (br. s, NHCO); 7.93 (s, 2 arom. H); 10.15 (s, 2 HCO); 11.62 (s, OH).

^{13}C-NMR ($CDCl_3$): 28.92 (CH_3); 19.37, 25.00 30.69, 35.86, 36.49, 37.65 (CH_2); 140.84 (arom. HC); 192.22 (HCO); 78.94, 79.84, 90.69, 116.90, 123.61, 157.28, 171.70, 173.26 (C).

FAB-MS: 417 (M^+).

***tert*-butyl {3-[6-(25, 26-dihydroxy-23-methyl-3, 7, 15, 19-tetraaza-tricyclo [19.3.1.1$^{9, 13}$]hexacosa-1(24), 9, 11, 13(26), 21(25), 22-hexaen-11-yl)-hex-5-ynoylamino]propyl}carbamate**

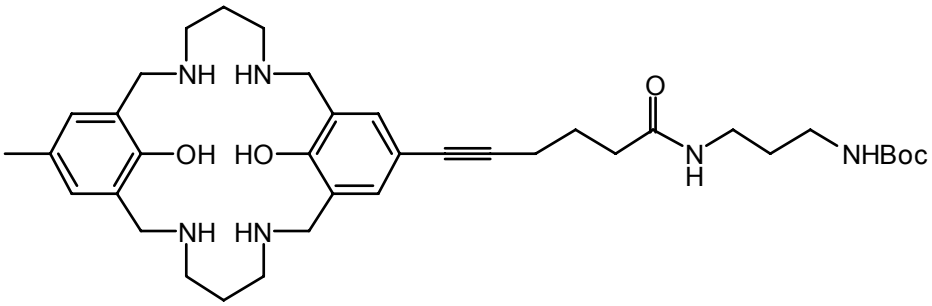

Compound **18**

The template condensation was carried out using the same procedure as for compound **10**. For this purpose, dialdehyde **17** (0.27 g, 0.65 mmol) and methylbenzene **9** (0.11 g, 0.65 mmol) in methanol (12 ml), a hot DMF solution (4 ml) of $Pb(OAc)_2 \cdot 3H_2O$ (0.24 g, 0.65 mmol) and $Pb(NO_3)_2$ (0.21 g, 0.65 mmol) and 1,3-diaminopropane (0.12 ml, 1.43 mmol) were used. Compound **18** was isolated from the mixture (0.35 g) of the three ligands (i.e.: $H_2L(R^1)_2$ / $H_2L\ R^1R^3$ (**18**)/ $H_2L(R^3)_2$ with $R^1 = CH_3$ and $R^3 = CC(CH_2)_3CONH(CH_2)_3NHBoc$ and with a statistical ratio of 0.25/0.50/0.25) by preparative RPHPLC (60%B) (0.1 g, 45% yield).

^{1}H-NMR (CD_3OD): 1.31 (s, 3 CH_3); 1.51 (quint., J = 6.62, 6.98, $HNCH_2C\mathbf{H_2}CH_2NHBoc$); 2.00 (quint., J = 7.35, 6.98, 2 $HNCH_2C\mathbf{H_2}CH_2NH$); 2.00 (quint., J = 7.35, 6.99, $CCH_2C\mathbf{H_2}$); 2.12 (s, CH_3); 2.23 (t, CH_2CO); 2.29 (t, CCH_2); 2.82 (t, $C\mathbf{H_2}NHBoc$); 2.96 (t, 2 $HNC\mathbf{H_2}CH_2C\mathbf{H_2}NH$); 3.08 (t, $HNC\mathbf{H_2}$); 4.11 (s, 2 $PhCH_2$); 4.12 (s, 2 $PhCH_2$); 7.08 (s, 2 arom. H); 7.31 (s, 2 arom. H).

^{13}C-NMR (CD_3OD): 20.32, 28.85 (CH_3); 24.67, 26.82, 29.34, 37.46, 37.56, 38.19, 38.59, 45.22, 45.37, 47.39, 47.72 (CH_2); 135.53, 135.74 (HC); 79.65, 79.93, 92.07, 114.76, 117.36, 120.92, 121.46, 121.76, 131.70, 133.34, 153.88 (C); 157.12, 177.18 (CO).

ESI: 665.41 ($[M + 1]^+$).

***N*-(3-amino-propyl)-6-(25, 26-dihydroxy-23-methyl-3, 7, 15, 19-tetraaza-tricyclo [19.3.1.1$^{9, 13}$]hexacosa-1(24), 9, 11, 13(26), 21(25), 22-hexaen-11-yl)-6-oxohexanamide**

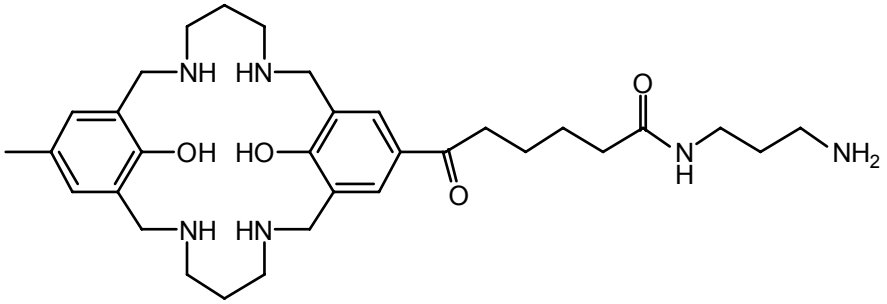

Compound H_2L_B (**19**)

Stirring overnight at 60˚C, alkyne **18** (100 mg, 0.15 mmol) in an acidic solution (TFA 10%, 5 ml) resulted in a quantitative hydration, affording lactone **19** (88 mg, quant.).

^{1}H-NMR (CD_3OD): 1.77 (br. quint., $COCH_2C\mathbf{H_2}C\mathbf{H_2}CH_2CO$); 1.94 (quint., J = 6.95, $HNCH_2C\mathbf{H_2}CH_2NH_2$); 2.21–2.25 (m, 2 $HNCH_2C\mathbf{H_2}CH_2NH$); 2.31(s, CH_3); 2.35 (t, J = 6.70, CH_2CO); 3.05 (tt, J = 7.46, 2 $C\mathbf{H_2}NH_2$); 3.12–3.22 (m, 2 $HNC\mathbf{H_2}CH_2C\mathbf{H_2}NH$+$CH_2CO$); 4.31 (s, 2 $PhCH_2$); 4.43 (s, 2 $PhCH_2$); 7.27 (s, 2 arom. H); 8.17 (s, 2 arom. H).

^{13}C-NMR (CD_3OD): 20.51 (CH_3); 24.81, 25.00, 26.78, 29.02, 37.04, 37.14, 38.09, 38.49, 45.21, 45.12, 47.36, 47.63 (CH_2); 135.52, 135.72 (HC); 114.90, 117.73, 120.56, 121.50, 121.87, 131.75, 133.24, 153.97 (C); 177.15, 199.85 (CO).

ESI-MS: 583.21 ($[M + 1]^+$).

$[(VO)_2(L_B)]^{2+}$

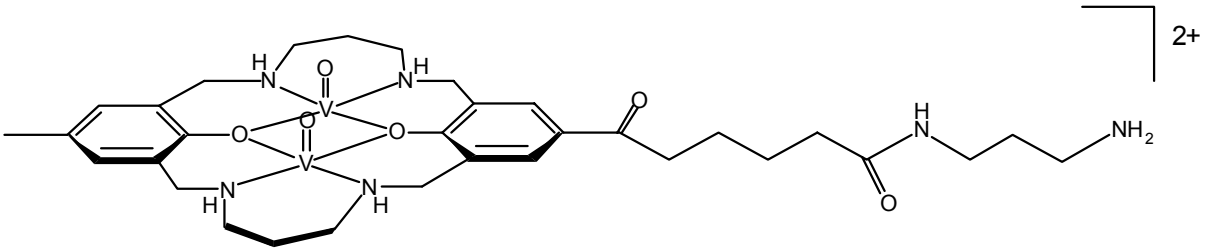

Compound **20**

The vanadium complex **20** was obtained by the same procedure as **13**, H_2L_B (**19**) (50 mg, 0.08 mmol) dissolved in methanol (3 ml), triethylamine (60 µl, 0.43 mmol) and trihydrated vanadyl sulfate (37 mg, 0.17 mmol) in methanol (3 ml) yielding the pale green salt **20** (52 mg, 75% yield).

ESI-MS: 811.14 ([**20**(µ-SO_4) + 1]$^+$).

2,6-Bis{[(3-aminopropyl)-amino]methyl}-4-methylphenol

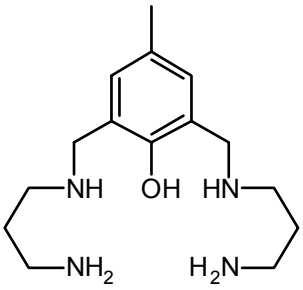

Compound HL_C (**21**)

Dialdehyde **9** (0.90 g, 5.50 mmol) was dissolved in methanol (50 ml) and charged with N-Boc-1,3-diaminopropane (2 ml, 11.5 mmol) in methanol (10 ml). The mixture was stirred at r.t. for 2 days. The solution was diluted with methanol (50 ml) and the product was reduced with $NaBH_4$ (2.10 g, 55 mmol). The reaction mixture was stirred for 4 h and evaporated to dryness. The product was deprotected by reaction in methanol (10 ml) and TFA (50 ml,10% in water) overnight. The crude product was purified by preparative RPHPLC (20% B) to afford the tetraamine ligand **21** as the TFA salt (1.54 g, 38% yield).

^{1}H-NMR (CD_3OD): 1.93.(quint., J = 7.72, 2 $CH_2C\mathbf{H_2}CH_2$); 2.09 (s, CH_3); 2.85 (t, 2 NH2C$\mathbf{H_2}$); 2.98 (t, 2 C$\mathbf{H_2}$NH); 4.05 (s, 2 $PhCH_2$); 7.07 (s, 2 arom. H).

^{13}C-NMR (CD_3OD): 20.26 (CH_3); 25.22, 37.85, 45.59, 47.88 (CH_2); 135.04 (CH); 121.73,132.41,153.61 (arom. C).

ESI-MS: 281.25 ([M + 1]$^+$).

Anal. calc. for $C_{15}H_{28}N_4O \cdot 4$ TFA: C 37.51, H 4.38, N 7.61; found C 37.61, H 4.23, N 7.40.

2,6-Bis{[(3-hydroxypropyl)-amino]methyl}-4-methylphenol

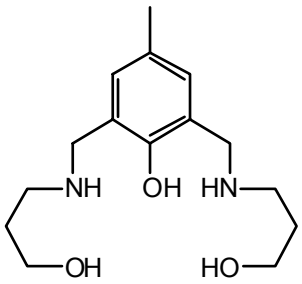

Compound H_3L_D (**22**)

A solution of dialdehyde **9** (1 g, 6.1 mmol) and 3-amino-1-propanol (4.6 ml, 61 mmol) in benzene (60 ml) was refluxed overnight with Dean Stark trap system. Evaporation of benzene afforded a yellow oil which was redissolved in methanol (60 ml) and reduced by addition of $NaBH_4$ (2.3 g, 61 mmol). Acidification with TFA (10%, 5 ml) followed by evaporation under vacuum afforded the TFA salt of **22** as a yellow oil. the crude product **22** was purified by preparative RPHPLC (20% B) to afford a white powder (2.9 g, 93% yield).
^{1}H-NMR (CD_3OD): 1.78.(quint., 2 $CH_2C\mathbf{H_2}CH_2$); 2.16 (s, CH_3), 3.04 (t, J = 7.15, 2 NHC$\mathbf{H_2}$); 3.55 (t, J = 5.70, 2 C$\mathbf{H_2}$OH); 4.10 (s, 2PhCH_2); 7.13 (s, 2 arom. H).

^{13}C-NMR (CD_3OD): 20.30(CH_3); 29.30, 47.19, 47.85, 60.64 (CH_2); 134.84 (CH); 121.78,132.42,153.60 (arom. C).

ESI-MS: 283.34 ($[M + 1]^+$).

Anal. calc. for $C_{15}H_{26}N_2O_3 \cdot 2$ TFA: C 44.71, H 5.53, N 5.49; found C 45.01, H 5.45, N 5.43.

$[Ni_2(L_C)](CF_3COO)_3(MeOH)$

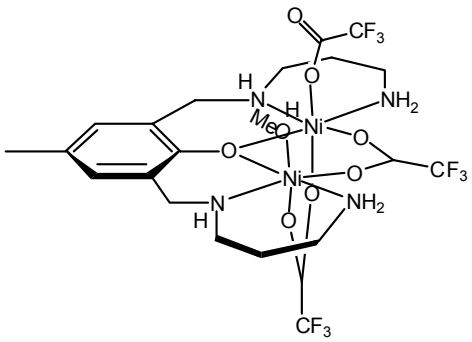

Compound (**23**)$(CF_3COO)_3(MeOH)$

To a solution of HL_A (**21**) · 4 TFA (100 mg, 0.14 mmol) in 2 ml of methanol was added a solution of $NiCl_2$ · 6 H_2O (65 mg, 0.28 mmol) in 2 ml of methanol. After addition of triethylamine (200 µl, 1.4 mmol) the color of the solution changed from dark green to pale blue. The resulting solution was allowed to stand at r.t. during one week producing X-ray quality blue crystals of $[Ni_2(L_C)](CF_3COO)_3(MeOH)$ ((**23**)$(CF_3COO)_3(MeOH)$). (107 mg, 85% yield).

ESI-MS (i-PrOH): 621 ((**23**)$(CF_3COO^-)_2]^+$),

567 ((**23**)$(CF_3COO^-)((CH_3)_2CHO^-)]^+$).

UV-Vis: 293 (2110), 243 (3240), 223 (2990), 605 (40).

IR: 2943s, 2605s, 1480s, 1671s, 1708s, 1445m.

Illustrative examples for the 96 well plate format screening of the coordination properties of HL_C (21) and H_3L_D (22).

In one well, a solution of $Cu_2(CH_3COO)_2{\cdot}H_2O$ (14 mg, 7.13 µmol) in ethanol (200 µl) was added to an ethanolic solution (100 µl) of HL_C (**21**) (1 mg, 3.57 µmol) and NEt_3 (1.8M in ethanol, 6 µl, 10.7 µmol). The resulting mixture was stirred one hour at r.t. and subjected to ESI-MS analysis.

ESI-MS (MeOH/(i-PrOH)): 403, 405 ($[Cu_2(L_C)]^+$).

A similar procedure was used with H_3L_D (**22**) (1 mg, 3.54 μmol) in ethanol (100 μl), NEt_3 (1.8M in ethanol) (10 μl,17.8 μmol) and Cu_2 $(CH_3COO)_2 \cdot H_2O$ (14 mg, 7.09 μmol) in ethanol (200 μl).

ESI-MS (MeOH/(i-PrOH)): 451, 453 ($[Cu_2(L_D)(EtO)]$ H^+).

8 X-ray Crystallography

8.1 Structure determination

Suitable crystals of $[(VO)_2(L_A - H^+)]_2(CF_3COO)_2$ were grown from methanol as violet plates. Intensity data were collected at 153 K on a Stoe Image Plate Diffraction system [87] using MoKα graphite monochromated radiation. Image plate distance 70mm, ϕ oscillation scans 0 - 191°, step Δϕ = 1.0°, 2θ range 3.27 – 52.1°, d_{max} -d_{min} = 12.45 - 0.81 Å. The structure was solved by direct methods using the programme SHELXS-97 [88].The refinement and all further calculations were carried out using SHELXL-97 [89]. The H-atoms were included in calculated positions and treated as riding atoms using SHELXL default parameters. The non-H atoms were refined anisotropically, using weighted full-matrix least-squares on F^2. The crystal was a twin and diffracted poorly to a maximumof 40° in 2θ and the average I/σ (I) was only 1.9. After Integration of the Image Plate data the reflections were treated using the program TWINXLI [90] which indicated that at least 30% of the data were overlapped and they were eliminated. The least-squares refinement with SHELXL-97 was then carried out using HKLF 5 and BASF (refined value 0.0967) to give a final R_1 value of 0.089 for 2998 observed reflections.

A blue crystal of compound (**23**)$(CF_3COO)_3$(MeOH) was mounted on a Stoe Imaging Plate Diffractometer System (Stoe & Cie, 1995) equipped with a one-circle φ goniometer and a graphite-monochromator. Data collection was performed at –120 °C using Mo-Kα radiation (λ = 0.71073 Å). 200 exposures (3 min per exposure) were obtained at an image plate distance of 70 mm with 0 < φ < 200° and with the crystal oscillating through 1° in φ. The resolution was d_{max} -d_{min} = 12.45 – 0.81 Å. The structure was solved by direct methods using the program SHELXS-97 [88] and refined by full matrix least squares on F^2 with SHELXL-97 [91]. The hydrogen atoms

were included in calculated positions and treated as riding atoms using SHELXL-97 default parameters. The figures were drawn with PLATON 99 [92].

8.2 Crystallographic data

The crystallographic data of compounds $[(VO)_2(L_A\text{-}H^+)]_2(CF_3COO)_2$ and (**23**)$(CF_3COO)_3(MeOH)$ are summarized in Table 2.3.

Table 2.3 Crystal data for $[(VO)_2(L_A\text{-}H^+)]_2(CF_3COO)_2$ and (**23**)$(CF_3COO)_3(MeOH)$.

	$[(VO)_2(L_A\text{-}H^+)]_2(CF_3COO)_2$	(**23**)$(CF_3COO)_3(MeOH)$
Chemical formula	$C_{72}H_{118}F_6N_8O_{28}V_4$ $(C_{58}H_{78}N_8O_{14}V_4)$ $(CF_3COO^-)_2 10CH_3OH$	$C_{22}H_{31}F_9N_4Ni_2O_8$
Formula weight	1861.50	767.93
Crystal system	Monoclinic	Monoclinic
Space group	P 2_1/c	C2/c
a [Å]	8.2731(5)	36.848(3)
b [Å]	21.3131(16)	9.1058(5)
c [Å]	24.8655(19)	17.5556(13)
α [°]	90	90
β [°]	101.869(8)	90.163(9)

γ [°]	90	90
V [Å^3]	4290.7(5)	5890.5(7)
Z	2	8
$\mu(MoK_\alpha)$/mm^{-1}	0.516	1.387
T/K	293(2)	153(2)
Reflections measured	20159	22573
Unique reflections	20159	5483
R(int)	0.0000	0.740
R_1, ωR_2 ($I>2\sigma(I)$)	0.0890, 0.1842	0.0386, 0.0931
R_1, ωR_2 (all data)	0.3310, 0.2549	0.0534, 0.0976

9 References

EN.REFLIST

Part 3 :

Synthesis of Mixed Phosphine-Phosphinite Ligands and their Use in the Enantioselective Hydrogenation of Olefins for the Quantification of Electronic Asymmetry

1 Introduction

1.1 Enantioselective catalysis: background

Transition metal-catalyzed asymmetric reactions are one of the most efficient methods for preparing a wide range of enantiomerically pure compounds. Design and synthesis of new efficient chiral ligands is crucial for the development of practical asymmetric catalytic reactions [1-3].

The high efficiency of diphosphines as chiral ligands for asymmetric reactions is attributable to their ability to form stable metal-containing chelate rings whose dissymmetric structures are retained through the reactions [4,5].

1.2 Enantioselective catalysis: early developments

The early success of Wilkinson's catalyst [$Rh(PPh_3)_3Cl$] [6-11], an achiral rhodium complex which catalyzes the hydrogenation of simple olefins in organic solvents under mild conditions, created a general awareness in the organic chemical community of the possibility for asymmetric synthesis.

In 1968, Horner [12,13] and Knowles [14] independently reported the first homogeneous asymmetric hydrogenation. The Wilkinson complex modified by incorporation of a chiral tertiary phosphine catalyzes the hydrogenation of certain olefins with an enantiomeric excess of 15%.

An important breakthrough in the area of asymmetric catalysis came with the introduction of C_2-symmetric diphosphine ligands [15]. In 1972, Kagan [16] reported the Rh(I) complex of chiral chelating diphosphine DIOP (Figure 3.1 (a)) used in the asymmetric

hydrogenation of α-acylaminoacrylic acids and esters. It is the first example of C_2 chiral ligand but it is also significant because it represents the first high-level (80% ee) catalytic asymmetric process. This report was rapidely followed by the development of the chelating P-chiral diphopshine DIPAMP (Figure 3.1 (b)) by the Mosanto group headed by Knowles [17]. This ligand led to the industrial production of *S*-DOPA (Figure 3.1 (c)) [18].

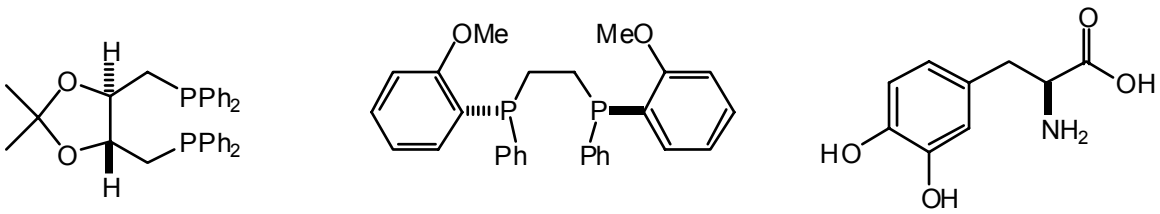

(a) (b) (c)

Figure 3.1 (a) (*R*,*R*)-DIOP, (b) (*R*,*R*)-DIPAMP, (c) (*S*)-DOPA.

Another major breakthrough was achieved in the 1980s by Noyori and coworkers [19-21]. Their fundamental work on Ru(II)-BINAP catalyst (Figure 3.2) enhanced the scope of enantioselective hydrogenation because the field of suitable substrates was found to be much wider than that of rhodium catalysts. Importantly, BINAP also finds its Rh-catalysis application in the industrial production of (*S*)-menthol [22].

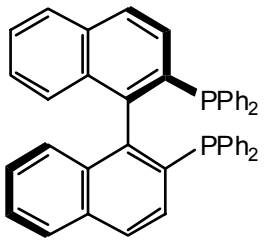

Figure 3.2 (*R*)-BINAP.

These achievements stimulated research on a variety of bidentate chiral diphosphines. Since then, hundreds of new phosphine ligands (where in most cases the C_2 symmetry plays an important role) have been synthesized and used as chiral ligand in the hydrogenation of olefins [23,24].

1.3 Enantioselective hydrogenation of olefins: scope and limitations

The classical application of rhodium asymmetric hydrogenation is the enantioselective synthesis of amino acids from dehydroamino acids. Traditionally, new ligands are tested on two key reactions, the hydrogenation of *N*-acylaminoacrylic acids to give amino acids and the hydrogenation of itaconic acids derivatives (Figure 3.3).

(a) (b)

R = H, aryl and R' = H, alkyl

Figure 3.3 Hydrogenation of new ligands is achieved on two classes of substrates: *N*-acylaminoacrylic acids (a) and itaconic acid (b) derivatives.

The number of successful practical applications has been rapidly increasing. Despite these impressive development, the scope of the Rh-catalyzed reactions is not very wide and knows many limitations.

First, the range of the substrates is limited to certain classes of alkenes bearing polar groups that can coordinate to the metal catalyst, like enamide and α,β-unsaturated carboxylic acids. The amino group in the reactant is normally protected as a carboxamide, but carbamates (Boc protected for example) are more useful intermediates in peptide synthesis. It has been shown that hydrogenation with enecarbamates is slower and less efficient [25]; but there are nevertheless some exceptions. In particular Etzkorn and coworkers, using the commercially available Rh(MeDUPHOS) (Figure 3.4(a)), showed that trisubstitued olefins containing Boc- and Cbz-protected amines can be hydrogenate in good ee and yield [26]. Secondly, successful reactants are limited to *Z*-α-dehydroamino acids and esters. There are some examples of reaction with *E*-isomers (using DIPAMP ligand (Figure 3.1(b))) but the reaction is slower than for its *Z* analog [27]. And finally, at least one hydrogen must be present on the double bond of the olefinic substrates. However, good results are obtained in

the hydrogenation of tetrasubstitued olefins using MeDuPhos (Figure 3.4(a)) [28,29] or TRAP (Figure 3.4(b)) [30,31] Rh catalysts.

(a) (b)

Figure 3.4 (*S*,*S*)-MeDuPhos (a) and (*R*,*R*)-(*S*,*S*)-TRAP (b).

Attempts to solve the problem of efficient practical methods for the enantioselective hydrogenation of unfunctionalized olefins is provided with synthesis of new ligands. The first encouraging results for hydrogenation of unfunctionalized alkenes were obtained using cyclopentadienyl complexes of titanium and zirconium [32] and later Brintzinger's [33] chiral titanocene and analogous zirconocene complexes [34,35] as catalysts. Pfaltz and co-workers reported iridium complexes of phosphinooxazoline (PHOX) (Figure 3.5) which gave enantioselectivities comparable of those obtained with Brintzinger's titanocene catalysts but with higher conversions [36-38].

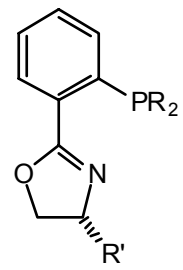

Figure 3.5 PHOX ligand.

1.4 Recent developments in enantioselective hydrogenation

Most of the ligands for enantioselective metal-catalyzed hydrogenation are homodonors ligands possessing C_2 symmetry, mainly diphosphines [39,40] and diphosphinites [41-43].

Recently, however, monodentate phosphinites and phosphites have been shown to be excellent ligands in the rhodium asymmetric hydrogenation of olefins by the research groups of Pringle [44], Reetz [45,46] and Feringa [47]. Amongst these, the monodentate phosphoramidite chiral ligand of Feringa's group, MonoPhos (Figure 3.6) gives excellent results in the rhodium-catalyzed hydrogenation of dehydroamino acid and itaconic acid derivatives (enantiomeric excess are comparable with those of a bidentate phosphoramidite ligand) [47].

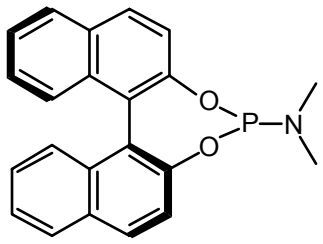

Figure 3.6 Feringa's (*S*)-MonoPhos.

The presence of C_2 symmetry axis within the chiral ligand is attractive because, in a enantioselective reaction, it reduces the number of possible competing diastereomeric transition state [15]. However, there is no fundamental reason why non-symmetrical ligands should be less effective. Non-symmetrical ligands with two different coordinating heteroatoms could allow more effective enantiocontrol than C_2-symmetric ligands [38].

That is why recently, chiral bidentate ligands with two different donors have attracted attention. Electronically asymmetric bidentate ligands P^N (PHOX ligand see Figure 3.5) were introduced by Helmchen [48], Pfaltz [49] and Williams [50].

A prochiral substrate is desymmetrized not only by steric factors but also through the

electronic asymmetry induced by the bidentate ligand [51-54]. The combination of different functionalities in a ligand has already proved beneficial in enantiodiscrimination [55]. If the metal center is coordinated by two different groups X and Y, the substituents of the double bond become electronically nonequivalent and thus are expected to display different reactivity.

The influence of electronic asymmetry in the ligands used in enantioselective hydrogenation appears like an evidence but how can one quantify the role of this electronic asymmetry? In an attempt to answer this question, we have designed and synthesized electronically asymmetric mixed phosphine-phosphinite ligands and studied their catalytic activities in the hydrogenation of simple functionalized olefins.

2 Quantification of electronic asymmetry

2.1 Electronic asymmetry

The concept of electronic differenciation was introduced by Faller [56]. In stoechiometric nucleophilic additions to allylmolybdenum complexes $[Mo(NO)(CO)(allyl)Cp)]^+$, the stereoselectivity of the reactions may be attributed to the asymmetry in charge distribution introduced by the nitrosyl ligand compared to the carbonyl ligand. Thus, this system provides a beautiful example wherein asymmetric induction in nucleophilic attack appears to be dominated by electronic rather than steric effects. A catalytic version of electronic differenciation was probed by Cesarotti with the ligand dpopyr (Figure 3.7(a)) which possess two differenciated P atoms [57]. The enantioselectivities obtained, in allylic alkylation reactions, were very low (20 and 30 %) and this led Helmchen to think that a more pronounced difference in electronic as well as steric properties was required and, therefore, chose the combination of a hard, N, and a soft, P or S donor in the PHOX ligand (Figure 3.5) [48]. The same concept was independently adopted by the groups of Pfaltz [58], Williams [59,60] as well as Brown with a different P-N chelating ligand (QUINAP) (Figure 3.7(b)) [61].

(a) (b)

Figure 3.7 (*S*)-dpopyr (a) and (*R*)-QUINAP (b).

Togni's Josiphos ligand (Figure 3.8(a)) and its derivatives are chiral chelating phosphines derived from ferrocene and they constitute a unique class of asymmetric ligands. Their rhodium or iridium complexes hydrogenate tetra-substituted C=C bonds (used for the preparation of (+)-biotin) or an imine (intermediate in the synthesis of the herbicide (*S*)-Metalochlor) respectively (Figure 3.8(b) and (c)) [62].

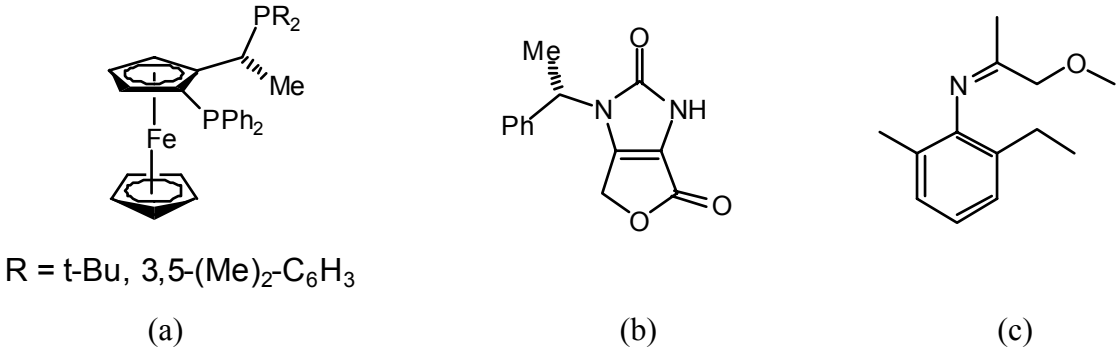

(a) (b) (c)

Figure 3.8 (*R*,*S*)-R-Josiphos (a), an intermediate in the synthesis of (+)-Biotin (b) and an intermediate in the synthesis of (*S*)-Metalochlor (c).

Depending of the nature of the substituents on the phosphine donors, Josiphos displays different catalytic activity and exhibits pronounced electronic effects on the stereoselectivity of the former reaction [63]. This has also previously been studied by Achiwa [55] in the context of his "respective control concept". He has studied the influence of the substituents on modified DIOP in various hydrogenation experiments. In particular, DIOCP ligand (which is a DIOP ligand modified by the incorporation of one bis-cyclohexyl instead of a bis-phenyl) is more effective than DIOP and Cy-DIOP in the asymmetric hydrogenation of ketopantolactone (Figure 3.9). This was confirmed by further experiments in which the cyclohexyl was replaced by other substituents considered to have less steric demand. So he concluded that, when one of the two phosphino groups is electron-rich, the activity and enantioselectivity of the catalyst is enhanced.

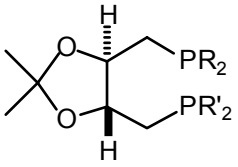

Figure 3.9 (*R*,*R*)-DIOP: R=R'=Ph; (*R*,*R*)-DIOCP: R=Cy, R'=Ph; (*R*,*R*)-Cy-DIOCP: R=R'=Cy.

Electronic effects have also been largely studied by RajanBabu in different asymmetric catalytic processes with ligands derived from glucose or fructose (Figure 3.10). Steric effects are kept constant while electronic effects are systematically varied to yield highly efficient catalysts [64-67].

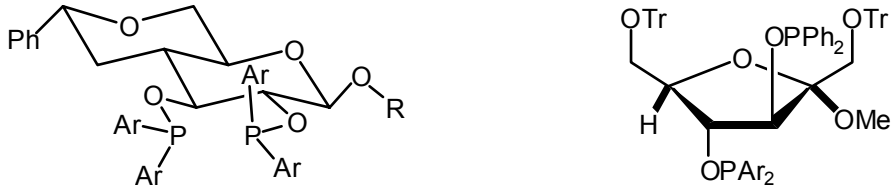

(a) (b)

Figure 3.10 Biphosphinite ligands obtained from *D*-Glucose (a) and *D*-Fructose (b).

2.2 Ligand design

In the enantioselective catalysis reactions described above, in which asymmetric ligands are involved, electronic asymmetry plays an important role in the stereoselectivity of the reaction. But, what is exactly the part due the electronic effect and mostly can the influence of the electronic asymmetry be quantified?

For this purpose, we have designed a new class of electronically asymmetric phosphine-phosphinite bidentate ligands which are *pseudo* C_S-symmetric (Scheme 3.1). This ensures that the enantioselectivity is caused by the electronic asymmetry, as the groove around the metal is nearly achiral from a steric point of view. This should allow us to quantify the importance of electronic asymmetry in various enantioselective catalytic reactions.

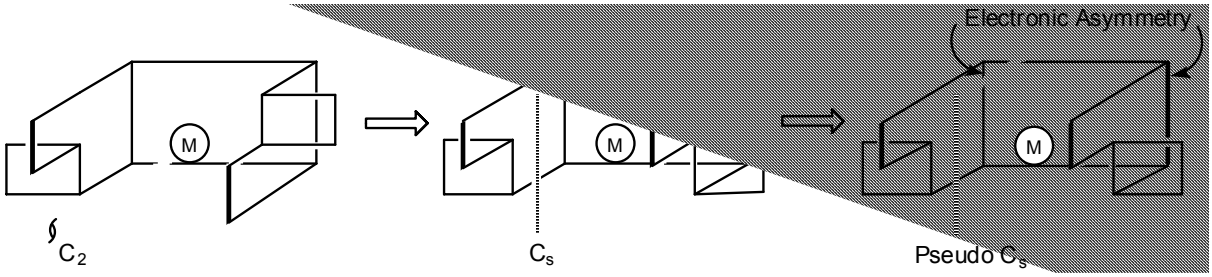

Scheme 3.1 Schematic representations of C_2, C_S and *pseudo* C_S symmetric environments around a square planar complex.

Previously in our group, Brändli described the synthesis of ligand POP, which is sterically achiral but electronically chiral (Figure 3.12) [69]. It appeared interesting to modify one arm (phosphine as well as phophinite arm) of this ligand by incorporation of an *o*-anisyl group instead of phenyl group. Thus led us to synthesize the *pseudo*-enantiomers of mixed phosphine-phophinite ligands POP$_{o\text{-An}}$ (**2**) and $_{o\text{-An}}$POP (**4**) (Figure 3.12).

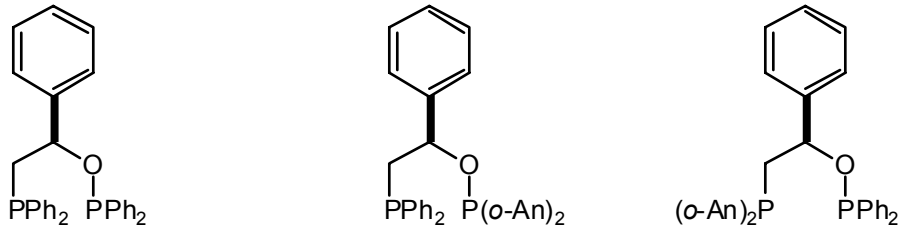

POP POP$_{o\text{-An}}$ (**2**) $_{o\text{-An}}$POP (**4**)

Figure 3.12 (*R*)-1,3-[bis(diphenylphosphin)]-2-phenyl-1-oxa-propane (POP), (*R*)-1-[bis-(*o*-methoxyphenyl)-phosphin]-3-(diphenylphosphin)-2-phenyl-1-oxa-propane (POP$_{o\text{-An}}$ (**2**)) and (*R*)-3-[bis-(*o*-methoxyphenyl)-phosphin]-1-(diphenylphosphin)-2-phenyl-1-oxa-propane ($_{o\text{-An}}$POP (**4**)).

2.3 Catalytic considerations

The POP ligand has already been tested in the asymmetric allylic alkylation of *rac*-1,3-diphenyl-2-propenyl acetate [69]. For comparison, this reaction will also be investigated with ligands POP$_{o\text{-An}}$ (**2**) and $_{o\text{-An}}$POP (**4**).

Allylic alkylation is based on *trans*-influence, which is a thermodynamic and ground-state effect. In metal complexes, the *trans*-influence is the effect of one ligand on the strength of the bond between the metal and a ligand in the *trans*-position with respect to it. The degree of enantioselectivity of the reaction depends on how well a chiral ligand in a Pd complex (for example) can direct the attack of the nucleophilic to one of the two allylic termini [70,71]. It is generally agreed that the nucleophilic attack takes place preferentially at the allylic terminus *trans* to the substitutent which possess the higher *trans* influence [72]. As shown by Togni, in a palladium-catalyzed asymmetric allylic amination using ferrocenyl phosphino-pyrazole ligand, the carbon atom *trans* to phosphorus atom is subjected to a much higher *trans* influence than the one *trans* to the pyrazole nitrogen, as refected by both the longer bond distance to palladium (Pd-$C_{trans\text{-}P}$ = 2.268 Å and Pd-$C_{trans\text{-}N}$ = 2.138 Å) [72]. These characteristics render this carbon more electrophilic than its counterpart *trans* to nitrogen. Thus, a nucleophile will attack $C_{trans\text{-}P}$.

Studies achieved by Brändli on mixed phosphine-phophinite ligands POP and POPPY (POPPY: (*R*)-3-diphenylphosphin-1-dipyrrolylphosphin-2-phenyl-1-oxa-propane) and their palladium complexes have shown that the differences of bond lenghts Pd-C or Pd-Cl in the complexes is not significant ([Pd(η^3-$Ph_2C_3H_3$)(POPPY)](OTf): Pd-$C_{trans\text{-}PO}$ = 2.252 Å and Pd-$C_{trans\text{-}P}$ = 2.219 Å and [$PdCl_2$(POP)]: Pd-$Cl_{trans\text{-}PO}$ = 2.351 Å and Pd-$Cl_{trans\text{-}P}$ = 2.338 Å) [69]. So we can conclude that *trans*-influence of phosphine and phosphinite are nearly identical.

Hydrogenation is based on *trans*-effect [73] which is a kinetic effect relating to the transition state. It is defined as "the effect of a coordinated group on the rate of substitution reaction of ligands *trans* to itself" [74]. Since the design of the ligands is more appropriate, the main study on these ligands is focused on the hydrogenation of olefins.

3 Synthesis of mixed phosphine-phosphinite ligands and their

platinum and rhodium complexes

3.1 *Pseudo*-enantiomer ligand syntheses

3.1.1 Synthesis of ligand $POP_{o\text{-}An}$ (2)

$Et_2NP(o\text{-}An)_2$ (**1**) is obtained by the nucleophilic substitution of the two chlorides of Et_2NPCl_2 by two *ortho*-lithiated molecules of anisole. $Et_2NP(o\text{-}An)_2$ (**1**) is acidified by HCl(g) to form $ClP(o\text{-}An)_2$. Addition of one equivalent of (*R*)-2-diphenylphosphin-1-phenyl-ethanol in the presence of base leads to the desired ligand $POP_{o\text{-}An}$ (**2**) (Scheme 3.2).

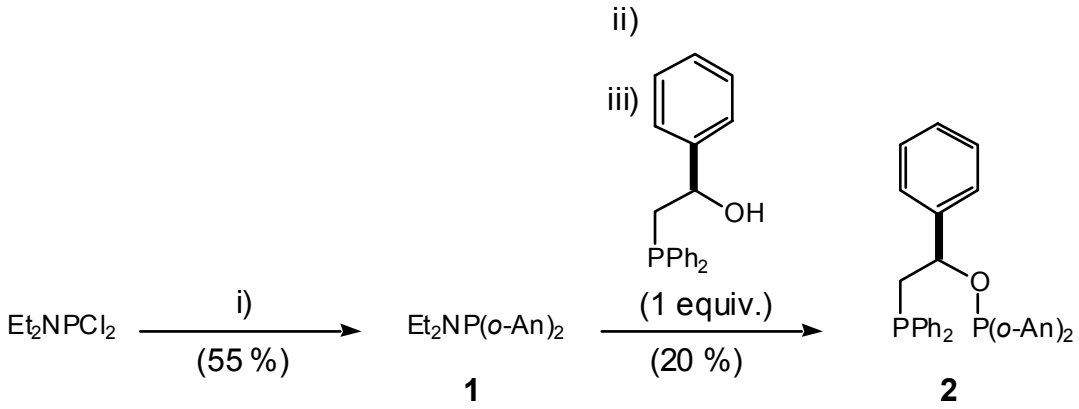

Scheme 3.2 Synthesis of ligand $POP_{o\text{-}An}$ (**2**).

i) Anisole (2 equiv.), TMEDA (2 equiv.), *n*-BuLi (2 equiv.), hexane, r.t. ii) HCl(g), ether, r.t. iii) NEt_3, ether, -20°C.

3.1.2 Synthesis of ligand $_{o\text{-}An}$POP (4)

The epoxyde ring of (*R*)-phenyloxirane is opened in the presence of base and bis-(*o*-methoxyphenyl)-phosphine leading to the formation of the phosphino alcohol **3**. Deprotonation by triethylamine and addition of chlorodiphenylphosphine gives the *pseudo*-enantiomer $_{o\text{-An}}$POP (**4**). To avoid degradation of the phosphine-phosphinite ligand **4**, borane protection proved beneficial in some cases. The deprotection of ligand **5** is achieved by action of DABCO in toluene (Scheme 3.3).

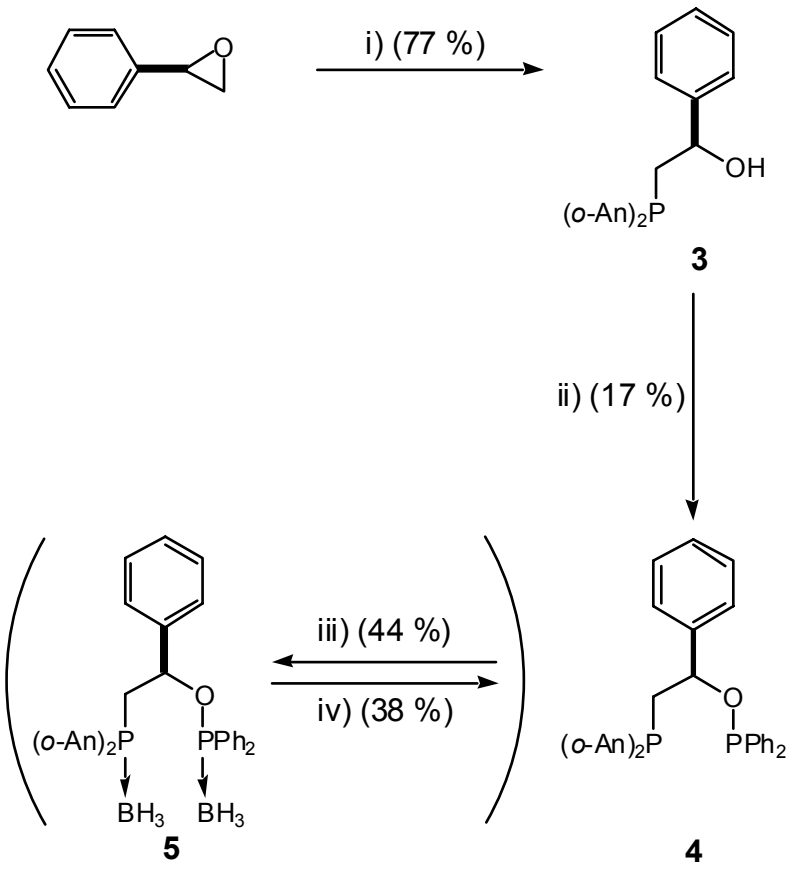

Scheme 3.3 Synthesis of ligand $_{o\text{-An}}$POP (**4**).

i) HP(*o*-An)$_2$ (1 equiv.), 50% aqueous solution KOH (1.25 equiv.), DMSO, 45˚C. ii) ClPPh$_2$ (1.1 equiv.), NEt$_3$ (1.5 equiv.), ether, -40˚C. iii) BH$_3$·SMe$_2$ (3 equiv.), ether, r.t. iv) DABCO (30 equiv.), toluene, r.t.

3.2 Platinum and rhodium complexes: synthesis and characterization

3.2.1 Overview of complexes: synthesis and characterization

The synthesis of metallic complexes of the ligands POP$_{o\text{-An}}$ (**2**) and $_{o\text{-An}}$POP (**4**) is important for structural (X-ray structure) and reactivity (^{31}P and ^{1}H NMR) studies of the two *pseudo*-enanantiomers. In particular, rhodium complexes are interesting because of their use in the catalytic hydrogenations. Rhodium complexes crystalize less easily than inert platinum complexes. Therefore, for metric comparison, square planar platinum complexes were synthesized.

3.2.2 Platinum complexes: [Pt(POP$_{o\text{-An}}$)Cl$_2$] (6) and [Pt($_{o\text{-An}}$POP)Cl$_2$] (7)

Platinum complexes of ligands POP$_{o\text{-An}}$ (**2**) and $_{o\text{-An}}$POP (**4**) are obtained by reaction of the ligands with [Pt(DMSO)Cl$_2$] in CH_2Cl_2 to give the corresponding complexes [Pt(POP$_{o\text{-An}}$)Cl$_2$] (**6**) and [Pt($_{o\text{-An}}$POP)Cl$_2$] (**7**). These complexes have been characterized by NMR and especially ^{31}P NMR which is a rapid and simple method to follow the metal-phosphorus bond formation (Pt-P coupling constants). The synthetic route is outlined in Scheme 3.4.

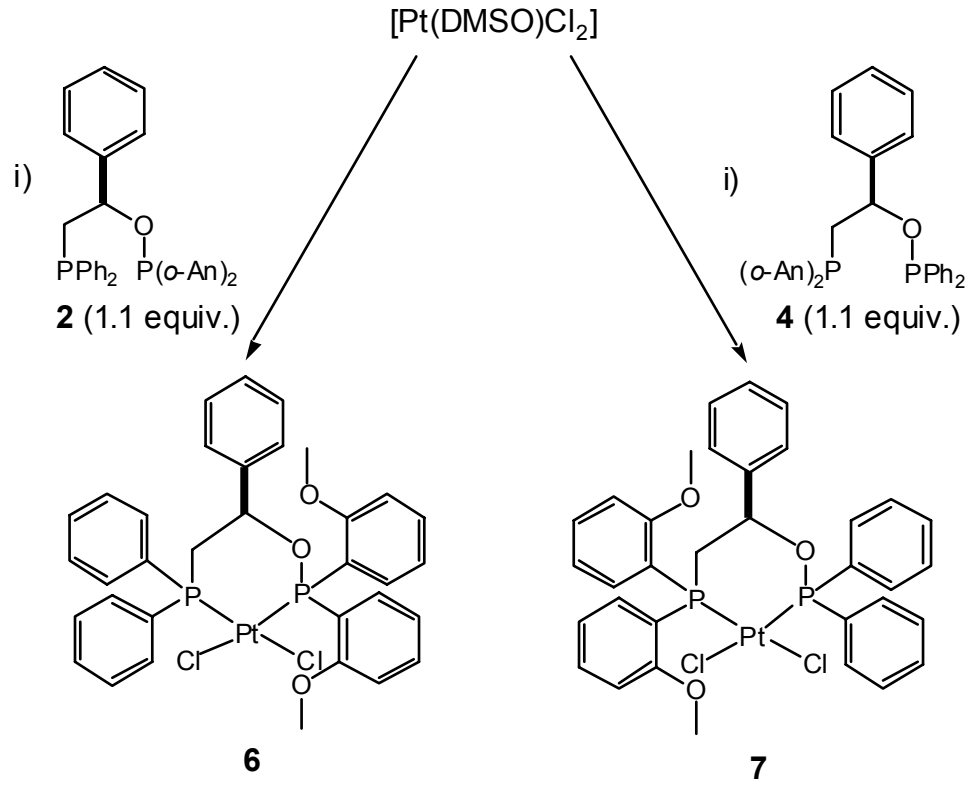

Scheme 3.4 Synthesis of platinum complexes **6** and **7**.
i) CH_2Cl_2.

Suitable crystals of [Pt($_{o}$-AnPOP)Cl_2] (**7**) for X-ray analysis are obtained by slow diffusion of hexane through the solvent of the reaction.The crystal structure of platinum complex [Pt($_{o}$-AnPOP)Cl_2] (**7**) is represented in Figure 3.13 and a selection of bond lengths and angles is collected in Table 3.1.

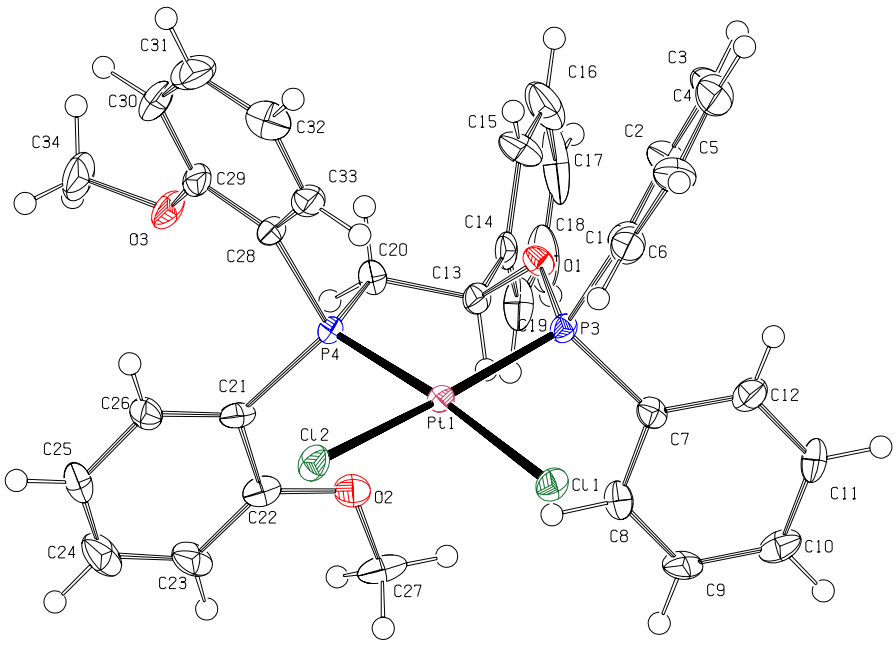

Figure 3.13 Molecular structure of [Pt(o-^{An}POP)Cl_2] (**7**). Thermal ellipsoids are at the 50% probability level. Solvent molecules (2 CH_2Cl_2) have been omitted for clarity.

Table 3.1 Selected bond lengths [Å] and angles [°] for [Pt(o-^{An}POP)Cl_2] (**7**).

	[Pt(o-^{An}POP)Cl_2] (**7**)
Pt(1)-P(3)	2.200(3)
Pt(1)-P(4)	2.242(2)
Pt(1)-Cl(1)	2.3562(19)
Pt(1)-Cl(2)	2.369(2)
P(3)-Pt(1)-P(4)	94.55(8)
P(3)-Pt(1)-Cl(1)	88.02(8)
P(4)-Pt(1)-Cl(1)	174.84(8)
P(3)-Pt(1)-Cl(2)	172.76(9)
P(4)-Pt(1)-Cl(2)	88.44(8)
Cl(1)-Pt(1)-Cl(2)	89.54(8)

The distances Pt-Cl (2.356 and 2.369 Å) are very close, this confirms the fact that in the ligand, phosphine and phosphinite have the same *trans*-influence. Platinum-phosphorus bond lengths (Pt-P(3) = 2.200 Å and Pt-P(4) = 2.242 Å) are concomittant with values

expected (observed range for Pt-P bond lenghts is 2.14 to 2.42 Å [75]). Unfortunately, no crystalline material of platinum complex [Pt(POP$_{o\text{-An}}$)Cl$_2$] (**6**) could be obtained.

3.2.3 Rhodium complexes: [Rh(COD)(POP$_{o\text{-An}}$)]$^+$ (8) and [Rh(COD)($_{o\text{-An}}$POP)]$^+$ (9)

Rhodium complexes [Rh(COD)(POP$_{o\text{-An}}$)]$^+$ (**8**) and [Rh(COD)($_{o\text{-An}}$POP)]$^+$ (**9**) are obtained as tetrafluoroborate salts by reaction of the ligands POP$_{o\text{-An}}$ (**2**) and $_{o\text{-An}}$POP (**4**) with [Rh(COD)$_2$](BF$_4$) in CH_2Cl_2. The synthetic route is outlined in Scheme 3.5. Unfortunately, crystals of rhodium complexes could not be obtained but results of NMR analysis and in particular ^{31}P NMR are characteristic of metal-phosphorus bond formation. Rh-P coupling constants of complex (**8**)(BF$_4$) ($J_{P\text{-}Rh}$ = 150.4 Hz) are slightly higher than those observed with complex (**9**)(BF$_4$) ($J_{P\text{-}Rh}$ = 145.2).

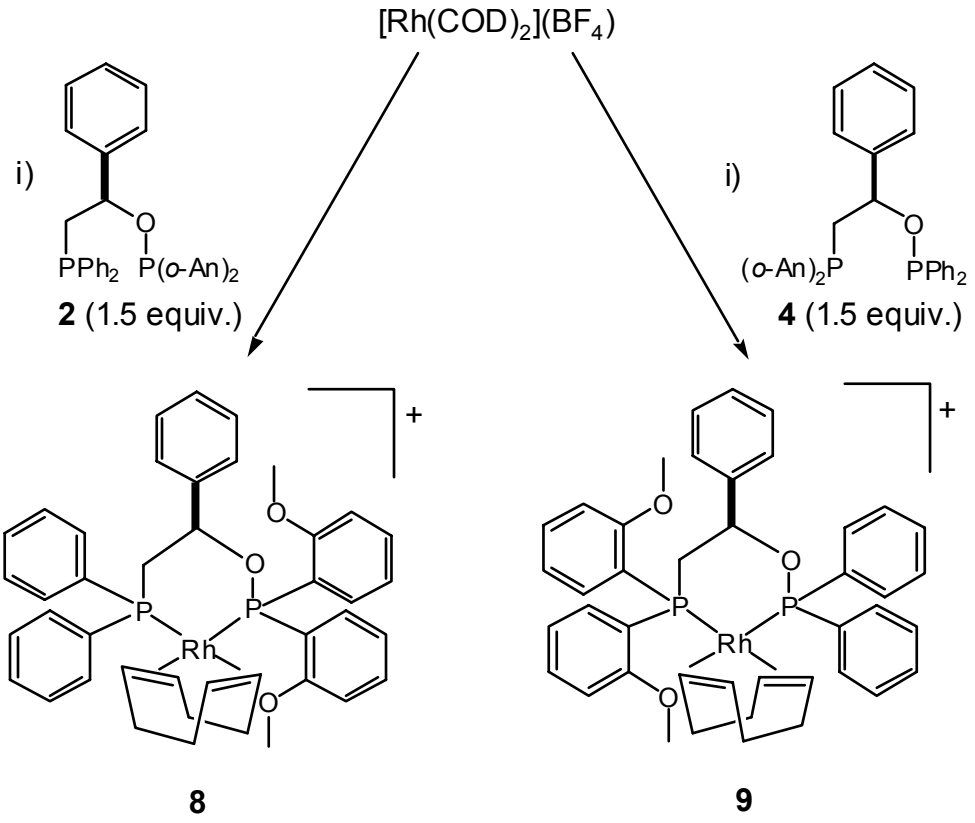

Scheme 3.5 **Synthesis of rhodium cationic salts** 8 **and** 9**.**
i) CH_2Cl_2.

4 Catalysis experiments

4.1 Asymmetric allylic alkylation

The two *pseudo*-enantiomers POP$_{o\text{-An}}$ (**2**) and $_{o\text{-An}}$POP (**4**) were tested in asymmetric allylic alkylation of *rac*-1,3-diphenyl-2-propenyl acetate (Scheme 3.6). Relevant results are summarized in Table 3.2.

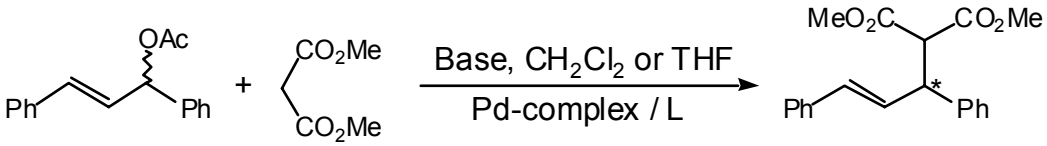

Scheme 3.6 Asymmetric allylic alkylation of *rac*-1,3-diphenyl-2-propenyl acetate catalyzed by [Pd(L)allyl]$^+$.

Table 3.2 Asymmetric allylic alkylation of *rac*-1,3-diphenyl-2-propenyl acetate catalyzed by palladium complex [PdClX]$_2$ (X = η□-C_3H_5 or η□-$C_{13}H_{15}$) and ligands POP$_{o\text{-An}}$ (**2**) or $_{o\text{-An}}$POP (**4**).

entry	ligand	equiv. L/Pd	[PdClX]$_2$ X=	solvent	base	%conv.[a]	%ee[a] (conf.)
1)	**2**	1/1	η□-C_3H_5	CH_2Cl_2	BSA/KOAc	100	5.5 (*R*)
2)	**2**	2/1	η□-C_3H_5	CH_2Cl_2	BSA/KOAc	100	12 (*S*)
3)	**2**	5/1	η□-C_3H_5	CH_2Cl_2	BSA/KOAc	100	7 (*S*)
4)	**2**	1/1	η□-$C_{13}H_{15}$	CH_2Cl_2	BSA/KOAc	100	2 (*R*)
5)	**2**	2/1	η□-$C_{13}H_{15}$	CH_2Cl_2	BSA/KOAc	100	2 (*R*)
6)	**2**	5/1	η□-$C_{13}H_{15}$	CH_2Cl_2	BSA/KOAc	100	4 (*R*)
7)	**4**	1/1	η□-$C_{13}H_{15}$	CH_2Cl_2	BSA/KOAc	100	14 (*S*)

8)	**4**	5/1	η□-$C_{13}H_{15}$	CH_2Cl_2	BSA/KOAc	100	25 (*S*)
9)	**2**	1/1	η□-$C_{13}H_{15}$	CH_2Cl_2/THF	NaH	100	0
10)	**2**	2/1	η□-$C_{13}H_{15}$	CH_2Cl_2/THF	NaH	100	2 (*S*)

[a] %conv. and %ee determined by HPLC analysis with a chiral stationary phase column (Daicel Chiralcel OD-H, 98/2 hexane/i-PrOH, flow 0.5 ml/min). t_R(*R*): 16.5 min, t_R(*S*): 17.7 min.

Allylic alkylation reactions can be performed in two different ways: deprotonation of dimethyl malonate by action of BSA in CH_2Cl_2 (entries 1 to 8) or by NaH in THF (entries 9 and 10). Because results are slightly better and also because reactions with BSA are easier and faster to carry out, this method was prefered to compare the activity of the ligands. In CH_2Cl_2 as solvent and BSA as base, two catalysts were tested: $[Pd(\eta^{□}\text{-}C_3H_5)Cl]_2$ and $[Pd(\eta^{□}\text{-}C_{13}H_{15})Cl]_2$ and proportions L/Pd varied (L = $POP_{o\text{-}An}$ (**2**) or $_{o\text{-}An}POP$ (**4**)).

As for ligand POP [69] the results are disappointing. Reactions are quantitative (100% conversion) but the enantiomeric excesses are very small. With $[Pd(\eta^{□}\text{-}C_3H_5)Cl]_2$ and ligand **2** as catalyst (entries 1 to 3), the absolute configuration of the product, which should be constant for one ligand, changes from *R* to *S*, depending of the number of equivalents of ligand added. But, ee are two small to conclude anything. Moreover, using $[Pd(\eta^{□}\text{-}C_3H_5)Cl]_2$ as catalyst, ligand **2** gives very poor ee close to zero (entries 4 to 6), one can suspect that ligand **2** has no enantioselective activity in the reaction. In the same conditions, reaction with ligand **4** ee gives better results but ee are not higher than 25% (entries 7 and 8).

Nevertheless, it is not surprising because asymmetric allylic alkylation which is based on thermodynamic factors (bond lenghts) is not appropriate to test the concept of the designed ligands. That is why hydrogenation of olefins, which is based on kinetic considerations, has been investigated with the ligands $POP_{o\text{-}An}$ (**2**) and $_{o\text{-}An}POP$ (**4**).

4.2 Hydrogenation of prochiral olefins

The two *pseudo*-enantiomers $POP_{o\text{-}An}$ (**2**) and $_{o\text{-}An}POP$ (**4**) as well as POP were tested in the hydrogenation of *N*-acylaminoacrylic acids and esters such as those described in Scheme 3.7.

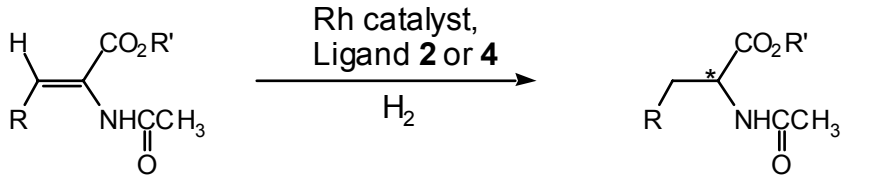

R = Ph or H
R' = Me or H

10 R = H, R' = H
11 R = H, R' = Me
12 R = Ph, R' = H
13 R = Ph, R' = Me

Scheme 3.7 Typical enantioselective hydrogenation reactions.

Results obtained in hydrogenation experiments are satisfactory. Reactions are quantitative (100% conversion) and enantiomeric excess relatively high for ligand **2** (80 %ee (*R*), entries 2, 4 and 10) and ligand **4** (36 %ee (*S*), entries 6 and 11). Under these conditions, hydrogenations with the POP ligand, despite quantitative conversion, give no enantiomeric excess. Enantiomeric excess obtained using $[Rh(COD)Cl]_2$ in ethanol or $[Rh(COD)_2](BF_4)$ in CH_2Cl_2 are more or less the same (entries 4 and 10). Hydrogenation of acid versus its analogous ester gives also the same enantiomeric excess (entries 1 and 2).

Table 3.3 Enantioselective hydrogenation of *N*-acylaminoacrylic acids and esters[a].

entry	product	ligand	Rh catalyst	solvent	%ee[b] (conf.)
1)	**10**	**2**	$[Rh(COD)Cl]_2$	ethanol	79 (*R*)
2)	**11**	**2**	$[Rh(COD)Cl]_2$	ethanol	80 (*R*)
3)	**12**	**2**	$[Rh(COD)Cl]_2$	ethanol	78 (*R*)
4)	**13**	**2**	$[Rh(COD)Cl]_2$	ethanol	80 (*R*)
5)	**10**	**4**	$[Rh(COD)Cl]_2$	ethanol	35 (*S*)
6)	**11**	**4**	$[Rh(COD)Cl]_2$	ethanol	36 (*S*)
7)	**12**	**4**	$[Rh(COD)Cl]_2$	ethanol	21 (*S*)
8)	**13**	**4**	$[Rh(COD)Cl]_2$	ethanol	23 (*S*)
9)	**11**	**2**	$[Rh(COD)_2](BF_4)$	CH_2Cl_2	72 (*R*)
10)	**13**	**2**	$[Rh(COD)_2](BF_4)$	CH_2Cl_2	80 (*R*)
11)	**11**	**4**	$[Rh(COD)_2](BF_4)$	CH_2Cl_2	36 (*S*)
12)	**13**	**4**	$[Rh(COD)_2](BF_4)$	CH_2Cl_2	22 (*S*)

[a] 100% conv., 48 h, 2 bars, r.t., 5%Rh, L/Rh 1.5/1, $[Rh(COD)Cl]_2$ in ethanol or $[Rh(COD)_2](BF_4)$ in CH_2Cl_2

[b] Determined by GC on chiral stationary phase (CHIRASIL-Val)

With the aim of quantifying electronic asymmetry, we have planned to use the Curtin-Hammett principle. This principle, which has been proposed in the 1950s by D.Y. Curtin and G.P. Hammett [68], says that in a chemical irreversible reaction that yields two enantiomers *R* and *S*, the product composition is controlled only by the difference in standard free energies ($\partial\Delta G^{\neq}$) of the respective transition states (Figure 3.11). Thus, the difference $\partial\Delta G^{\neq}$ can be expessed in function of the proportion of enantiomers *R* and *S* obtained in a reaction, by the relation $\ln [R]/[S] = \partial\Delta G^{\neq} / RT$, and we can plot the curve $\partial\Delta G^{\neq}$=f(ee) (Curve 3.1).

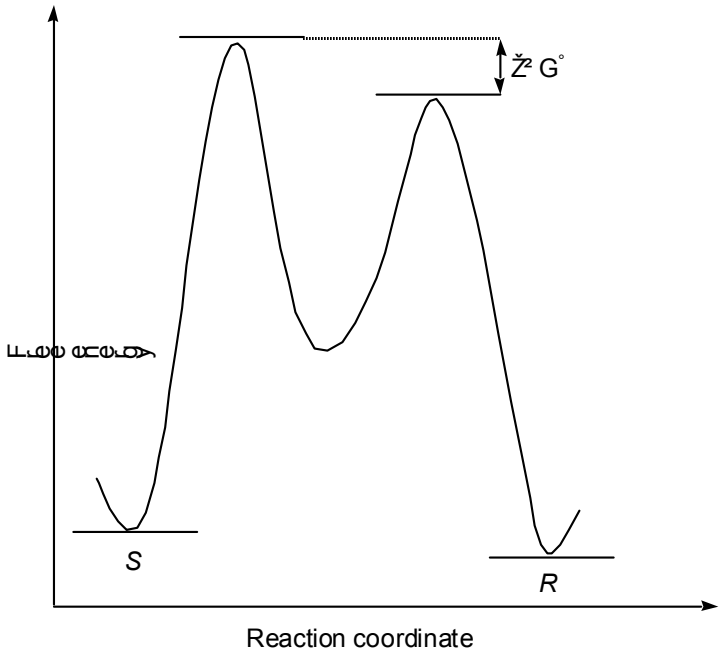

Figure 3.11 Representation of the energetic profile for the transformation of a prochiral substate into enantiomers *R* and *S*.

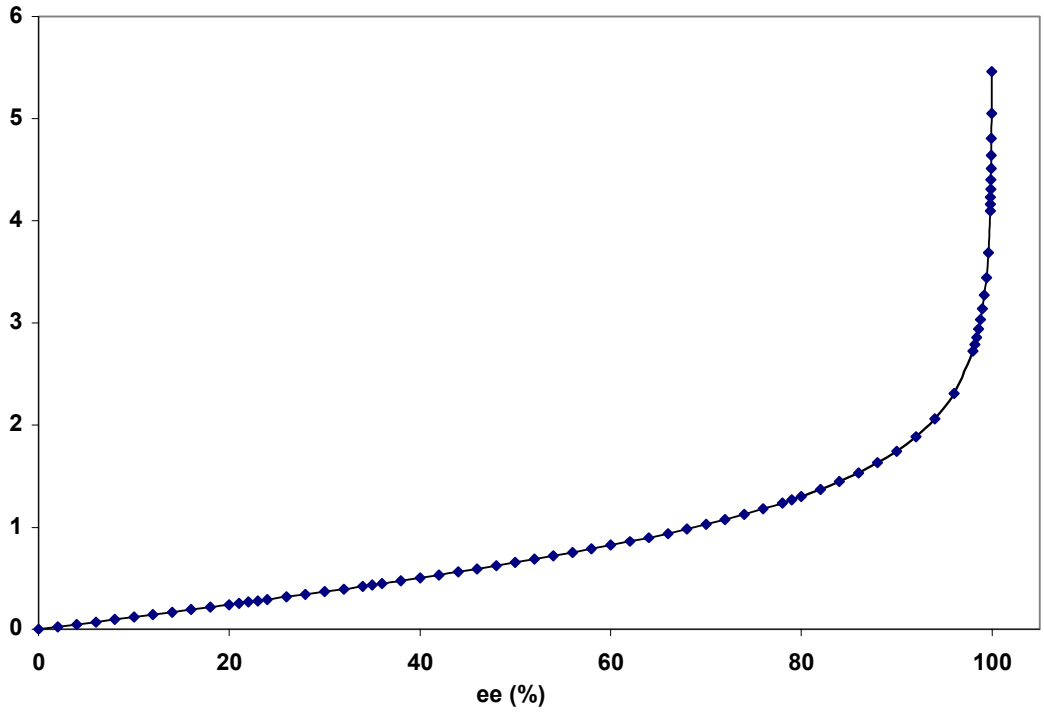

Curve 3.1 Curtin-Hammett Principle: $\partial \Delta G^{\neq} = f(ee)$, with R = 1.99 cal/K/mol and T = 298 K.

We have calculated, according to the Curtin-Hammett principle, the observed ($\partial\Delta G^{\neq}_{obs}$) and theorical ($\partial\Delta G^{\neq}_{th}$) values for the difference of free energy $\partial\Delta G^{\neq}$ as a function of enantiomeric excess. The difference between the enantiomeric excess expected for enantiomeric ligands (i.e. CH_2 instead of oxygen atom) (ee_{th}) and those obtained because of their *pseudo*-enantiomeric structure (ee_{obs}) is due to electronic asymmetry. Or in terms of free energy, the difference $\partial\Delta G^{\neq}_{obs}$-$\partial\Delta G^{\neq}_{th}$ yields the contribution of electonic asymmetry in the reaction. The results are summarized in Table 3.4.

We can observe that the contribution of electronic asymmetry in the reactions studied fluctuates between 0.63 and 1.03 kcal/mol (entries 5 and 6). Esters (products **11** and **13**) give slightly higher differences of $\partial\Delta G^{\neq}$ than their analogous acids (products **10** and **12**). Better differences are also obtained with *N*-acetyl phenylalanine **12** (and its methyl ester **13**) as product of the hydrogenation compared to *N*-acetyl alanine **10** (and its methyl ester **11**). And finally, the biggest effect of electronic asymmetry of the ligands (1.02 and 1.03 kcal/mol, entries 4 and 6) is observed in the case of the hydrogenated product **13** (*N*-acetyl phenylalanine methyl ester).

Table 3.4 Quantification of electronic asymmetry.

entry	L	product	$\%ee_{obs}$ (R)	$\partial\Delta G^{\neq}_{obs}$[a]	$\%ee_{th}$ (R)	$\partial\Delta G^{\neq}_{th}$	$\partial\Delta G^{\neq}_{obs}$- $\partial\Delta G^{\neq}_{th}$
1)	**2**	**10**	79	1.27			
	4		- 35	- 0.43	- 79	- 1.27	0.84
2)	**2**	**11**	80	1.30			
	4		- 36	- 0.45	- 80	- 1.30	0.85
3)	**2**	**12**	78	1.24			
	4		- 21	- 0.25	- 78	- 1.24	0.99
4)	**2**	**13**	80	1.30			
	4		- 23	- 0.28	- 80	- 1.30	1.02
5)	**2**	**11**	72	1.08			
	4		- 36	- 0.45	- 72	- 1.08	0.63
6)	**2**	**13**	80	1.30			
	4		- 22	- 0.27	- 80	- 1.30	1.03

[a] $\partial\Delta G^{\neq}$ in kcal/mol

5 Conclusion

With the aim of quantifying electronic asymmetry, *pseudo*-enantiomers of mixed phosphine-phosphinite ligands have been designed for use in hydrogenation of prochiral olefins.

Electronically asymmetric ligands $POP_{o\text{-}An}$ (**2**) and $_{o\text{-}An}POP$ (**4**) have been synthesized and characterized by X-ray crystallography and ^{31}P NMR spectroscopy. After hydrogenation catalysis with the two *pseudo*-enantiomers, we can conclude that the hydrogenation of prochiral olefins (derivatives of *N*-acetamidoacrylic acids and esters) is induced electronically by use of mixed phosphine-phosphinite ligands **2** and **4**.

The results obtained in quantification of electronic asymmetry induced by asymmetric ligands, in enantioselective hydrogenation reactions are promising and stimulate us to continue the studies on this type of ligand. Based on the same concept, we project to study the influence of electronically asymmetric *pseudo*-enantiomers of POP ligand-type, mixing substituents such as cyclohexyl, pyrrol, phenyl, *o*-anisyl, *o*-ethylphenyl.

6 Experimental Section

6.1 General considerations

NMR spectra were recorded on either a VARIAN XL 200 or BRUKER AMX 400. Chemical shifts are given in ppm and coupling constant in Hz. Signals are referenced against H_3PO_4 (^{31}P, external reference) and tetramethylsilane (^{1}H, ^{13}C, internal reference).
All experiments were carried out under a nitrogen atmosphere using standard Schlenk techniques.
Solvents (THF, ether, CH_2Cl_2, hexane) were distilled under nitrogen with standard desicating agents or degassed prior to use (DMSO, ethanol).
Bis-(*o*-methoxyphenyl)-phosphine was synthesized from P(*o*-An)$_3$ [76] or PCl_3 [77]; the synthesis of $Et_2NP(o\text{-An})_2$ was inspired by litterature method [78]; (*R*)-2-diphenylphosphin-1-phenyl-ethanol [69], (*R*)-1,3-bis-(diphenylphosphin)-2-phenyl-1-oxa-propane (POP) [69] and $[Pt(DMSO)_2Cl_2]$ [79] were synthesized according to litterature methods.

6.2 Syntheses

***N*, *N*- Diethylamino-bis-(*o*-methoxyphenyl) phosphine** (Compound **1**)

Anisole (6.25 ml, 58 mmol) and TMEDA (8.6 ml, 58 mmol) were dissolved in hexane (150

ml), cooled at 0˚C and then a solution 1.6M of *n*-BuLi (36 ml, 58 mmol) was slowly added. The reaction mixture was stirred 20 h at r.t. A solution of Et_2NPCl_2 (4.2 ml, 28.7 mmol) in hexane (20 ml) was added to the resulting suspension and the mixture was once again stirred 20 h at r.t. After hydrolizing, the product was extracted with CH_2Cl_2, dried over $MgSO_4$ and evoporated to dryness. After recrystallisation in hexane the product **1** was obtained as a white powder (5.0 g, 55% yield).

^{1}H NMR ($CDCl_3$): 0.89 (t, J = 7.0, 6H, CH_3); 3.02 (quint., 4H, CH_2); 3.72 (s, 6H, arom. CH_3); 6.88-7.60 (m, 8 arom. H).

^{13}C NMR ($CDCl_3$): 13.9, 57.11, 57.19 (CH_3); 42.18, 42.22 (CH_2); 112.95, 113.01, 122.43, 122.63, 134.97, 135.63, 138.45, 138.58 (CH); 105.70, 106.75, 161.75, 161.78 (arom. C).

^{31}P{^{1}H} NMR ($CDCl_3$): 42.0 (s).

ESI-MS (CH_2Cl_2/i-PrOH): 318.3 ($[M + 1]^+$).

(*R*)-1-[Bis-(*o*-methoxyphenyl)-phosphin]-3-(diphenylphosphin)-2-phenyl-1-oxa-propane

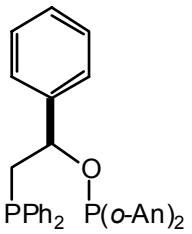

Compound $POP_{o\text{-An}}$ (**2**)

A solution of **1** (1.74 g, 5.49 mmol) in ether (200 ml) was acidified with $HCl_{(g)}$ during 15 min. The suspension was then filtered and the solution was evaporated to dryness to afford $ClP(o\text{-}An)_2$ as a white powder. To a solution of chloro di(*o*-anisyl)phosphine (1.54 g, 5.49 mmol) in ether (150 ml) was added a solution of (*R*)-2-diphenylphosphin-1-phenyl-ethanol (1.68 g, 5.49 mmol) and NEt_3 (4.14 ml, 30 mmol) in ether (50 ml) at –20˚C. The mixture was stirred 24 h at r.t. and after filtration over celite, the solution was evaporated to dryness affording **2** as a white gum. The crude product was purified by flash chromatography on neutral alox using toluene as eluant to afford **2** as a white powder (620 mg, 20% yield).

^1H NMR ($CDCl_3$): 2.63 (dd, J = 7.2, J = 13.6, 1H, CH_2); 3.55 (s, CH_3); 3.74 (s, CH_3); 3.00 (dd, CH_2); 5.05 (quint., J = 7.0, CH); 6.71-7.45 (m, 23 arom. H).

^{13}C NMR ($CDCl_3$): 55.59, 55.87 (CH_3); 39.76, (d, $J_{C\text{-}P}$ = 15.2, CH_2); 121.25, 121.34, 121.36, 121.49, 121.50, 126.90, 127.61, 127.63, 128.24, 128.47, 128.51, 128.61, 128.70, 128.84, 128.90, 128.92, 128.98, 129.07, 129.11, 129.20, 131.10, 131.24, 132.08, 132.13, 133.28, 133.54, 133.55, 133.81, 135.92, 136.20 (CH); 110.46, 111.23, 138.92, 139.52, 160.51, 160.83, 161.08 (arom. C).

$^{31}P\{^1H\}$ NMR ($CDCl_3$): -23.00 (d, $^4J_{P\text{-}P}$ = 2.7, PCH_2); 92.00 (d, PO).

ESI-MS (CH_2Cl_2/i-PrOH): 589.2 ($M + K^+$).

(*R*)-2-[Bis-(*o*-methoxyphenyl)-phosphin]-1-phenyl-ethanol

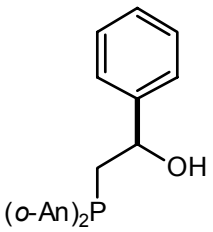

Compound **3**

To a solution of bis-(*o*-methoxyphenyl)-phosphine (0.70 g, 2.8 mmol) and a 50% aqueous solution of KOH (3.5 mmol) in DMSO (50 ml) was added dropwise the (*R*)-phenyloxirane (0.33 ml, 2.8 mmol) in DMSO (10 ml) at 45˚C. After heating one night at 45˚C, the mixture

was diluted water and extracted with toluene. The organic extract was dried over Na_2SO_4 and evaporated under vaccum to afford compound **3** as a white powder (0.80 g, 77% yield).

^1H NMR ($CDCl_3$): 2.75 (m, CH_2); 3.25 (brs, 6H, CH_3); 5.05 (m, CH); 6.29-7.40 (m, 13 arom. H).

^{13}C NMR ($CDCl_3$): 56.32, 56.63 (CH_3); 42.57 (d, J = 14.3, CH_2); 127.11, 127.26, 127.33, 127.43, 127.55, 127.77, 127.82, 128.39, 128.58, 131.64, 131.67, 132.81, 132.90, 133.62, 133.73 (CH); 108.66, 109.27, 159.82, 160.38, 160.76 (arom. C).

$^{31}P\{^1H\}$ NMR ($CDCl_3$): -41.1 (s).

ESI-MS (CH_2Cl_2/i-PrOH): 367.1 ($[M + 1]^+$).

(*R*)-3-[Bis-(*o*-methoxyphenyl)-phosphin]-1-(diphenylphosphin)-2-phenyl-1-oxa-propane

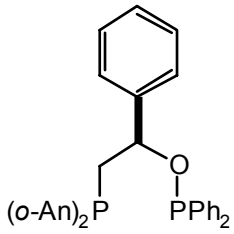

Compound $_{o\text{-An}}$POP (**4**)

A solution of alcohol **3** (0.81 g, 2.2 mmol) in ether (70 ml) and NEt_3 (0.45 ml, 3.3 mmol) was added to a solution of chlorodiphenylphosphine (0.44 ml, 2.4 mmol) in ether (35 ml) cooled at –40˚C. The mixture was stirred overnight at r.t. and after filtration over celite, the solution was evaporated to dryness. The crude product was then borane protected, purified by flash chromatography, deprotected and purified again by flash chromatography under nitrogen to

afford the pure phosphine **4** as a white gum (0.2 g, 17% overall).

^{1}H NMR (C_6D_6): 2.94 (dd, J = 7.0, J = 15.0, 1H, CH_2); 3.15 (s, CH_3); 3.19 (s, CH_3); 3.27 (dd, 1H, CH_2); 5.30 (quint., J = 7.0, CH); 6.39-7.80 (m, 23 arom. H).

^{13}C NMR (C_6D_6): 55.60, 55.86 (CH_3); 39.76 (d, J = 14.8, CH_2); 127.99, 128.21, 128.24, 128.32, 128.43, 128.57, 128.63, 128.65, 128.73, 128.80, 128.86, 128.92, 129.07, 129.19, 129.26, 129.38, 129.59, 130.84, 130.99, 131.77, 131.85, 133.01, 133.20, 133.32, 133.51, 139.39, 139.52 (CH); 111.22, 112.67, 143.09, 144.52, 160.83, 161.08, 161.26 (arom. C).

^{31}P{^{1}H} NMR (C_6D_6): -34.69 (d, $^4J_{P\text{-}P}$ = 4.4, PCH_2); 110.33 (d, PO).

ESI-MS (CH_2Cl_2/i-PrOH): 589.1 ($M + K^+$).

(*R*)-3-[Bis-(*o*-methoxyphenyl)-phosphinborane]-1-(diphenylphosphinborane)-2-phenyl-1-oxa-propane

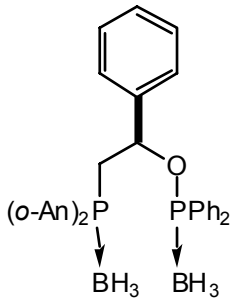

Compound **5**

A solution (94%) of borane methyl sulfide complex (0.7 ml, 6.5 mmol) was added to a solution of phosphine **4** (1.2 g, 2.2 mmol) in ether (50 ml) and the mixture was stirred at r.t. for 2 h. After addition of ethyl acetate (50 ml) the resulting solution was hydrolized with HCl 1M and the organic phase was dried over Na_2SO_4 and then evaporated. The crude product was purified by flash chromatography on silicagel (ethylacetate/hexane 2.5:7) to give the phosphine borane **5** as a white powder (0.56 g, 44 % yield).

^{1}H NMR ($CDCl_3$): 1.35 (br s, 6H, BH_3); 2.65-3.15 (m, CH_2); 3.36 (br s, 6H, CH_3); 5.90 (m, CH); 6.12-7.72 (m, 23 arom. H).

^{13}C NMR ($CDCl_3$): 51.64, 51.47 (CH_3); 35.70 (CH_2); 127.59, 128.51, 128.54, 128.62, 129.33, 129.47, 129.53, 129.66, 129.74, 129.81, 130.16, 130.22, 130.27, 130.39, 130.48, 130.57, 131.64, 131.89, 132.67, 132.75, 135.11, 135.20, 135.27, 135.31 (CH); 111.29, 112.52, 143.69, 143.89, 161.83, 163.18, 163.56 (arom. C).
$^{31}P\{^{1}H\}$ NMR ($CDCl_3$): 12.8 (br s, PCH_2); 106.5 (br s, PO).

ESI-MS (CH_2Cl_2/i-PrOH), positive mode: 563.2 ($[M\text{-}1\text{-}BH_3]^+$), negative mode: 559.3 ($[M\text{-}1\text{-}H_2O]^-$).

Deprotection:

The phosphine borane **5** (0.56 g, 1 mmol) was dissolved in toluene (50 ml) containing DABCO (3.30 g, 30 mmol) and the mixture was stirred for 2 days at r.t.
The DABCO in excess was eliminated by washing with a buffer solution pH=8 and the organic phase was evaporated. The crude product was purified by flash chromatography under nitrogen on neutral alox (ethylacetate/hexane 8:7) to afford the phosphine **4** as a white gum (0.2 g, 38%).

[Pt(POP$_{o\text{-An}}$)Cl$_2$]

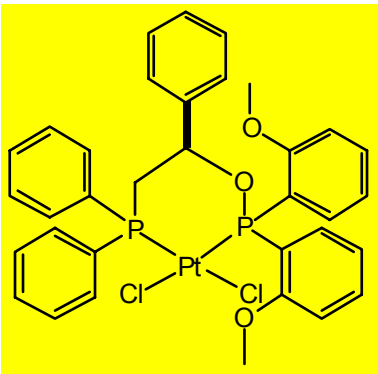

Compound **6**

A solution of the ligand **2** (10 mg, 0.018 mmol) in CH_2Cl_2 (1 ml) was added to a solution of $[Pt(DMSO)_2Cl_2]$ (7 mg, 0.016 mmol) in CH_2Cl_2 (1 ml). The mixture was stirred a few minutes and then let at r.t. overnight. Colorless crystals of **6** were obtained by slow diffusion of hexane through a CH_2Cl_2 solution.

^1H NMR ($CDCl_3$): 2.50-2.80 (m, CH_2); 3.49 (s, CH_3); 3.86 (s, CH_3); 4.90-5.10 (m, CH); 6.80-8.20 (23 arom. H).

^{13}C NMR ($CDCl_3$): 55.61, 56.28 (CH_3); 23.05 (CH_2); 114.61, 120.40 (d, $^3J_{C-P}$ = 14.4), 120.65 (d, $^3J_{C-P}$), 125.62, 128.23, 128.69, 128.77, 128.88, 128.93, 128.97, 129.23, 129.35, 129.58, 132.25, 132.28, 133.59, 133.70, 134.34, 134.86, 135.03, 135.13 (CH); 111.48 (d, $^2J_{C-P}$ = 5.6), 112.17 (d, $^2J_{C-P}$), 106.34, 107.23, 143.23, 144.02, 161.02, 161.15, 163.51 (arom. C).

$^{31}P\{^1H\}$ NMR ($CDCl_3$): 1.74 (dd, $^4J_{P-P}$ = 19.2, J_{P-Pt} = 3550.4, PCH_2), 83.30 (dd, J_{Pt-P} = 3887.0, PO).

ESI-MS (CH_2Cl_2/i-PrOH): 781.2 ($[M - Cl]^+$).

[Pt(*o*-AnPOP)Cl$_2$]

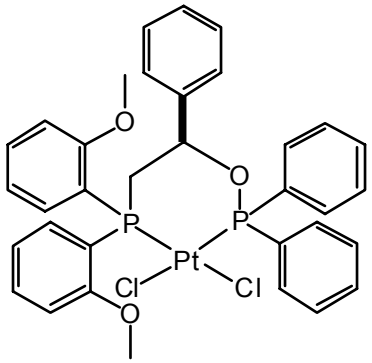

Compound **7**

A solution of the ligand *o*-AnPOP (**4**) (10 mg, 0.018 mmol) in CH_2Cl_2 (1 ml) was added to a solution of $[Pt(DMSO)_2Cl_2]$ (7 mg, 0.016 mmol) in CH_2Cl_2 (1 ml). The mixture was stirred a few minutes. Colorless crystals of **7** were obtained by slow diffusion of hexane through

CH_2Cl_2 solution.

^1H NMR ($CDCl_3$): 2.50-3.10 (m, CH_2); 3.73 (s, CH_3); 3.83 (s, 3H, CH_3); 5.10-5.30 (m, CH); 6.90-8.30 (23 arom. H).

^{13}C NMR ($CDCl_3$): 55.91, 56.07 (CH_3); 23.35 (CH_2); 115.01, 121.27, 124.41, 125.83, 128.41, 128.53, 128.78, 129.13, 132.85, 132.94, 133.45, 133.76, 134.67, 135.75, 137.40, 141, 01, (CH); 111.52, 143.74, 159.59, 160.48, 163.24 (arom. C).
$^{31}P\{^1H\}$ NMR ($CDCl_3$): 3.18 (dd, $^4J_{P\text{-}P}$ = 19.2, $J_{P\text{-}Pt}$ = 3541.6, PCH_2); 85.44 (dd, $J_{Pt\text{-}P}$ = 3855.6, PO).

ESI-MS (CH_2Cl_2/i-PrOH): 781.1 ($[M - Cl]^+$).

[Rh(COD)(POP*o*-An)]$^+$

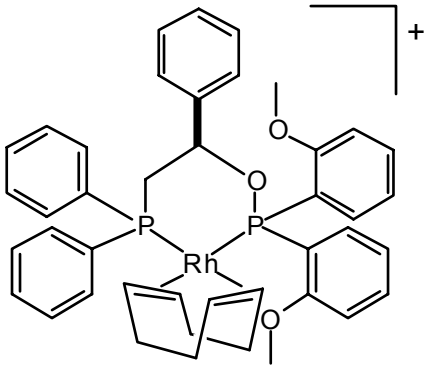

Compound **8**

A solution of $[Rh(COD)_2](BF_4)$ (2.5 mg, 0.006 mmol) in CH_2Cl_2 (1 ml) was added to a solution of ligand **2** (5mg, 0.009 mmol) in CH_2Cl_2 (0.5 ml). After few minutes of stirring, the solution was evaporated to dryness and washed sevral times with hexane to afford the tetrafluoroborate salt of cation **8** as a yellow powder.

^1H NMR ($CDCl_3$): 2.10-2.40 (m, 8H, CH_2); 2.70-2.88 (m, 2H, CH_2); 3.97 (s, CH_3); 4.03 (s, CH_3); 5.32 (br s, 1H, CH); 5.62 (br s, 4H, CH); 6.76-7.89 (23 arom. H).
^{13}C NMR ($CDCl_3$): 55.98, 56.39 (CH_3); 28.42 (CH_2); 115.32, 120.83, 126.01, 128.64,

129.09, 129.15, 129.34, 129.45, 129.60, 129.70, 132.29, 132.43, 133.70, 133.96, 134.07 (CH); 111.76 (d, $^2J_{C-P}$ = 4.8), 145.72, 162.05, 162.34, 164.61 (arom. C).

$^{31}P\{^1H\}$ NMR ($CDCl_3$): 23.04 (dd, $^4J_{P-P}$ = 50.2, J_{P-Rh} = 150.4, PCH_2); 112.57 (dd, J_{P-Rh} = 165.0, PO)

ESI-MS (CH_2Cl_2/i-PrOH): 761.3 (M^+).

[Rh(COD)(*o*-AnPOP)]$^+$

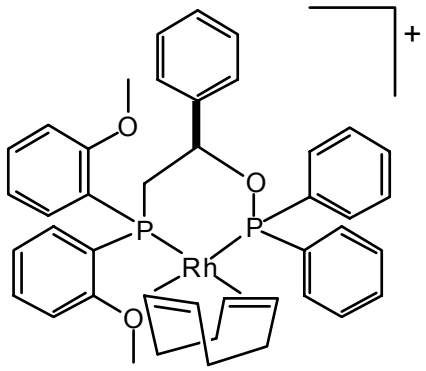

Compound **9**

A solution of $[Rh(COD)_2](BF_4)$ (2.5 mg, 0.006 mmol) in CH_2Cl_2 (1 ml) was added to a solution of ligand **4** (5mg, 0.009 mmol) in CH_2Cl_2 (0.5 ml). After few minutes of stirring, the solution was evaporated to dryness and washed sevral times with hexane to afford the tetrafluoroborate salt of cation **9** as a yellow powder.

^1H NMR ($CDCl_3$): 2.30-2.60 (m, 8H, CH_2); 2.90-3.20 (m, 2H, CH_2); 3.98 (s, CH_3); 4.06 (s, CH_3); 5.39 (br s, 1H, CH); 5.60 (br s, 4H, CH); 6.97-7.71 (23 arom. H).

^{13}C NMR ($CDCl_3$): 56.09, 56.54 (CH_3); 28.42 (CH_2); 112.13 (d, $^3J_{C-P}$= 17.6), 125.85, 128.82, 129.08, 129.21, 129.35, 129.46, 129.59, 129.69, 130.97, 131.08, 132.45, 132.58, 132.81 (CH); 107.92, 139.43, 143.62, 161.37, 163.15 (arom. C).

$^{31}P\{^1H\}$ NMR ($CDCl_3$): 14.80 (dd, $^4J_{P-P}$ = 45.8, J_{P-Rh} = 145.2, PCH_2); 125.79 (dd, J_{P-Rh} =161.9, PO)

ESI-MS (CH_2Cl_2/i-PrOH): 761.3 (M^+).

Typical procedure for Pd-catalyzed allylic alkylation

Entry 8 (Table 3.2): A mixture of $[Pd(\eta^3\text{-}C_{13}H_{15})Cl]_2$ (4 mg, 0.006 mmol), ligand **4** (16.30 mg, 0.030 mmol) and KOAc (0.82 mg, 0.006 mmol) in CH_2Cl_2 (2.5 ml) was added to a solution of *rac*-1,3-diphenyl-2-propenyl acetate (30 mg, 0.118 mmol) BSA (58 µl, 0.237 mmol) and dimethyl malonate (27 µl, 0.237 mmol) in CH_2Cl_2 (3 ml) under nitrogen. The solution was stirred at r.t. and monitored by TLC (eluent: ethyl acetate/hexane 1:5, product R_f=0.37). After 2 h to 24 h, the reaction mixture was quenched with a small amount of saturated NH_4Cl aqueous solution. The mixture was extracted two times with CH_2Cl_2, dried over $MgSO_4$ and the organic phase was evaporated. The conversion and the enantiomeric purity were determined by HPLC analysis with a chiral stationary phase column, Chiralcel OD-H (98/2 hexane/i-PrOH, 0.5 ml/min).

Entry 10 (Table 3.2): A mixture of $[Pd(\eta^3\text{-}C_{13}H_{15})Cl]_2$ (2.65 mg, 0.004 mmol), ligand **2** (4.35 mg, 0.008 mmol) in CH_2Cl_2 (2 ml) was added to a solution of *rac*-1,3-diphenyl-2-propenyl acetate (20 mg, 0.079 mmol) and sodium dimethyl malonate (0.158 mmol) (obtained from addition of NaH (4 mg ,0.158 mmol) to dimethyl malonate (18 µl, 0.158 mmol)) in THF (2 ml) under nitrogen. The solution was stirred at r.t. and monitored by TLC (eluent: ethyl acetate/hexane 1:5, R_f=0.37). The reaction mixture was worked up as described above.

Typical procedure for Rh-catalyzed hydrogenation

Entry 2 (Table 3.3): A solution of catalyst $[Rh(COD)Cl]_2$ (0.3 mg, 0.6 µmol) and ligand **2** (1 mg, 1,8 µmol) in ethanol (0.2 ml) was added to a solution methyl-2-acetamidoacrylate (3.5 mg, 24.2 µmol) in ethanol (1 ml) under nitrogen. The reaction mixture was purged, charged with H_2 (2 bars) and stirred at r.t. After 48 h, the solution was filtered through a small amount of silicagel and analyzed by CG (chiral stationary phase column, CHIRASIL-Val).

7 X-ray crystallography

7.1 Structure determination

Suitable crystals of [Pt(o-AnPOP)Cl_2] (**7**) were obtained as colourless prism-like crystals by recrystallization in CH_2Cl_2 / hexane. The intensity data were collected at 153K on a Stoe Image Plate Diffraction System [80] using MoKα graphite monochromated radiation. Image plate distance 70mm, ϕ oscillation scans 0 - 190°, step Δϕ = 1.1°, 2θ range 3.27 – 52.1°, d_{max} - d_{min} = 12.45 - 0.81 Å. The structure was solved by direct methods using the programme SHELXS-97 [81]. The refinement and all further calculations were carried out using SHELXL-97 [82]. The H-atoms were included in calculated positions and treated as riding atoms using SHELXL default parameters. The non-H atoms were refined anisotropically, using weighted full-matrix least-squares on F^2. An empirical absorption correction was applied using the DIFABS routine in PLATON [83]. The anisotropic displacement parameters for atom C54 was made equal to that of C20, as it would not refine anisotropically. The compound crystallized with two independent molecules (molecules A & B) and two molecules of dichloromethane, per asymmetric unit. The molecular structure and crystallographic numbering scheme are illustrated in the PLATON [83] drawing (Figure 3.13).

7.2 Crystallographic data

The crystallographic data of compound **7** are summarized in Table 3.5.

Table 3.5 Crystal data for [Pt(o-AnPOP)Cl_2] (**7**).

	7
Chemical formula	$C_{35}H_{34}Cl_4O_3P_2Pt$ $C_{33}H_{30}O_3P_2Pt$. $2CH_2Cl_2$
Formula weight	901.45
Crystal system	Monoclinic
Space group	P 2_1
a [Å]	11.8367 (7)
b [Å]	22.3112 (18)
c [Å]	13.2453 (8)
α [°]	90
β [°]	91.338 (7)
γ [°]	90
V [Å^3]	3497.0 (4)
Z	4
$\mu(MoK_\alpha)/mm^{-1}$	4.444
T/K	153 (2)
Reflections measured	26491
Unique reflections	13053
R(int)	0.0415
R_1, ωR_2 ($I>2\sigma(I)$)	0.0257 (0.0626)

R_1, ωR_2 (all data)	0.0435 (0.0731)

8 References

EN.REFLIST

General Conclusion

Catalysis is the backbone of chemical industry. It is the key to the production of fabrics, foodstuffs, fuels and pharmaceuticals, as well as a fundamental feature of all life processes. Finding new homogeneous catalysts which complete with the best heterogeneous catalysts and enzymes or provide enantiomerically pure products is one of the challenge of modern synthetic chemistry.

In the context of the present thesis, we have designed organic ligands and studied their coordination properties for applications as catalysts in the field of transition metal catalysis.

The first part of this thesis describes the coordination properties of Kläui's tripodal ligand toward Zr(IV). The primary goal of this project was to confirm that this ligand is an cyclopentadienyl analog (Cp^-). It was expected that complexed with d^0 metals such as Zr(IV), the resulting complexes could be used as homogeneous catalysts in the olefin polymerization. But, in contrast to the Cp_2Zr-based chemistry, this chemistry is characterized by octahedral environments around zirconium and thus the ligand does not behave like a Cp^-.

Inspired by the structure and reactivity of metalloenzymes, we have designed and synthesized dinuclear transition-state analogs (haptens) for the production of catalytic antibodies as well as dinuclear coenzymes for incorporation into the host protein. These antibodies associed with coenzymes were designed as catalysts for oxydase-, catalase-, oxygenase-reactions. Despite repeated efforts, it was unfortunately impossible to couple the hapten to the carrier protein, thus hampering the production of catalytic antibodies.

In the last project, a new class of electronically asymmetric phosphine-phosphinite bidentate ligands were designed and synthesized. The use of these ligands in hydrogenation reactions allowed us to quantify the contribution of electronic asymmetry in enantioselective catalysis. Modifying phosphino and phosphinito substitutents should allow to optimize the

enantiomeric excess to values comparable to those obtained with traditional ligands where steric interactions dominate.

The last three decades have seen in the scientific study of catalysis, a progressive shift from phenomenological approaches to structured and mechanistic investigations at the molecular level. Using new sophisticated and powerful instrumentation, quantum chemical calculations and other computational methods, catalysis comes now to molecular design. The transfer of ideas and approaches between different scientific disciplines (chemistry, biology, physics, mathematics...) created the development of *interdisciplinarity* which is a benefit for chemistry as well as for the other domains.